Improvements and Applications of Atmospheric Soundings from Geostationary Platform

by

Zhenglong Li

A dissertation submitted in partial fulfillment of

the requirements for the degree of

Doctor of Philosophy

(Atmospheric and Oceanic Sciences)

at the

UNIVERSITY OF WISCONSIN – MADISON

2009

Abstract

A unique feature of the Geostationary Operational Environmental Satellite (GOES) Sounder over the polar orbiting sounders is that it observes the atmosphere and the surface on an hourly basis with a nominal spatial resolution of 10 km. The temporally and spatially dense observations are of great importance for improving short-term weather forecasting or nowcasting. To further demonstrate how the GOES clear-sky sounding products can help nowcasting, an improved clear-sky physical retrieval algorithm for atmospheric temperature and moisture is developed. The use of the GOES Sounder is usually limited to clear skies to avoid cloud contamination of the derived profiles. However, the chance for a GOES Sounder field-of-view (FOV) to be clear is only about 34 %. Until the advent of a microwave sounder in geostationary orbit, the search for viable soundings in cloudy conditions will continue. This thesis extends the sounding retrievals from clear sky to cloudy regions, by developing a synthetic regression-based cloudy sounding retrieval algorithm. A comparison with the microwave radiometer measured total precipitable water (TPW) at the Southern Great Plains (SGP) Cloud and Radiation Testbed (CART) site from June 2003 to May 2005 shows that the clear sky TPW retrievals are improved by 0.4 mm over the legacy GOES Sounder TPW product. Comparisons against radiosondes at SGP CART site from August 2006 to May 2007 and the conventional radiosonde network over the Continental United States (CONUS) from January 2007 to November 2008 both show

that the retrievals of moisture under thin cloud conditions perform as well as those with the clear sky conditions. The largest improvement to the Global Forecast System (GFS) first guess is found in the upper level (roughly 300 – 700 hPa) integrated precipitable water vapor (PW) or PW3; the RMS is reduced by 0.4 mm. In the case of low thick clouds, PW3 is significantly improved; the improvement of RMS is about 0.21 mm. The new GOES algorithms are applied to three severe storm cases, demonstrating that the new soundings provide additional information that can lead to better short term severe storm forecasting.

Acknowledgements

My deepest gratitude is to my research advisors, Dr. Jun Li and Dr. W. Paul Menzel, for the opportunity to work with them on this project. It's been my greatest fortune to have advisors like them, who gave me so much support, help, guidance and freedom. It has always been great experience to discuss with them, no matter what the topic is. Dr. Steven A. Ackerman, my academic advisor, is always a reliable person to look for help, no matter it is about research or academy. I am deeply grateful to my committee members: Dr. Grant W. Petty, Dr. Ralf Bennartz, Dr. Pao K. Wang, and Dr. A-xing Zhu. I cannot thank them enough for their kindness and the advices. I am grateful to Mr. James P. Nelson III for providing various data base, to Mr. Harold M. Woolf for providing the fast radiative transfer model, and to Sarah Bedka for generating Figure 20 and Figure 21. Additional thanks to Dr. Jun Li's group, including Dr. Jinlong Li, Dr. Elisabeth Weisz, Dr. Xin Jin, and Chian-Yi Liu. Cooperation with them makes the work much easier. I want to thank Connie Linehan, Maria Vasys and Don Moskowitz for their support during the past years.

Special thanks to Dr. Yinghui Liu and Dr. Xuanji Wang. They both provided tremendous help, support and encouragement to me since I arrived here. I want to thank my Chinese fellows in AOS building for the happy memories, including Dr. Jun Huang, Hong Zhang, Longtao Wu, Dr. Li Bi, Dr. Yafang Zhong, Fang Wang, Agnes Huei Ni, Wei Huang, Wei Zhou, Feng He, Wei Liu, Yun Liu, Guangshang Chen, Jun Cheng, Shu Wu, and Fuyao Wang. I am also grateful to Brent Maddux, whom I shared a lot of good memories with in Room 1345.

I cannot thank enough to my wife, Haiying Zhang, for her selfless supports, sacrifice and endless love. Her encouragement and supports always give me confidence. Last, but not the least, I would like to express my sincere gratitude to my parents for their patience with me.

Some data were obtained from the Atmospheric Radiation Measurement (ARM) Program sponsored by the U.S. Department of Energy, Office of Science, Office of Biological and Environmental Research, Environmental Sciences Division. This program is supported at CIMSS by NOAA GIMPAP program NA06NES4400002.

Table of Contents

Chapter 1 Background

1.1 Motivation

Satellite observations have greatly improved the weather forecasting by providing global measurements of the atmosphere and the surface. However, short-term severe storm forecasting still remains challenging. One of the difficulties is that not enough pre-convective information is available for the numerical weather prediction (NWP) models.

The sounders on geostationary satellites (GEOS), such as the Geostationary Operational Environmental Satellite (GOES), are positioned to provide the temporally and spatially dense observations needed in order to improve short term forecasting, or nowcasting. Unlike the sounders on polar orbiting satellites (POES), the GOES Sounder monitors and measures the atmosphere and the surface on an hourly basis. The repeated measurements greatly complement the missing information needed for nowcasting. One of the goals of this study is to further demonstrate how the GOES sounding products can help nowcasting. For that purpose, an improved clear-sky physical retrieval algorithm will be developed and applied to GOES-12 Sounder measurements.

A second goal of this study is to extend the sounding retrievals from clear sky to cloudy regions, because completely clear-sky observations for the GOES Sounder occur only about 1/3 of the time. Unlike sounders on POES, the GOES Sounder has no microwave component; thus soundings to date have been restricted to clear skies only. The potential to perform soundings in thin clouds and low opaque conditions will be explored.

1.2 IR Sounder and Weather Forecasting

Satellite measurements continue to be an important global observation. They enhance the conventional surface observations in both space and time. Over the ocean and remote land areas where few humans live, satellites are the best way to observe the atmosphere and surface. Even over the land, where the radiosonde observations (RAOBs) are available, satellites are able to fill the temporal and spatial gaps. In addition, according to McPherson (1999), the number of RAOBs over the land is expected to decline in the near future. This urges better use of satellite measurements in weather forecasting.

Two of the important satellite instruments for observing the weather and environment are the sounder and imager. These two are different instruments in several aspects. The sounder has better spectral resolution and more spectral bands. Meantime, viewing the same area for the same time will result in less incoming energy for the sounder. Therefore, the sounder usually has a lower signal-to-noise ratio (SNR). One way to increase the incoming energy for the sounder is to increase the size of field-of-view (FOV), so that the sounder usually has coarser spatial resolution. The different characteristics of the two instruments are defined by their applications. The imager's better spatial resolution and SNR make it useful for applications that study such events as forest fires, clouds/fog, pollution, volcanic eruption and ice/snow cover, and etc. Although sounder observations can assist these studies, the primary application of a sounder is vertical sounding of the atmosphere.

Measurements from sounders on satellites help improve weather forecasts. The retrievals and the derived products from the radiance measurements provide information for forecasters to monitor and predict weather system developments. Claud et al. (1991) demonstrated that the temperature field derived from the TIROS-N Operational Vertical Sounder (TOVS) (Smith et al., 1979) helped to detect a storm undetected by the standard synoptical network, and to describe another storm incorrectly described by the conventional measurements. Dostalek and Schmit (2001) showed that the derived total precipitable water (TPW) from the GOES soundings has more representative spatial gradients and temporal changes than the Eta forecast model in the Great Plain dry-line environment. Li et al. (2008 and 2009) demonstrated that the derived lifted index (LI) from GOES-12 soundings can successfully reveal the pre-convective environment surrounding a supercell.

Most of these above applications are in a descriptive case study form. More quantitative utilization of sounder measurements occurs through data assimilation of the retrievals and the derived products, or of the radiance measurements. Theoretically, the radiance assimilation is superior to the retrieval assimilation for traditional low-spectrum sounder measurements because necessary assumptions made for the observational error statistics are better justified in radiance assimilation than in retrieval assimilation (Eyre et al. 1993). Studies (English et al., 2000) at the European Centre for Medium-Range Weather Forecasts (ECMWF) have proved the assimilation of TOVS and the Advanced TIROS Operational Vertical Sounder (ATOVS) measurements under the clear sky greatly improves the forecast. The development of new hyperspectral instruments offers more opportunities for improvement. McNally et al. (2006) demonstrated that assimilation of clear-sky radiances from the Atmospheric Infrared Sounder (AIRS) outperformed the assimilation from either the Advanced Microwave Sounding Unit-A (AMSU-A) or the High-resolution Infrared Radiation Sounder (HIRS).

1.3 The GOES Sounder

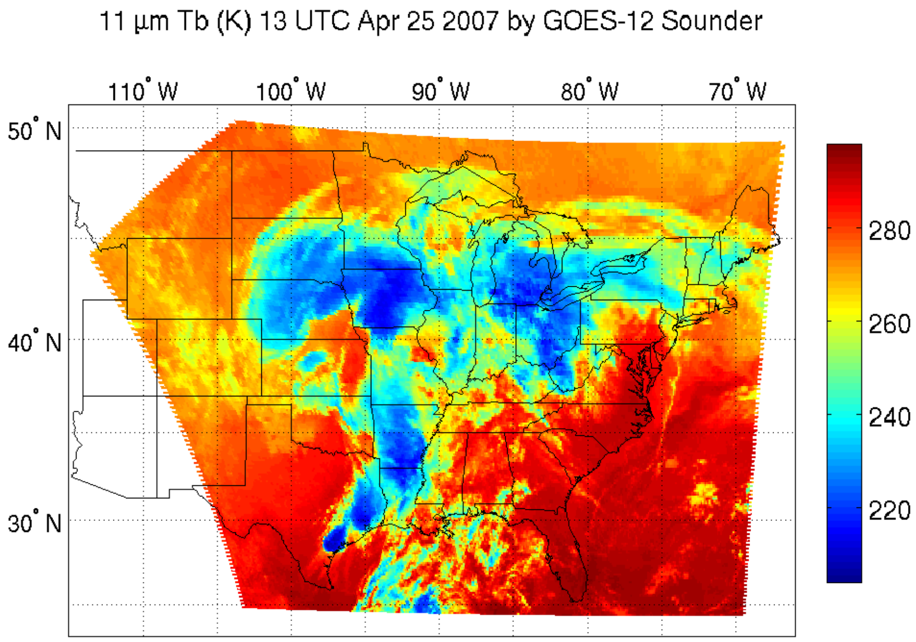

Figure 1. 11 µm brightness temperatures (K) at 13 UTC on 25 April 2007 shows the spatial coverage of the GOES-12 Sounder

Since 1994 the GOES Sounders (GOES-8/9/10/11/12/13) have been measuring radiances in 18 infrared (IR) spectral bands, ranging from approximately 3.7 to 14.7 µm, over North America and adjacent oceanic regions. According to Menzel et al.

(1998), the role of the GOES Sounder is to (a) provide simultaneous hourly observations over extended regions, especially measurements over data-poor oceans; (b) complement the twice-daily international suite of balloon observations by filling in space and time data gaps; (c) depict rapid changes in regional temperature, water vapor, and cloud cover for nowcasting severe weather; and (d) infer wind profiles by detecting thermal gradients and tracking H_2O features that are particularly useful for aviation and tropical storm forecasts. More specifically, the GOES Sounder provides the temperature, moisture and wind field, and the surface and cloud properties, especially when the conventional measurements are not available. Table 1 shows the characteristics of GOES-12 Sounder and purpose of each channel.

Compared with POES sounders, the application of GOES Sounder measurements to weather forecasting is limited by the spatial coverage. POES have global coverage. Studies (English et al., 2000) have shown TOVS and ATOVS help reduce the forecast error by 20 % in the Southern Hemisphere and only 5 % in the Northern Hemisphere. Although the GOES satellites observe about 1/3 of the earth surface as a disk, the GOES Sounders primarily work over the Continental United States (CONUS) and adjacent oceans (see Figure 1 for GOES-12 Sounder spatial coverage). The dense conventional observations (such as RAOB and radars) do not leave much room for the current GOES Sounder measurements to improve the weather forecast. Additionally, the presence of clouds reduces the clear sky coverage of the GOES Sounder. According to Schreiner et al. 2001, the probability of a clear FOV for GOES Sounder is about 34 %. The cloudy or cloud-contaminated FOVs observed by GOES Sounders are usually rejected for use by NWP models; for POES sounders, the microwave sounders are used to extract profile information from the cloud contaminated FOVs.

Table 1. The GOES-12 Sounder instrument characteristics. The unit is mW/(m²·sr·cm⁻¹) for NEDR, and K for NEDT.

	Chan	Wavelength(μm)	Band	NEDR	NEDT	Purpose
Long wave	1	14.71	Carbon Dioxide	0.77	0.81 @ 224 K	Stratosphere T
	2	14.37	Carbon Dioxide	0.61	0.66 @ 222 K	Tropopause T
	3	14.06	Carbon Dioxide	0.45	0.42 @ 237 K	Upper-level T
	4	13.64	Carbon Dioxide	0.39	0.32 @ 252 K	Midlevel T
	5	13.37	Carbon Dioxide	0.35	0.27 @ 260 K	Low-level T
	6	12.66	Water Vapor	0.14	0.095 @ 277 K	Surface T, W
	7	12.02	Window	0.11	0.072 @ 280 K	Surface T, W
Medium wave	8	11.03	Window	0.11	0.079 @ 280 K	Surface T
	9	9.71	Ozone	0.14	0.15 @ 256 K	Total Ozone
	10	7.43	Water Vapor	0.099	0.20 @ 260 K	Low-level W
	11	7.02	Water Vapor	0.059	0.19 @ 250 K	Midlevel W
	12	6.51	Water Vapor	0.11	0.86 @ 230 K	Upper-level W
Short wave	13	4.57	Carbon Dioxide	0.0062	0.13 @ 270 K	Low-level T
	14	4.52	Carbon Dioxide	0.0062	0.21 @ 260 K	Midlevel T
	15	4.45	Carbon Dioxide	0.0066	0.61 @ 240 K	Upper-level T
	16	4.13	Nitrogen	0.0024	0.099 @ 275 K	Boundary-layer T
	17	3.98	Window	0.0022	0.10 @ 280 K	Surface T
	18	3.74	Window	0.00094	0.075 @ 280 K	Surface T, W

However, two unique characteristics make the GOES Sounder ideal for improving weather forecasting, especially severe storm nowcasting: the temporal resolution of one hour and the nominal spatial resolution of 10 km at nadir. Data assimilation of radiances from POES sounders has produced significant improvements in NWP model forecasts (English et al., 2000; McNally et al., 2006) — however, they can only visit the same location somewhere between 12 hours to a few days, depending on the scanning swath width. One of the difficulties in forecasting severe storms is the short lifetime (typically just a few hours). If the model initialization does not correctly capture the pre-storm environment, it is unlikely the NWP model will predict where and when a severe storm is going to form. Another difficulty is the relatively small scale of the severe storm, especially during the early formation stage (typically a few to tens of kilometers). When assimilating POES sounder measurements, the data are usually thinned to allow faster computations at the expense of coarser resolution. The resolution of 50 km or worse makes it hard to capture the pre-convective environment. On the other hand, the GOES Sounder observes the same location on an hourly basis with a spatial resolution of 10 km at nadir. Any systems lasting longer than 1 hour with a size larger than 10 km are likely to be sampled by the GOES Sounder.

Studies have shown that the GOES sounding products are able to improve weather forecasting (Menzel et al., 1998; Schmit et al., 2002; Li et al., 2008 and 2009) by providing better-than-forecast moisture products. Figure 2 shows how the legacy physical TPW retrievals (Ma et al., 1999, currently running at the Cooperative Institute for Meteorological Satellite Studies (CIMSS)) improve the first guess of the Global Forecasting System (GFS) forecast from the National Centers for Environmental Prediction (NCEP), as compared with the ground-based microwave radiometer (MWR) measured TPW from the Atmospheric Radiation Measurement (ARM) Program at the Southern Great Plains (SGP) at the Cloud and Radiation Testbed (CART) site. For the legacy physical retrievals, the RMS is reduced from 2.80 mm to 2.61 mm, but the bias is increased from -0.46 mm to -0.67 mm. This improvement is insignificant and illustrates why the application of GOES Sounder measurements to NWP is challenging. Currently, there are only limited GOES Sounder measurements and products assimilated into operational NWP models. The retrieved clear sky TPW and cloud top pressure (CTP) are assimilated into the Rapid Update Cycle (RUC) model, and the clear-sky radiances (mostly over the water) are assimilated into the GFS model and the North American Mesoscale (NAM) model at NCEP.

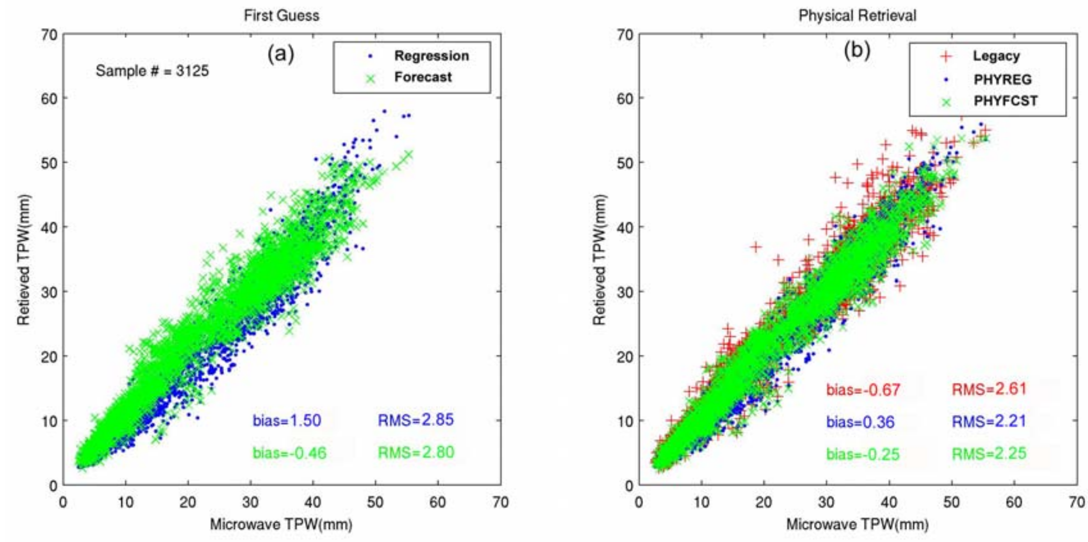

Figure 2. TPW retrievals versus ARM microwave radiometer measured TPW at the SGP CART site from June 2003 to May 2005. The x-axis presents microwave measured TPW as the true, and the y-axis presents (a) the first guess and (b) different physical retrievals applied to the GOES-12 Sounder. PHYREG and PHYFCST are the improved physical retrievals using regression and GFS forecast as first guess respectively. The legacy physical retrieval uses the GFS forecast as first guess. The RMS and bias of the differences are provided.

1.4 IR Sounding Retrievals in Cloudy Regions

For IR sounders, a profile retrieval usually excludes cloud-contaminated FOVs due to the strong absorption and scattering of IR radiances by clouds. This avoidance of IR measurements in cloudy regions does not mean the measurements are not important. Satellite observations show that the possibility of a FOV being clear is much smaller than to it being cloudy or cloud-contaminated. According to Schreiner et al. 2001, the possibility for the current GOES Sounder to see a clear FOV is about 34 %. Wylie et al. (2005) showed that completely clear-sky observations from the HIRS, with a spatial resolution of 17.4-km at nadir, occur only 23 % during the sixteen years of observations, globally. New hyperspectral instruments, such as AIRS with a spatial resolution of 13.5-km at nadir, reveal even fewer clear-sky observations; the chance for a footprint to be clear is less than 10 % (Huang and Smith, 2004). Studies also show that cloudy regions are more important for NWP error development (McNally 2002) and exhibit more forecast error than clear skies. Therefore, for better employment of IR sounder measurements, it is necessary to include cloudy measurements, albeit very carefully.

Different methods have been developed to extract atmospheric information in cloudy regions. Cloud-clearing (Joiner and Rokke, 2000; Susskind et al., 2003; Li et al., 2005; Cho and Staelin, 2006) has been used to derive clear radiances within a partly cloudy FOV. A basic assumption of cloud clearing is that differences of earth surface and atmosphere conditions between adjacent FOVs are small. By using sounders with other collocated measurements, for example, combining AIRS with the

Moderate Resolution Imaging Spectroradiometer (MODIS) measurements (Li et al., 2005), or AIRS with AMSU measurements (Susskind et al., 2003; Cho and Staelin, 2006), it is possible to derive the equivalent clear radiances within a partly cloudy AIRS FOV. The difference between MODIS/AIRS cloud-clearing and AMSU/AIRS cloud-clearing is that the former preserves the single FOV for AIRS clear column radiances, while the latter degrades the spatial resolution to AMSU footprint (3 by 3 AIRS FOVs). When it is overcast, combining the IR and microwave measurements (Chevallier et al., 2002), enables simultaneous retrieval of atmospheric profiles and cloud parameters. This method is especially useful when clouds are opaque as demonstrated by Huang and Smith (1986). These methods focus on removing the effect of clouds so that atmospheric soundings can be achieved from clear equivalent radiances. Another method is to identify channels unaffected by clouds for an FOV (McNally and Watts, 2003; Carrier et al., 2007). For a hyperspectral IR instrument, even when clouds are present, some channels are not affected by the clouds. Channels peaking in upper troposphere do not ‘see’ lower clouds, and thus are able to provide useful atmospheric information above the clouds.

Recent studies (Weisz et al., 2007; Zhou et al., 2007) demonstrated that hyperspectral IR measurements are able to retrieve atmospheric profiles along with cloud parameters in two conditions. One, when clouds are optically thin, the observed IR radiation includes a contribution from below the cloud down to the surface. With the simultaneously retrieved cloud information, such as CTP, cloud optical thickness (COT) and cloud effective particle size, the algorithm is able to account for the cloud effect and retrieve the temperature and moisture profile information. Second, when the cloud is optically thick, contribution from below the cloud is hidden, but a sounding above the cloud can be retrieved.

In this study, the possibility of extending the GOES soundings from clear sky to cloudy regions is explored. The focus will be on thin clouds (defined as having retrieved COT smaller than 2.0) and low thick clouds (defined as having retrieved CTP larger than 850 hPa and retrieved COT larger than 2.0). In this study, optically thin clouds include high thin cirrus clouds and low-level cloud edges. When a FOV is only partly covered by scattered low clouds, the effective optical thickness is not large. Even low stratus clouds or other thick clouds, at cloud edge, are considered as thin clouds for increasing sounding coverage. According to Warren et al. (1985), low clouds have an occurrence frequency of 15 % between 30º – 60º N. Chang and Li's (2005) study shows the global single-layer cirrus clouds have an occurrence frequency of 12 % under cloudy conditions.

Chapter 2 Data Set

Several data sets used for the retrievals are introduced in this chapter.

1. The RAOB/GOES/GFS-2003 match-up database contains 9884 temporally and spatially collocated conventional RAOBs, GOES-12 Sounder brightness temperature (Tb) measurements, and NCEP GFS model forecast profiles from June 2003 to September 2004 over the CONUS, which are collected at CIMSS at the University of Wisconsin at Madison (UW). The GOES-12 Sounder Tb is averaged using a 3 by 3 box to reduce the random noise in the measurements. This database is used mainly for training purpose.
2. The RAOB/GOES/GFS-ARM match-up database contains temporally and spatially collocated RAOBs, the GOES-12 Sounder Tb measurements and the NCEP GFS model forecast profiles from August 2006 to May 2007. The RAOB are collected at the ARM SGP CART site at Lamont, OK (C1, 36°37' N, 97°30' W). The ARM RAOBs have better overall quality than the conventional RAOB (Turner et al., 2003; see section 4.2 for more details on ARM RAOB). The GOES-12 Tb measurements are spatially averaged using the inverted cone method (see section 3.2.3). It will be mainly used for cloudy retrieval validation as an independent database. Additionally, the 4-times-per-day observations are perfect for testing the time continuity technique. The sample size is 765, among which 362 are cloudy samples.
3. The RAOB/GOES/GFS-2007 match-up database contains temporally and

spatially collocated conventional RAOBs, GOES-12 Sounder Tb measurements, and NCEP GFS model forecast profiles over the CONUS from January 2007 to November 2008. The GOES-12 Tb measurements are spatially averaged using the inverted cone method. The sample size is 53037, in which 21607 are cloudy. Figure 3 shows the station locations and monthly sample distribution of the collected conventional RAOB. This database is mainly for validation purpose, in both clear and cloudy conditions.

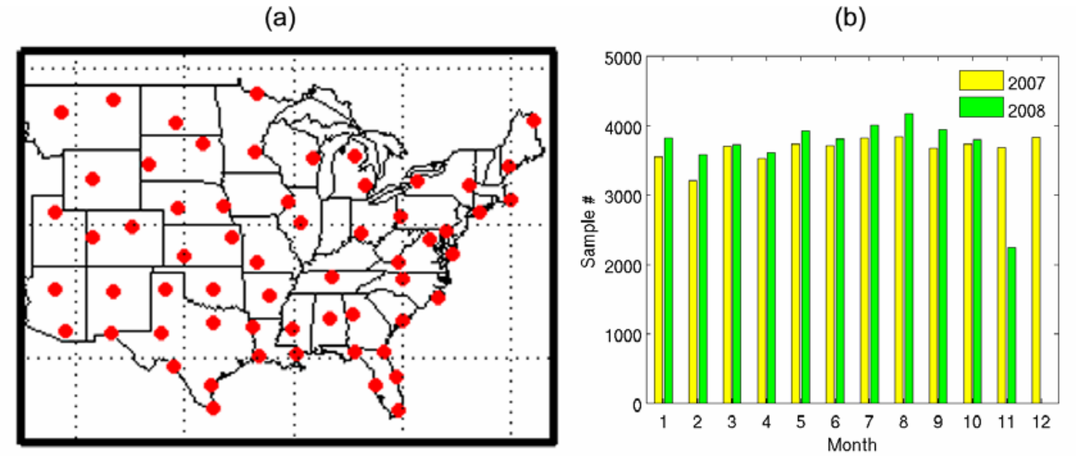

Figure 3. a) The conventional radiosonde station locations over the CONUS; b) the monthly sample distribution of collected radiosonde observations from the RAOB/GOES/GFS-2007 match-up database

4. The SeeBor training database (Borbas et al., 2005) contains about 15000 global profiles of temperature, moisture and ozone from National Oceanic and Atmospheric Administration (NOAA)-88, ECMWF, the Thermodynamic Initial Guess Retrieval-3 (TIGR-3), ozonesondes and desert radiosondes. A physically based characterization of the surface skin temperature and the surface emissivity are also included in this database. This database are widely used at CIMSS for synthetic regression retrievals for skin temperature, surface emissivities and

profiles, when there is no real match-up data. In this study, the data set is used as a training set for cloudy retrievals.

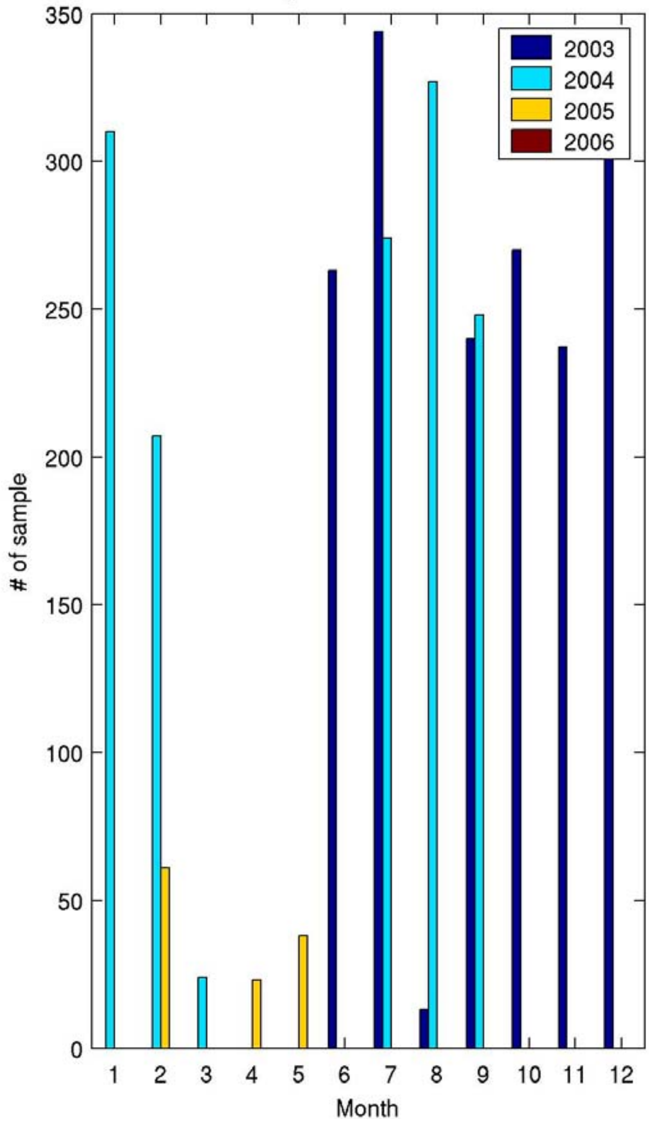

Figure 4. The monthly sample distribution of the collected microwave radiometer measured TPW at SGP CART site from June 2003 to May 2005. The collocated GOES-12 Sounder measurements are averaged using a 3 by 3 box.

5. The MWR/GOES/GFS-ARM match-up database contains temporally and spatially collocated TPW measured by a ground-based MWR, the GOES-12 Sounder Tb measurements and the NCEP GFS model forecast profiles. Every

five minutes, an MWR at the SGP CART site provides measurements of column-integrated amounts of water vapor [http://www.arm.gov/instruments/instrument.php?id=mwr]. This microwave radiometer measured TPW, with accuracy of ± 0.7 mm, is excellent for TPW retrieval validation. The time coverage is from June 2003 to May 2005. The collocated GOES-12 Sounder measurements are averaged using a 3 by 3 box. Figure 4 shows the distribution of samples in different month and year.

6. The UW-Madison Baseline Fit Emissivity Database (Seemann et al., 2008) is derived using input from MODIS operational land surface emissivity product (MOD11). It is a monthly averaged global database at ten wavelengths (3.6, 4.3, 5.0, 5.8, 7.6, 8.3, 9.3, 10.8, 12.1, and 14.3 microns) with 0.05 degree spatial resolution. The Baseline Fit method, which is based on a conceptual model developed from laboratory measurements of surface emissivity, is applied to fill in the spectral gaps from 3.6 to 14.3 μm.

Chapter 3 Clear-sky Sounding Improvements

The major difference between the GOES Sounder and POES operational sounders is that the GOES Sounder monitors and measures the atmosphere and the surface on an hourly basis. The temporal dense measurements greatly complement the missing information needed for short-term weather nowcasting. Previous studies have shown the clear-sky GOES sounding products are helpful for weather forecasters (Menzel et al., 1998; Schmit et al., 2002; Li et al., 2008 and 2009; Jin et al., 2008). To further demonstrate that, an improved clear-sky physical retrieval algorithm is developed and applied to GOES-12 Sounder measurements, with emphasis on the comparisons to the old version —— the legacy version (Ma et al., 1999) and operational NWP models. Meanwhile, the repeated observations offer an opportunity to explore the concept of the time continuity on GOES sounding.

3.1 Newtonian Nonlinear Method

In clear sky conditions, if atmospheric scattering is negligible, the exiting radiance at the top of the atmosphere for a given GOES-12 Sounder channel with wavenumber ν is

$$R_\nu = \varepsilon_\nu B_\nu(T_s)\tau_s - \int_0^{p_s} B_\nu(T)d\tau(0,p) + (1-\varepsilon_\nu)\int_0^{p_s} B_\nu(T)d\tau^* + R_\nu^{'} \qquad (1)$$

where R_ν is the exiting radiance at the top of the atmosphere or GOES-12 Sounder IR radiance, ε_s is the surface emissivity, $B_\nu(T)$ is Planck function, $\tau(0,p)$ is the atmospheric transmittance from the top to the atmospheric pressure p, subscript s denotes surface, $\tau^* = \tau_s^2 / \tau$ is the downwelling transmittance, and $R_\nu^{'}$ is the reflected solar radiation, which is considered negligible in IR region when wavelength is larger than 4.0 μm. As shown in equation (1), the GOES-12 IR radiance has three major contributions: the surface emission, the upwelling atmosphere emission, and the reflection of the downwelling atmosphere emission by the surface.

The retrieval problem is to inversely solve atmospheric profiles and surface parameters for given satellite IR radiance measurements. It is an ill-posed inverse problem (Plokhenko and Menzel, 2001 and 2003; Plokhenko et al., 2003). Neglecting impacts from ozone and other trace gases, the radiative equation could be linearized in Tb space to the first order as

$$\delta T_b = K_{T_s} \delta T_s + K_\varepsilon \delta\varepsilon + \sum K_T \delta T + \sum K_Q \delta \ln Q \quad (2)$$

or $\delta T_b = K \delta x + \sigma$ (2a)

where δT_b is the Tb difference between the observed and the calculated Tb from the first guess; $K = [K_{Ts} \quad K_\varepsilon \quad K_T \quad K_Q]$ is the matrix of weighting functions for surface skin temperature, surface emissivity, temperature profile, and moisture profile; $\delta x = \begin{bmatrix} \delta T_s \\ \delta\varepsilon \\ \delta T \\ \delta \ln Q \end{bmatrix}$ is the vector of the perturbation of the retrieval parameters, defined as the differences between the first guess and the truth; and σ is the satellite observation noise plus the forward model uncertainty. From equation (2), for any channel, the Tb difference has four contributions: the surface skin temperature, the surface emissivity, and the temperature and moisture profiles. Any perturbations between the true and the first guess will result in a departure of the calculated Tb away from the observed Tb.

If it is a well-posed problem, then the solution could be obtained using a simple linear algebra method or the least square method

$$\delta x = \left(K'E^{-1}K\right)^{-1} K'E^{-1}\delta T_b \quad (3)$$

or in iteration form:

$$x_{i+1} = x_0 + (K'E^{-1}K)^{-1}K'E^{-1}[\delta T_b + K(x_i - x_0)] \quad (4)$$

where x_{i+1} is the (i+1)th iteration of x, x_0 is the first guess, and $E = \begin{bmatrix} \sigma_1^2 & & & & \\ & \sigma_2^2 & & 0 & \\ & & \cdots & & \\ & 0 & & \sigma_{n-1}^2 & \\ & & & & \sigma_n^2 \end{bmatrix}$ is the measurement noise.

Because the actual sounding retrieval is an ill-posed problem, there is no way to find the inverse of $K'E^{-1}K$. As a result, the iteration of equation (4) is usually unstable. One way to handle this is to regularize the solution or solutions by posing either or both of two constraints: a) the iterated x can only be adjusted according to a known background condition; b) the iterated x can not be too far away from the first guess. Mathematically, the two constraints could be realized using a cost function (Li et al., 2000; Eyre et al., 1993)

$$J(x) = \delta Tb^{T} E^{-1} \delta Tb + \gamma\left(x - x^{0}\right)^{T} S_0^{-1}\left(x - x^{0}\right) \quad (5)$$

where S_0 is the error covariance matrix of the background, and γ is the regularization parameter. The aim is to find the best estimate of x, so that the cost function is a minimum. There are two constraints on the cost function. First, the solution should meet the condition that the difference between the observed and the calculated Tb is a minimum. Second, the solution cannot be too far away from the first guess. The regularization parameter balances the relative importance of the two constraints. A larger γ gives more weight to the second constraint. As a result, the iteration might be under-adjusted. A smaller γ gives more weight to the first constraint (closer to the least square method), which means more freedom on the adjustment. As a result, the iteration might not converge (over-adjusted). The value of γ is usually determined empirically, and could be adjusted in iterations. If the iteration fails to converge, larger regularization parameters are used to allow less adjustment of *x* (Li and Huang 1999).

Usually, the solution of equation (5) is obtained by minimizing the cost function or letting *J'(X)* = 0. However, due to the non-linearity, the iteration is usually not fast enough and the solution can be unstable. A better and faster solution can be obtained using the inverse Hessian method (Ma et al., 1999)

$$x_{i+1} = x_i - J''(x_i)^{-1} J'(x_i) \qquad (6)$$

And the iteration solution, which is called Quasi-Newton nonlinear iteration, is

$$x_{i+1} = x_0 + (\gamma S_0^{-1} + K' E^{-1} K)^{-1} K' E^{-1} [\delta Tb + K(x_i - x_0)] \qquad (7)$$

This is the method used by Li et al. (2000), and is called the regularization method. When γ is 1, equation (7) changes to the classical Newton nonlinear iteration

$$x_{i+1} = x_0 + (S_0^{-1} + K' E^{-1} K)^{-1} K' E^{-1} [\delta Tb + K(x_i - x_0)] \qquad (7a)$$

Compared with the linear algebra solution in equation (4), there is one extra term γS_0^{-1} in equation (7) or S_0^{-1} in (7a). Mathematically, this term adds positive values along the diagonal direction of $K'E^{-1}K$ and makes the inverse possible. Physically, this term controls the iterations by providing background information and the relative importance of the two terms in equation (5). S_0 has to be consistent with the first guess. Too small diagonal values of S_0 make the adjustment too small in iterations, and therefore the iteration might have difficulty to converge to the optimal point. Too large diagonal values of S_0 make the adjustment too large, which could result in failure of convergence.

Equation (7) is a little different from the one used by Ma et al., (1999). Their solution is derived using the Marquardt-Levenberg algorithm (Marquardt 1963; Levenberg 1944), and has a hybrid iterative solution combining the classical Newton method and the steepest descent method (Press et al., 1990 and 1992) and looks

$$x_{i+1} = x_0 + (S_0^{-1} + K^{'}E^{-1}K + \gamma_i I)^{-1}\{K^{'}E^{-1}[\delta Tb + K(x_i - x_0)] + \gamma_i(x_i - x_0)\} \qquad (8)$$

where terms associated with γ_i are presented from the steepest descent method.

In this study, a hybrid form of iteration equation combining equation (7) (Li et al., 2000) and equation (8) (Ma et al., 1999) is used

$$x_{i+1} = x_0 + (\gamma S_0^{-1} + K^{'}E^{-1}K + \gamma_i I)^{-1}\{K^{'}E^{-1}[\delta Tb + K(x_i - x_0)] + \gamma_i(x_i - x_0)\} \qquad (9)$$

This equation represents different forms depending on the values of γ and γ_i. If γ is 1, equation (9) becomes Marquardt-Levenberg solution; if γ_i is zero, it becomes Quasi-Newton nonlinear iteration; and if γ is 1 and γ_i is zero, it becomes classical Newtonian iteration method. The advantage of this hybrid form of iteration equation is simpler coding. One algorithm could be used for three different iteration methods. As will be shown later, the actual iteration method used in this study is the classic Newtonian iteration method.

All the atmospheric and surface parameters could be retrieved using the physical retrieval algorithm, including temperature, moisture and ozone profiles (Jin et al., 2008), the surface skin temperature, and the surface emissivities for each channel. However, this thesis focuses on retrieving the temperature and moisture profiles.

3.2 Improvements of the Physical Retrieval Algorithm

From equation (7a), there are six variables in the right hand, which will greatly affect the retrievals: the first guess, the background error covariance matrix, the measurements, the calculated radiances, the weighting functions, and the covariance matrix of the measurements. The improvements will focus on the first four variables. The impact from the weighting functions will be discussed at the end of the chapter.

3.2.1 Improvements of First Guess —— Regression Algorithm

In the algorithm, the GOES single FOV (SFOV) clear-sky sounding algorithm starts with a statistical linear regression technique instead of using the NWP model forecast (Ma et al., 1999). This method was first introduced by Smith et al. (1970). A summary for regression sounding retrievals follows.

Sounding retrieval pursues a relationship between satellite measurements and atmospheric soundings, or

$$Y(n) = K(n,m)X(m) \qquad (10)$$

where *Y(n)* is a vector of retrieval parameters (*n* is the number of unknowns, including cloud, surface and atmospheric parameters), *X(m)* is a vector of measurements (*m* is the number of knowns, including satellite measurements and other known variables), and *K(n,m)* is an operator matrix to calculate *Y* for given *X*. With a training database, the linear regression coefficients can be obtained using the least square method or linear algebra

$$K = YX^T (XX^T)^{-1} \qquad (11)$$

The predictors for the regression include: 1) the radiances (Tb in the algorithm, including the quadratic terms of Tb); 2) the surface pressure; 3) the local zenith angle; 4) the observed surface temperature and moisture if available; and 5) the NCEP GFS forecast profiles. The predictants include the surface skin temperature, the surface emissivity, and the profiles of temperature, moisture and ozone. A little more explanations about the regression algorithm are given below.

1) The radiances provide primary information about the temperature and moisture profiles. However, due to the non-linearity of the radiative transfer equation, the quadratic terms are included as predictors. Also, due to the correlation between different channels, the interaction terms are included.

2) To take advantage of high accuracy of NWP model forecast data, the NCEP GFS forecast are used as predictors in the regression algorithm. This ensures better first guess than the forecast data.

3) Measurements of surface air temperature and surface air water vapor are used as predictors to help the boundary layer retrieval (following the work by Smith et al., 1985; Smith and Woolf, 1988; Ma et al., 1999; Li et al., 2000).

4) The logarithm of the mixing ratio is used for both predictants and predictors to account for the non-linearity of moisture in the radiative transfer equation.

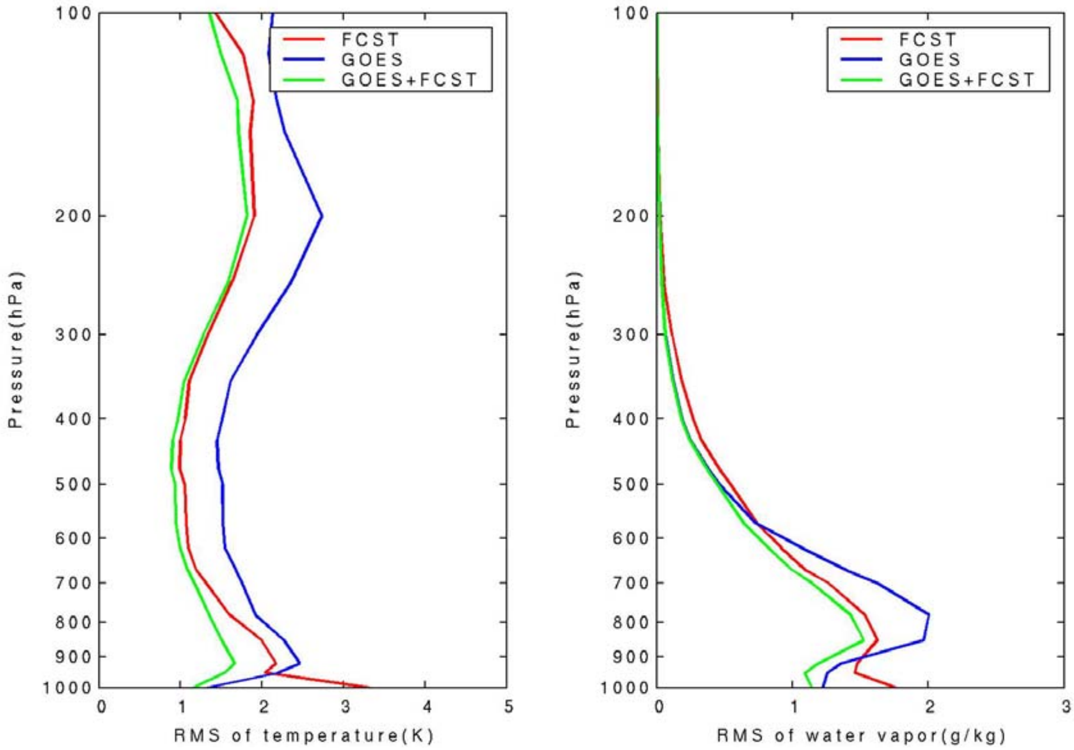

Figure 5. The RMS of regression retrieved temperature (left) and moisture (right) profiles compared with RAOB. The red lines are the GFS forecast, the blue lines are the regression retrievals from GOES alone (no forecast profiles used as predictors), and the green lines are the regression results with the GFS forecast as predictors.

By using 90 % of the RAOB/GOES/GFS-2003 match-up dataset as training, the other 10 % of the dataset are used as independent dataset for validation of the regression retrievals of the profile information. Figure 5 shows how the regression retrievals improve the first guess of the GFS forecast. The bias profiles are not shown because they are close to zero. For RMS, smaller values indicate better results——more similar to RAOB profiles. Without the forecast data as predictants, the retrieval of temperature and moisture (blue lines) are not as good as the GFS forecast for most of the layers. On the contrary, with the forecast, the regression retrievals are better than forecast. Notice the profiles near the surface are improved the most due to the high-quality surface observations included as the predictors. Actually, by including the surface observation, even the regression without forecast has better results than forecast near the surface.

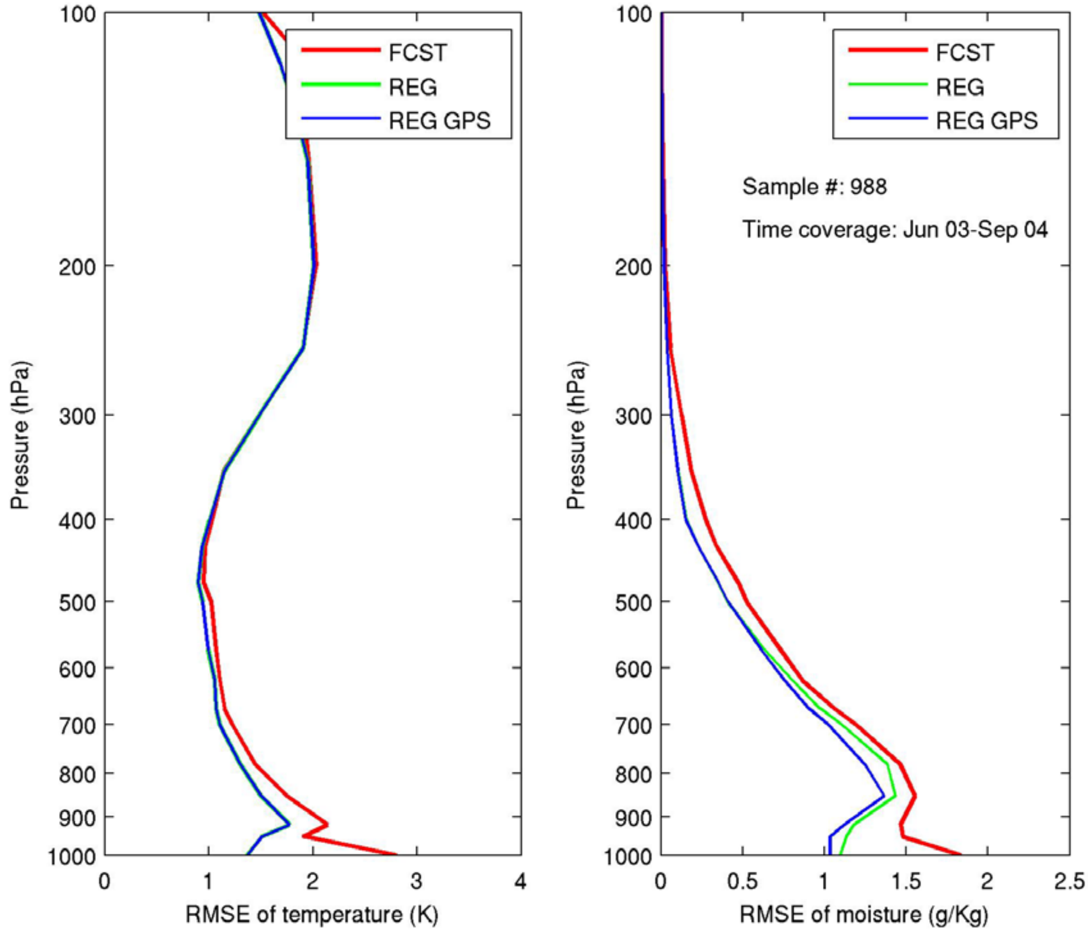

Figure 6. The RMS of regression retrieved temperature (left) and moisture (right) profiles compared with RAOB. The red lines are the GFS forecast, the green lines are the regression retrievals without GPS TPW as a predictor, and the blue lines are the regression retrievals with the GPS TPW as a predictor. The same 10 % of the RAOB/GOES/GFS-2003 match-up database are used for comparison as in Figure 5.

The results shown above are statistical results from real measurements. This does not mean the regression retrievals are always better first guesses than the GFS forecast. Actually, both the regression retrievals and the GFS forecast will be used as first guess in the physical iteration algorithm depending on the weather conditions. There will be a test to determine which one to use. See section 3.3.1 for more details.

GPS retrieved TPW on regression

The global positioning system (GPS) has been proven useful on moisture retrievals (Bevis et al., 1992, Duan et al., 1996). This offers another great opportunity to improve the GOES sounding retrievals. Compared with other moisture measurements, such as RAOB and the ground-based MWR, the GPS has obvious advantages: 1) The high temporal resolution of 30 min, which is much better than the RAOB (12 hours); 2) The global coverage with decent spatial resolution (around 400 stations over the CONUS, compared with less than 80 RAOB stations over the CONUS); 3) compared with ground-based microwave radiometers (MWR), the GPS are airborne. It is therefore much cheaper for GPS to have global coverage than the ground-based MWR; and 4) GPS works almost under all conditions of weather.

The GPS TPW is used as an additional predictor to help improve the first guess of the profile information. Since there is no match-up database including GPS-based TPW, the RAOB profiles in the RAOB/GOES/GFS database are used to calculate TPW. The simulated GPS retrieved TPW is generated with a standard deviation (STD) of 0.15 cm and a mean of zero (Birkenheuer, D., and S. Gutman, 2005). The same 90 % of the RAOB/GOES/GFS-2003 match-up database are used to train the regression coefficients, and the other 10 % are used for validation. Figure 6 shows the results.

The GPS TPW has no impact on temperature retrievals, but has a strong impact on the moisture profile retrievals, especially in the lower atmosphere.

3.2.2 Background Error Covariance Matrices

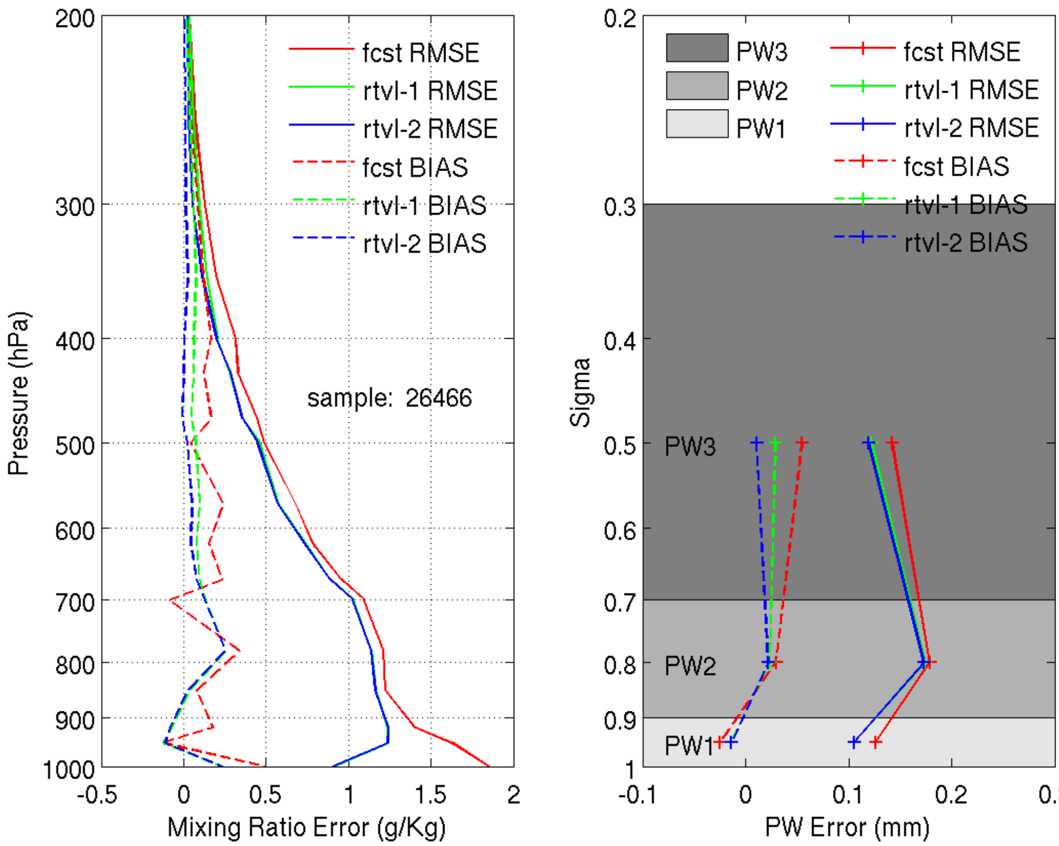

Figure 7. The impacts of off-diagonal elements of the inverse of error covariance matrix of the background on moisture retrieval of (left) the mixing ratio profiles, and (right) the three layer PWs using the RAOB/GOES/GFS-2007 match-up database. The solid lines are the RMS of difference as compared with RAOB, and the dashed lines are the bias. FCST represents the NCEP GFS forecast profiles. RTVL-1 represents physical retrievals without off-diagonal elements, and RTVL-2 represents physical retrievals with off-diagonal elements.

Among the four variables, the background error covariance matrix might be the most important one. In the iteration algorithm, what really matters is the inverse of the error covariance matrix of the background (IECMB). Different authors have different ways to calculate IECMB. For example, in Li et al., 2000, only diagonal elements of IECMB are retained. The background covariance matrix is estimated based on empirical evidence. In Ma et al., 1999, an error correlation matrix instead of a covariance matrix is used to "keep the same scale of the relationship between temperature and the natural logarithm of the water vapor mixing ratio". Clearly, neither of them used real error covariance matrix in the algorithm.

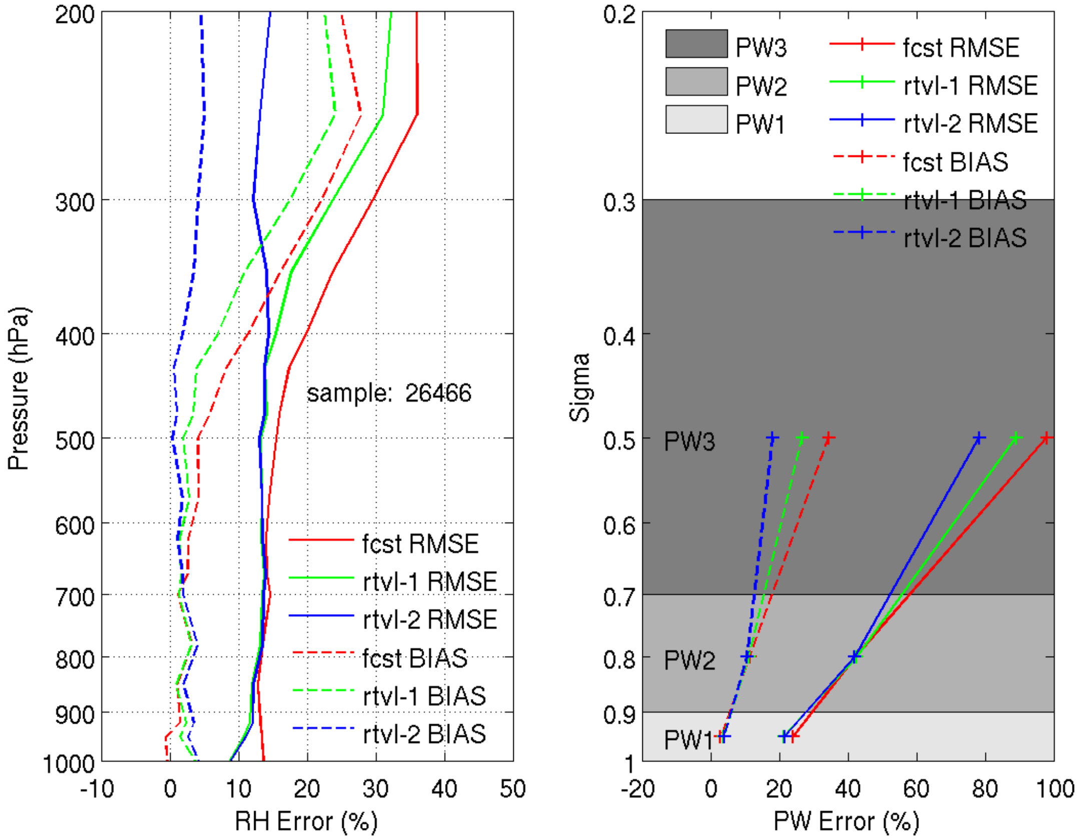

Figure 8. Same as Figure 7 except (left) the relative humidity profiles, and (right) the three layer PWs error percentage.

It is found in this study that a real IECMB not only increases the retrieval precision, but also makes the iteration more stable and converge faster. Using the

RAOB/GOES/GFS-2003 match-up database, two sets of IECMB are calculated: one for regression and the other for the GFS forecast. The method to calculate them is described.

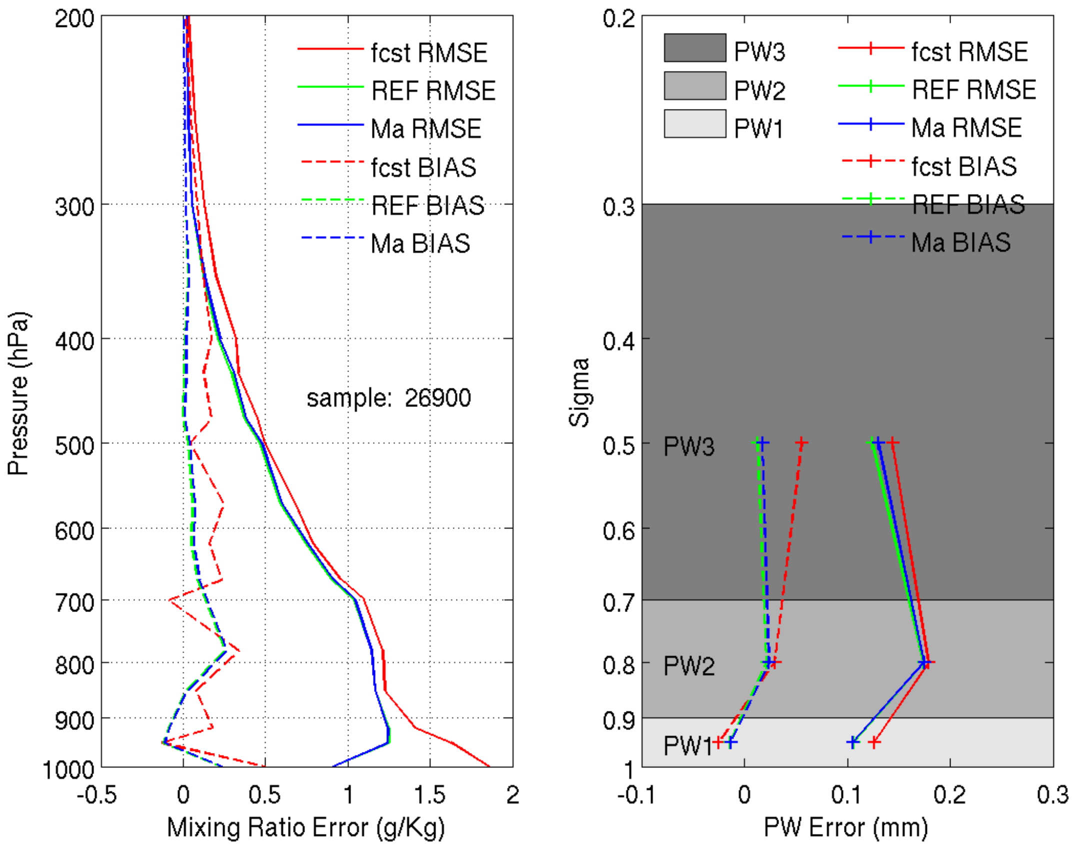

Figure 9. Comparison of different physical retrievals of (left) the mixing ratio profiles, and (right) the three layer PWs using the RAOB/GOES/GFS-2007 match-up database. The solid lines are the RMS of difference as compared with RAOB, and the dashed lines are the bias. FCST represents the NCEP GFS forecast profiles. REF represents physical retrievals using the classic Newtonian iteration method, and Ma represents physical retrievals using method of Ma et al., 1999.

Assume *E(m,n)* is the error profiles (compared to RAOB), where *m* is the number of the profiles, and *n* is the number of profile level. The IECMB is calculated using

$$S_0^{-1} = (E^T E / m)^{-1} \qquad (12)$$

where E is the covariance matrix of the background error information, and $()^{-1}$ is the inverse.

Different from Li et al. (2000), the off-diagonal elements of IECMB are also retained and used in the physical algorithm. The off-diagonal elements explain the correlations of temperature and moisture between adjacent levels. They were not used in Li et al. (2000) because they could cause the iteration to be unstable. Figures 7 and 8 show how the off-diagonal elements of IECMB affect the moisture retrievals. Both the mixing ratio (Figure 7a) and the relative humidity (Figure 8a) show that the off-diagonal elements have positive impacts on moisture retrieval, especially in the upper troposphere, where level correlations are more significant than in the lower troposphere. By using the off-diagonal elements, the bias of mixing ratio and relative humidity is improved for pressure smaller than 600 hPa, and the RMS is improved for pressure smaller than 400 hPa, which is more significant in Figure 8a.

Figure 7b and Figure 8b shows the impacts of the off-diagonal elements of IECMB on the 3 layer precipitable water (PW) retrievals. The 3 layer PW is integrated precipitable water in sigma coordinates. PW1 is from the surface to 0.9 (roughly 900 hPa), PW2 is from 0.9 to 0.7 (roughly 900 to 700 hPa), and PW3 is from 0.7 to 0.3 (roughly 700 to 300 hPa). In other words, the 3-layer PW depicts the moisture in the lower, middle and upper troposphere. As expected, PW3 is improved by using the off-diagonal elements; both RMS and bias are reduced in Figure 7 (b) and Figure 8 (b). Although the improvement of RMS in Figure 7 (b) is not significant, the improvements of both RMS and bias are about 5 % in Figure 8 (b). Therefore, in this study, the off-diagonal elements are retained in the physical iteration.

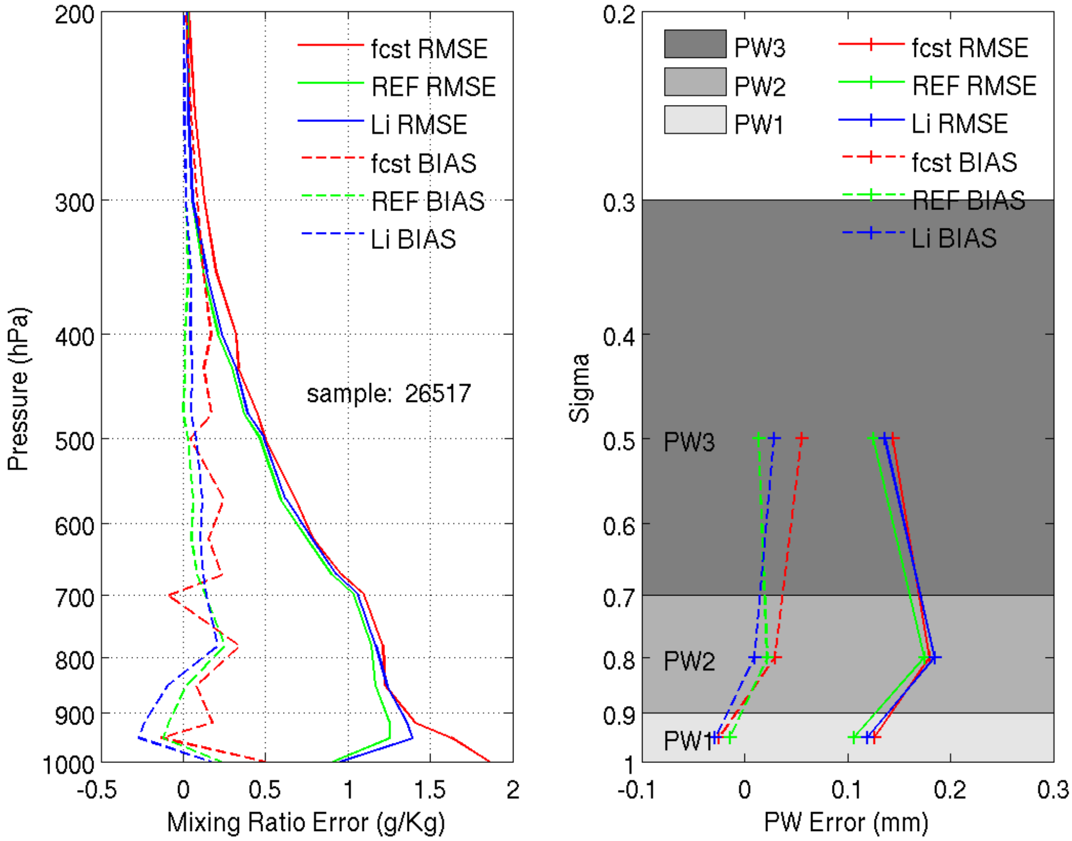

Figure 10. Same as Figure 9 except Li represents physical retrievals using method of Li et al., 2000.

One advantage of using real IECMB is more stable iterations and faster convergence. Therefore, no extra parameters (such as γ_i and γ in equation (9), which actually decrease the retrieval accuracy) are needed. Figure 9 shows the comparisons of the retrievals of moisture by the classic Newtonian iteration method and Ma et al. (1999). Figure 10 shows the comparisons of the retrievals of moisture by the classic Newtonian iteration method and Li et al. (2000). In the comparison, the three algorithms use the same background error covariance matrix, which is calculated using equation (12). The differences among the three algorithms are described in section 3.1. The RAOB/GOES/GFS-2007 match-up database is used.

From Figure 9, the classic Newtonian method looks very similar but shows slightly better results than Ma's; only PW3 sees about 0.02 mm improvement of RMS. It will be shown later that the classic Newtonian iteration with the new IECMB yields much better results than the legacy retrievals using Marquardt-Levenberg method (Ma et al., 1999). From Figure 10, the improvement by the classic Newtonian iteration method over the Quasi-Newton iteration is substantial, especially in the lower troposphere. Therefore, in the improved physical retrieval algorithm, the classic Newtonian iteration method is used, and with the realistic IECMB, the algorithm has no problem with convergence, which is typically reached within 3 steps.

3.2.3 Improvements of Measurements——Noise Reduction

All satellite measurements include noise. Typically, there are two types of noise in GOES Sounder observation. Random noise exists in all channels due to the spectroscope and bit truncation. Different channels have different scale of random noise. Column 5 (radiance) and 6 (Tb) in Table 1 show the noise characteristics of each channel for GOES-12 Sounder. There are a lot of noises in the sounder measurements, especially in channels 1, 2, 12 and 15. The other type is the systematical noise, which could also come from the instrument and the pre-processing. However, one important contributor is the instrument drifting as it becomes older. Both the random noise and the systematical noise have to be handled prior to any retrieval using satellite measurements.

Random Noise

A commonly used method to reduce random noise is the spatial averaging method. This could be done because of spatial continuity. For example, GOES-12 Sounder channel 1 is designed for measuring stratosphere temperature. Unlike the lower troposphere, the stratosphere is very smooth in temperature distribution. For channels like this (such as channels 1, 2 and 15), spatial averaging over a large box (such as 15 by 15 FOVs) is effective on reducing the random noise.

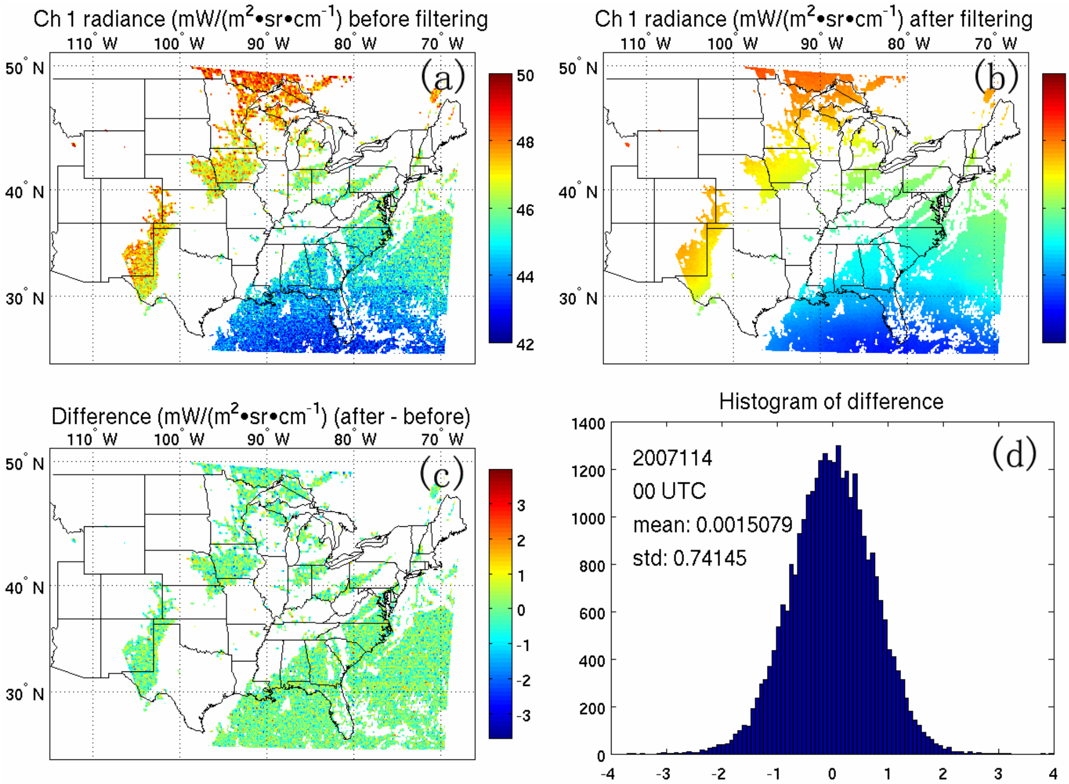

Figure 11. The demonstration of the inverted cone method on random noise reduction in clear sky conditions for channel 1. a) the original measurements of channel 1 radiances at 0 UTC on 24 April 2007; b) channel 1 radiances after filtering using the inverted cone method; c) the differences of the radiances (after minus before); and d) the histogram of the differences.

The upper troposphere is still smooth in temperature but can be affected by high clouds. Along the boundaries between different air masses, gradients can also be found. Continued averaging using a large box will result in losing important atmospheric temperature and moisture gradients. For these channels, a smaller box, as well as considerations of preservation of gradients (which will be shown), is needed.

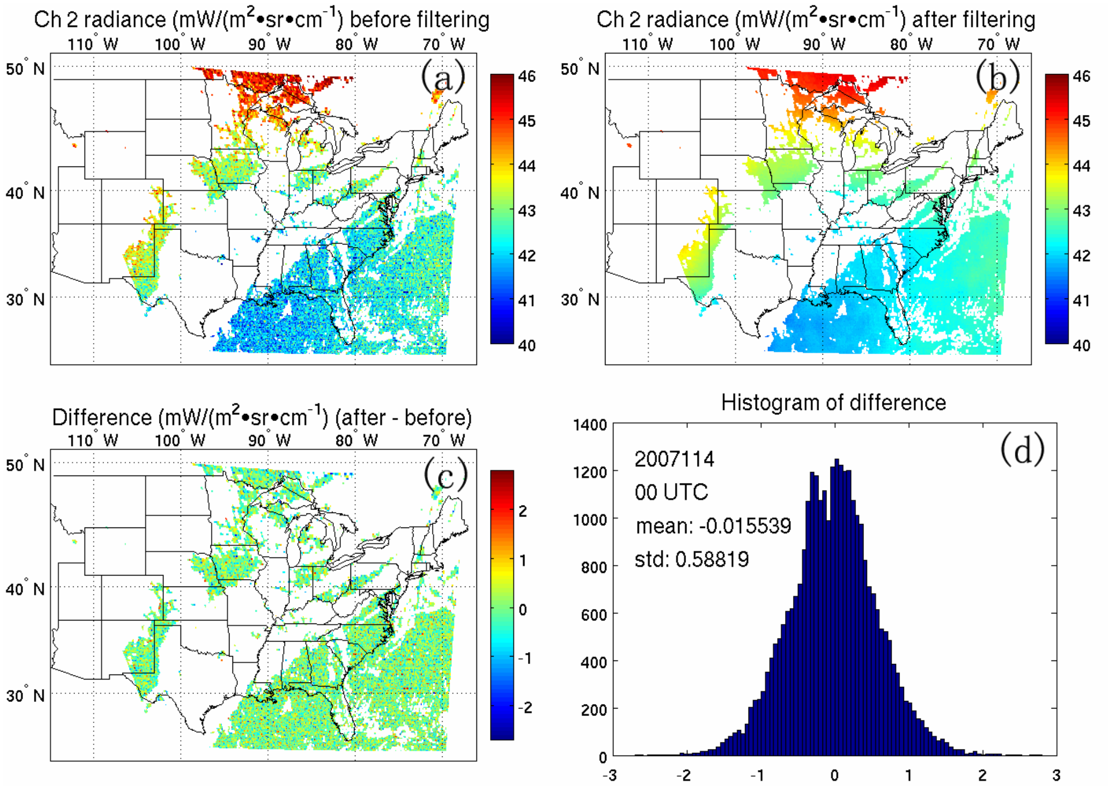

Figure 12. Same as Figure 11 except for channel 2.

Further down in the lower troposphere, the temperature is not smooth; neither is the water vapor. Large gradients are more frequently observed. For channels sensitive to this layer of atmosphere, the averaging box needs to be reduced. However, using the simple averaging method, one may find some problem in areas of large gradients: the cold side is warmed up and the warm side is cooled down. As a result, the gradient is reduced. In order to preserve the gradients, extra weights are added into the averaging

$$w_k(i,j) = \exp(-a\frac{\delta R^2}{\varepsilon_k^2} - b\frac{\delta r^2}{r^2}) \qquad (13)$$

where $w_k(i,j)$ is the weight for the FOV at location (i,j), k is channel index, δR is the radiance difference between the center of the box and location (i,j) in $mw/(sr \cdot m^2 \cdot cm^{-1})$, ε_k is the channel noise, δr is the physical distance, r is the radius of the box, and a and b are two empirically determined constants. Here two constraints are imposed. First, due to the spatial continuity of the lower troposphere, the closer FOVs (smaller δr) have more weights than others. Second, FOVs with similar radiances are given more weights than others to preserve the gradients. All the channels except 1, 2 and 15 are filtered using weights from equations (13).

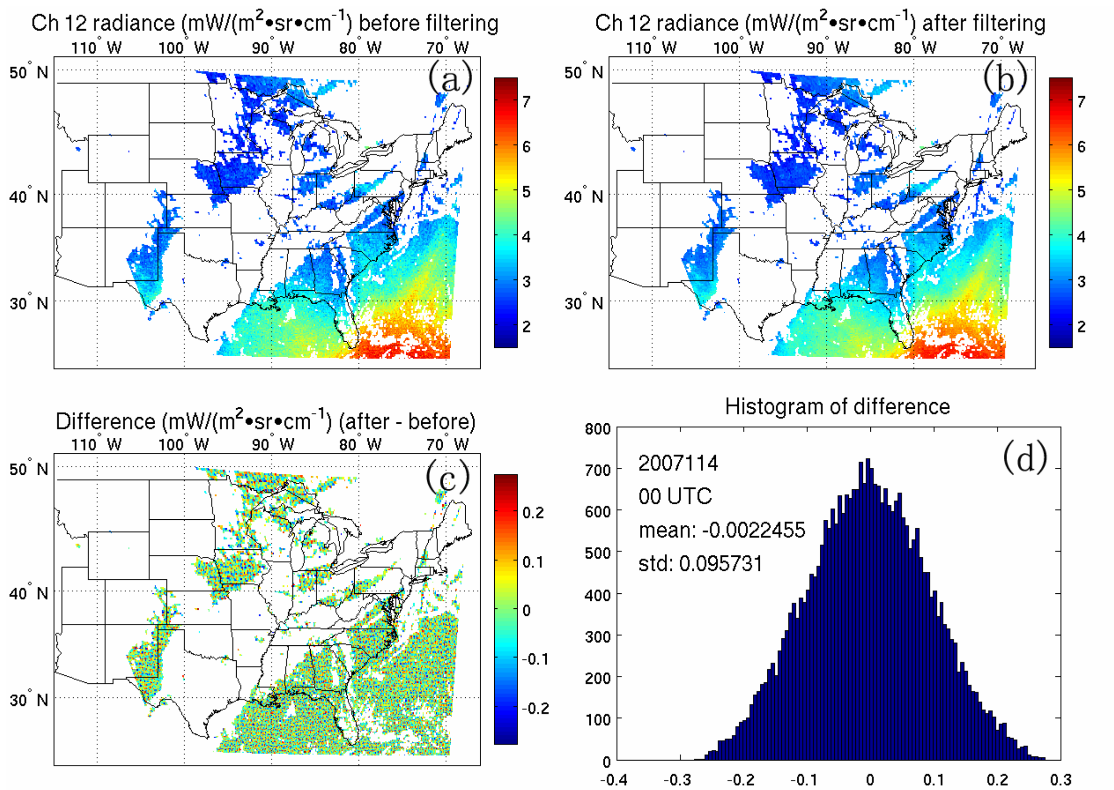

Figure 13. Same as Figure 11 except for channel 12.

The method described above is so-called inverted cone method (Plokhenko and Menzel 2001). One example is shown in Figures 11 - 13 for channel 1, 2 and 12.

From channel 1 and 2, it is clear that the simple averaging using a large box is enough. As mentioned previously, one of the disadvantages of the simple averaging method is its inability to preserve gradients. However, since the spatial gradients in channel 1 and 2 are so small, there is no obvious gradients loss; note the noises are geographically randomly distributed in the difference image. Channel 12 obviously has much more gradients than channel 1 and 2. The randomly distributed noises in Figure 13 (c) again indicate no obvious loss of gradients.

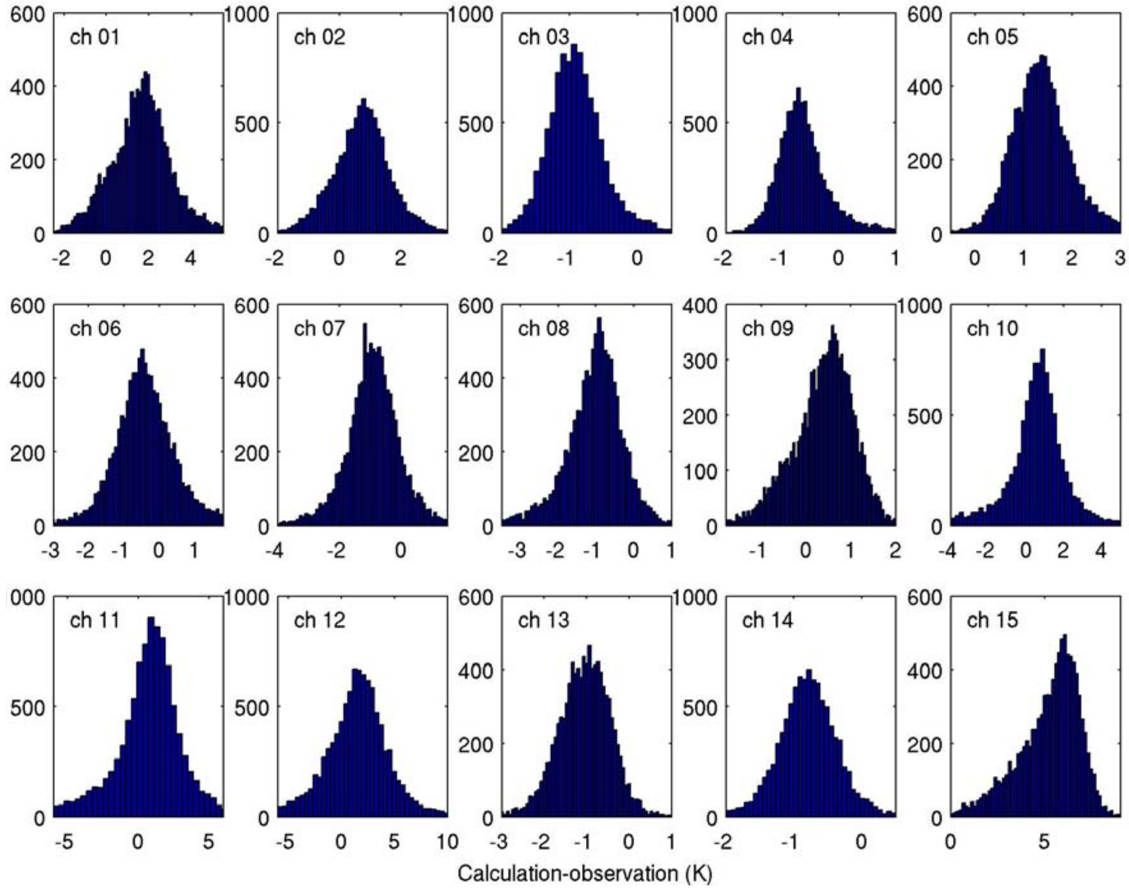

Figure 14. The histograms of the differences between calculated and observed Tb (former minus the later) for the GOES-12 Sounder's first 15 channels from June 2003 to September 2004. The RAOB/GOES/GFS-2003 match-up database is used for calculation. The RAOB observed profiles are used to calculate Tb.

Table 2. The mean and STD of the differences between the bias-adjusted and true (calculated) Tb using the old and the new scheme.

Channel	old		new	
	mean	STD	mean	STD
1	0.17	1.36	0	1.04
2	0.13	0.93	0	0.75
3	0.06	0.60	0	0.43
4	0.37	0.63	0	0.35
5	0.10	0.66	0	0.51
6	0.21	0.98	0	0.69
7	0.54	0.99	0	0.59
8	0.65	0.96	0	0.51
9	-0.38	0.78	0	0.40
10	0	1.62	0	1.58
11	0.51	2.86	0	2.78
12	1.83	3.80	0	3.18
13	0.31	0.52	0	0.29
14	0.44	0.72	0	0.33
15	0.28	1.39	0	0.42

Bias Adjustment

The inverted cone method is useful for random noise reduction, but it cannot remove systematical noise or the radiance bias. For GOES Sounder observations, there are two sources of biases. One, as mentioned before, comes from the satellite measurements, including the spectroscopy, instrument drifting, and the pre-processing including calibration and bit truncation. These biases usually are fixed or changes slowly as the instruments getting older. The other error source is the radiative transfer model used. These biases are typically related to the air masses (the radiative transfer calculation deficiency in some weather condition) and spectroscopy database used. While the ideal way to remove radiance bias is to find and remove the absolute bias associated with the satellite measurements and the radiative transfer model individually, it is not necessary and realistic to do so in the retrieval algorithm. The importance is to ensure that the measurements do not appear biased as compared to simulated radiances.

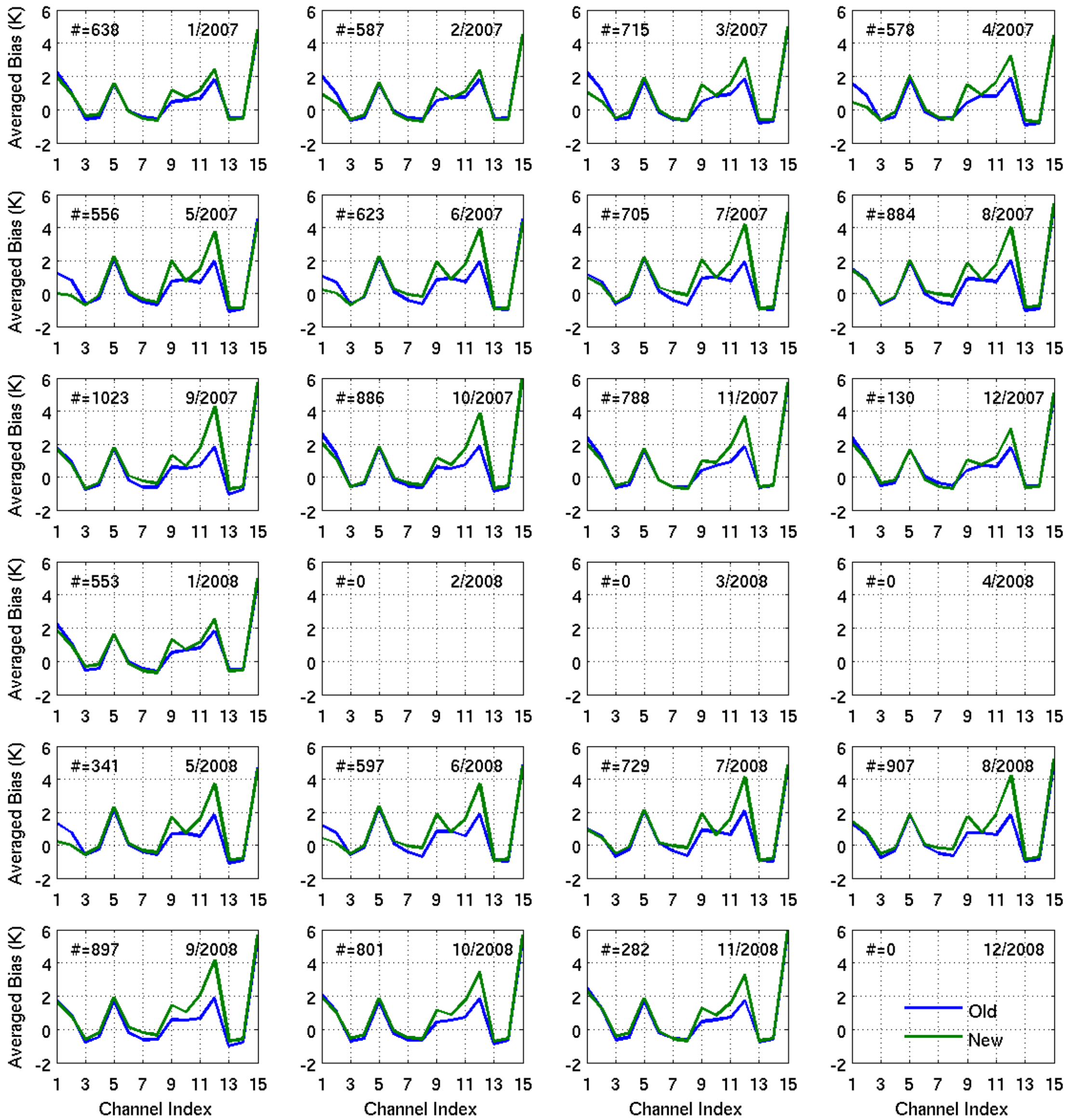

Figure 15. The monthly averaged radiance biases from Jan 2007 to Nov 2008. The blue lines (old) represents the radiance biases derived using the old bias regression coefficients (2006). The green lines (new) represent the actual radiance biases (the calculation minus the observation).

Figure 14 shows the histogram of the differences between the observed and the calculated Tb using the RAOB observations (the latter minus the former) using the RAOB/GOES/GFS-2003 match-up database. All of the channels have biases——the distribution does not center around zero. Some of the channels even have biases larger than 1 K, such as channel 1, 5, 12 and 15. In Ma et al. (1999), a regression method called “shrinkage estimation” (Schmit 1996) is used to remove radiance bias for GOES-8 Sounder. In this method, besides the radiance measurements, the latitude and longitude are used as predictors to remove geography-related bias; the solar and local zenith angles are used to remove bias related with satellite’s viewing angle; and the surface skin temperature is used to remove air masses-related bias. In this study, an improved version for bias correction is used. In the improved scheme, the satellite measurements are still the primary predictors. Besides, in order to account for the correlation between channels, the quadratic terms are included as predictors. The hourly surface air temperature and air moisture observations are used as predictors to account for different air masses instead of the surface skin temperature.

The regression training uses 90 % of the RAOB/GOES/GFS-2003 match-ups in the database; the remaining 10 % is used for validation. Table 2 shows the mean and STD of the differences between the bias-adjusted radiances and the true as calculated from the RAOB. A good bias adjustment scheme should minimize the differences so that the distribution of the differences should be Gaussian with a mean of zero and a small STD. In Table 2, some channels still have biases using the old bias adjustment method. As a comparison, the new bias adjustments show much better results; the mean of the differences is zero, and the STD is smaller.

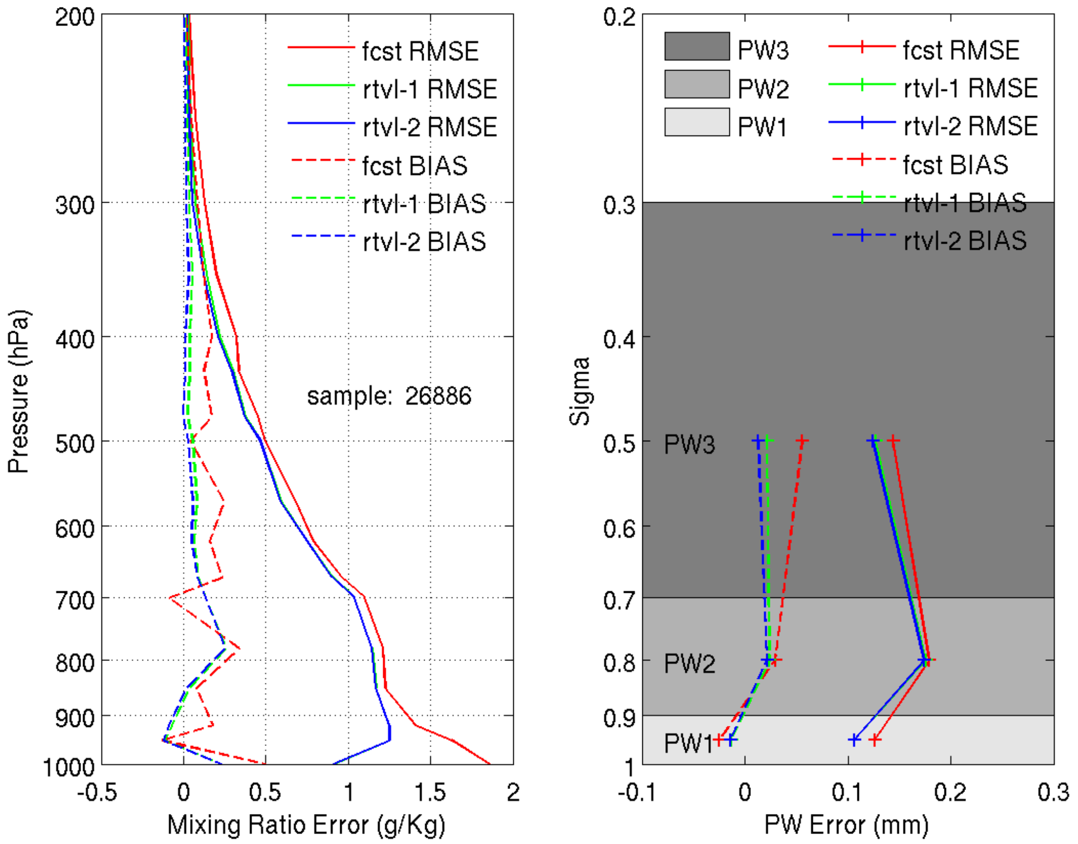

Figure 16. The impacts of different bias regression coefficients on moisture retrieval of a) the mixing ratio profiles, and b) the three layer PW using the RAOB/GOES/GFS-2007 match-up database. The solid lines are the RMS, and the dashed lines are the bias. RTVL-1 represents physical retrievals using radiance bias-adjusted from old (2006) regression coefficients, and RTVL-2 represents physical retrievals using radiance bias-adjusted from new (2007-2008) regression coefficients.

In the operational use, the bias regression coefficients are updated frequently because the instrument's performance drifts. Figure 15 shows the monthly averaged radiance biases from January 2007 to November 2008. The blue lines (old) represent the differences of the bias adjusted radiances and the observed radiances (the former minus the latter). The bias is adjusted using the old bias adjustment coefficients, which is derived from the RAOB/GOES/GFS-ARM match-up database (see Chapter

2 for more information about this database). The green lines represent the differences of the calculated radiances and the observed radiances (the former minus the latter). These are the actual radiance biases needed to be removed. If the old bias adjustment coefficients work for the time period from January 2007 to November 2008, then the blue lines and the green lines should overlap.

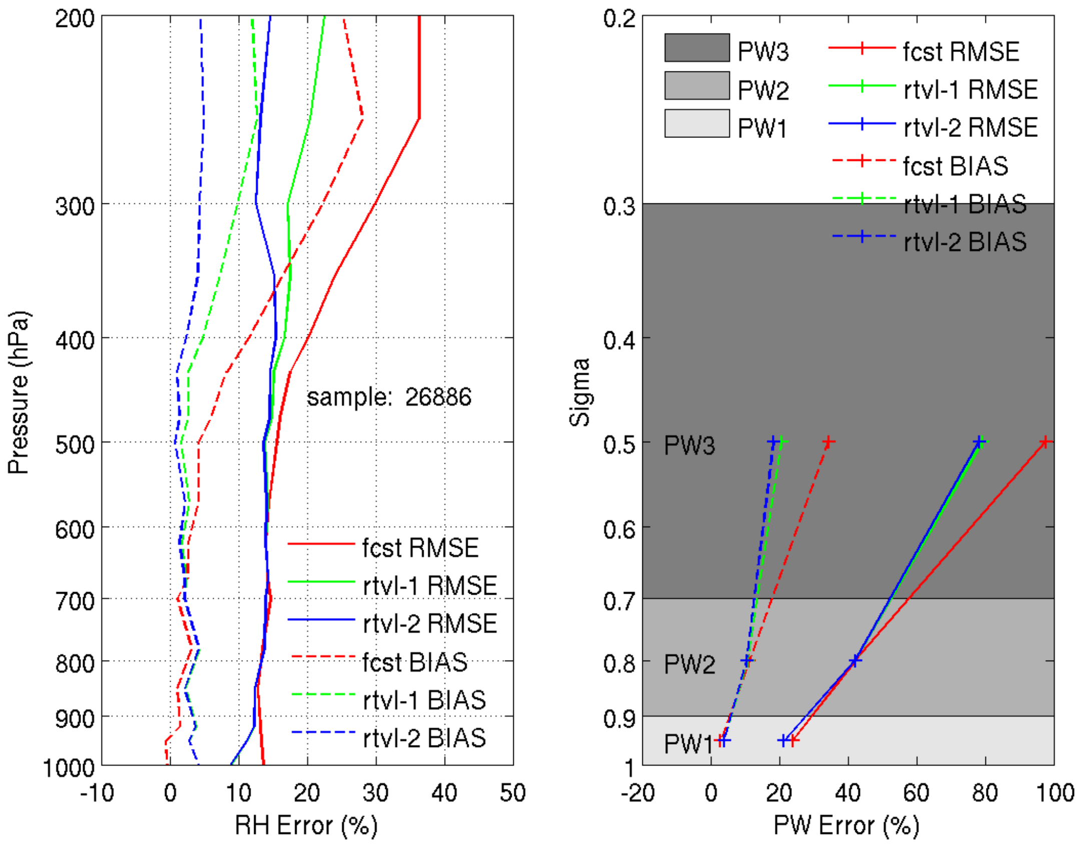

Figure 17. Same as Figure 16 except a) the relative humidity profiles, and b) the three layer PWs error percentage.

As shown in Figure 15, the green and the blue lines agree mostly except for channels 1, 2, 9 (not used in the algorithm), 11 and 12. Channels 1 and 2 are temperature channels, so the old bias adjustment coefficients will have negative impacts on temperature retrievals in stratosphere and tropopause (not shown). Channels 11 and 12 are moisture channels sensitive to upper troposphere, so the old bias adjustment coefficients will have negative impacts on the moisture retrievals in the upper troposphere. Channels 7 and 8 see some differences in Figure 15 during summer time (June to September). But both channels are not very sensitive to moisture, so the impacts on moisture retrieval should not be significant.

Figures 16 and 17 show how different radiance bias adjustment regression coefficients affect the moisture retrievals. Both the mixing ratio (Figure 16 (a)) and the relative humidity (Figure 16 (a)) show the new bias adjustment coefficients have positive impacts on moisture retrieval, especially in the upper troposphere, where more radiance biases are found in channels 11 and 12 in Figure 15. Using the new radiance bias adjustment coefficients, the bias of mixing ratio and relative humidity (RH) is improved for levels with pressure smaller than 600 hPa, and the RMS is improved for levels with pressure smaller than 400 hPa, which is more significant in Figure 17 (a). As a result, PW3 is slightly improved by using the new radiance bias adjustment coefficients; both RMS and bias are reduced in Figure 16 (b) and Figure 17 (b).

3.2.4 Radiative Transfer Model (RTM)

Same as the operational use at NOAA's National Environmental Satellite, Data, and Information Service (NESDIS), this study uses the Pressure-Layer Fast Algorithm for Atmospheric Transmittance (PFAAST) models (Hannon et al., 1996) to calculate the GOES-12 Sounder radiances. PFAAST is based on the line by line radiative transfer model (LBLRTM) version 8.4 (Clough and Iacono, 1995) and the high-resolution transmission molecular absorption database-2000 (HITRAN-2000) (Rothman et al., 1992) with updates (aer_hitran_2000_updat_01.1). The new 101-level PFAAST calculates the radiances with better accuracy and less model bias than the old 42-level one used by Ma et al. (1999) for operational GOES Sounder product.

Since the PFAAST does not calculate weighting functions (Jacobian or K-matrix), an analytical approximation method is used to calculate the weighting functions in this study (Zeng, 1974; Li, 1994). This method is superior to the one used on TOVS in that the non-fixed surface emissivity and solar reflectivity are included in the calculation.

3.2.5 Other Important Algorithm Considerations

Eigenvector

The physical iterations involve a lot of matrix operations. The PFAAST used in the algorithm is based on 101-level profiles. For each FOV, there are $101 \times 3 + 1 = 304$ parameters to be retrieved (temperature/moisture/ozone profile and the surface skin temperature). If the hourly surface observations are regarded as two extra "channels" (Li et al., 2000), there are totally 20 channels (some of the channels are turned off due to solar contamination). The dimension of background covariance matrix is 304 by 304, and 20 by 304 for weighting functions. The calculation associated with these matrices is highly time-consuming. For computational efficiency, eigenvectors are used. Any profile perturbation $\delta x = x_i - x_0$ during ith iteration could be expanded using a set of eigenvectors (Smith and Woolf, 1976)

$$\delta x = \sum_{j=1}^{m} f_j \mathbf{v_j} = \mathbf{Vf} \quad (14)$$

where $\mathbf{V} = [\mathbf{v_1} \quad \mathbf{v_2} \quad \dots \quad \mathbf{v_m}]$ is the matrix of eigenvectors and $\mathbf{f} = [f_1 \quad f_2 \quad \dots \quad f_m]$ is the expansion coefficient vector, and m is the number of eigenvectors. Using equation (14), it can be shown that equation (9) could be rewritten as

$$\mathbf{f_{i+1}} = (\gamma \widetilde{S}_0^{-1} + \widetilde{K}' E^{-1} \widetilde{K} + \gamma_i I)^{-1} [\widetilde{K}' E^{-1} (\delta Tb + \widetilde{K} \mathbf{f_i}) + \gamma_i \mathbf{f_i}] \quad (15)$$

where $\widetilde{S}_0^{-1} = \mathbf{V}' S_0^{-1} \mathbf{V}$ is the inverse of the background error covariance matrix in eigenvector domain, $\widetilde{K} = K\mathbf{V}$ is the matrix of weighting functions in eigenvector domain. Therefore, the retrieval problem is simplified to find a set of expansion coefficients, which could be converted to retrieval parameters through equation (14).

Due to the correlation of temperature and moisture between adjacent levels, it is not necessary to use all the eigenvectors to reproduce δx. In this study, it is empirically found that 10 eigenvectors (5 for temperature, 3 for moisture, 1 for ozone and 1 for skin temperature) are optimal for the physical iterations. This reduces the dimension of the background covariance matrix to 10 by 10, and the dimension of the weighting functions to 20 by 10. The smaller size of background covariance matrix and weighting functions greatly speed up the computation.

Convergence Check

In each iteration, two variables are calculated in order to determine whether the iteration continues or stops. One is the brightness temperature residual

$$r = \sqrt{\frac{1}{n}\sum_{i=1}^{n}(R_o^i - R_c^i)^2} \qquad (16)$$

where r is the averaged brightness temperature residual, n is the number of channels used, and R_o^i and R_c^i are the observed and calculated brightness temperature for channel i. The other one is the norm of the eigenvector expansion coefficients

$$\boldsymbol{\delta}\mathbf{f} = \mathbf{f}_{\mathbf{i+1}} - \mathbf{f}_{\mathbf{i}} \quad (17)$$

The iteration stops is any of the following condition is met

a) r is smaller than a given threshold (0.2 K in the algorithm), which indicates there is no room for the algorithm to improve. The retrieval is considered an excellent one.

b) r is larger than another given threshold (10 K in the algorithm), which indicates the retrieval is way off the true. The retrieval is considered a failed one.

c) $\boldsymbol{\delta}\mathbf{f}$ is smaller than a given threshold (0.05 in the algorithm), which indicates the iteration is converged.

Otherwise, the iteration continues until the maximum allowed iteration number is reached.

Table 3. Definition of the PI based on the value of the residual.

PI	0	1	2	3	4	5	6	7	8	9	10
Residual (K)	2	1.5	1.25	1.1	.95	.8	.65	.5	.35	.2	0

Precision Index

After exiting from iterations, a precision index (PI) is assigned to each retrieval. For a failed retrieval, PI is set to 0. For an excellent retrieval, PI is set to 10. For others, PI values are assigned based on the brightness temperature residuals according to Table 3. For example, if the residual is 0.57 K, because it is larger than 0.5 and smaller than 0.65, then PI is 7. If the residual is larger than 2.0, the retrieval is considered as a failure.

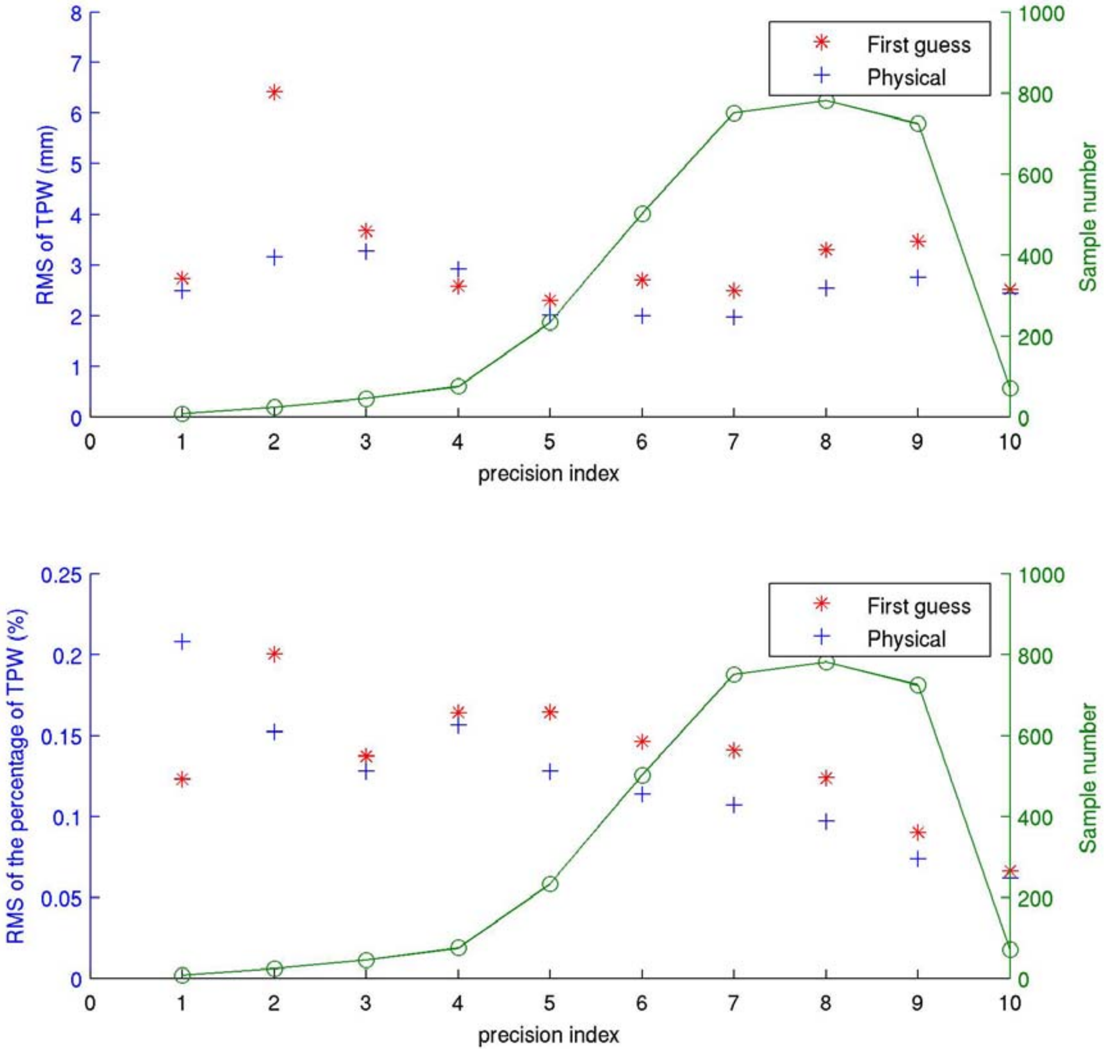

Figure 18. The RMS of (upper) TPW difference, and (bottom) RMS of TPW difference in percentage with respect to different precision index as compared with MWR measured TPW from June 2003 to May 2005 at the SGP CART site. The red stars represent the RMS of the GFS forecast. The blue pluses represent the physical retrievals. The green lines show the sample distribution.

It is expected that larger PI is associated with better retrieval precision. To evaluate this, the physical retrieval algorithm is applied to the

MWR/GOES/GFS-ARM match-up database (see chapter 2 for more details about the database). The retrieved TPW is compared with the MWR measured TPW. Figure 18 shows how the RMS of TPW error and TPW error percentage change with PI. All retrievals with PI >= 5 show significant improvement of TPW over the GFS forecast in both panels. However, when PI <= 4, it is hard to evaluate the retrievals because the two panels show different results (see PI = 1 and 4). More importantly, the sample distribution shows retrievals with PI <= 4 are not common. Therefore, retrievals with PI <= 4 are not considered with good precision in this study.

Quality control

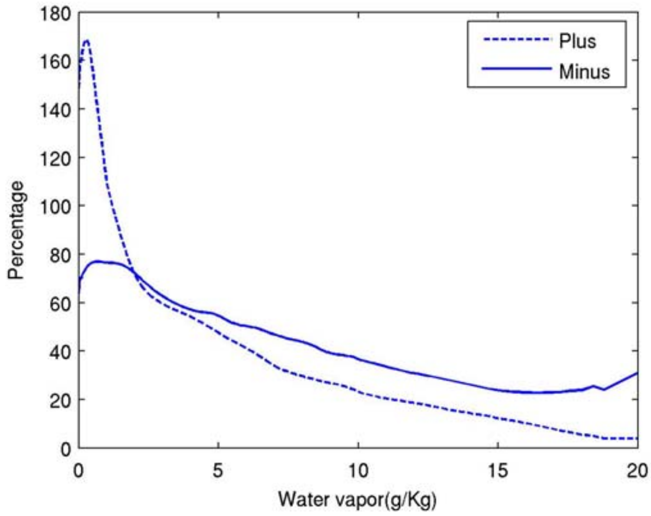

Figure 19. The maximum adjustment allowance for moisture update in iterations for both positive and negative adjustments, calculated from the RAOB/GOES/GFS-2003 match-up database. The dotted line represents the positive adjustment, and the solid line represents the negative adjustment.

Due to the non-linearity of moisture with respect to Tb, the adjustment of moisture in iterations needs more caution. Any over-adjustment of the moisture profiles makes it hard for the iteration to converge. Two constraints of moisture are applied in the algorithm.

a) Saturation check

In iterations, the RH at any level is set to 0.98 if it is larger than 0.98. Similarly, it is set to 0.02 if it is smaller than 0.02.

b) Maximum allowed adjustment

The first guess RH error profile typically has large errors in the upper troposphere and small errors in the lower troposphere. In iterations, more adjustment is needed for upper troposphere moisture, and less adjustment for lower troposphere moisture. For each sample in the RAOB/GOES/GFS-2003 match-up database, the adjustment allowance is the difference between the first guess and the RAOB

$$p = \log(w_{raob}) - \log(w_{fg}) \quad (18)$$

where p is the adjustment allowance, w_{fg} and w_{raob} are the mixing ratio for the first guess and the RAOB respectively. An averaged adjustment allowance is calculated for different mixing ratio in two categories; a positive/negative value indicates a positive/negative adjustment is needed. Figure 19 shows the maximum adjustment allowance (2 times the averaged adjustment allowance) with respect to different mixing ratio values. The dotted line represents positive adjustment allowance, and the solid line represents negative adjustment allowance. For example, if the mixing ratio is 10 g/Kg, the adjustment allowance could not be smaller than -0.37 for a negative adjustment, neither could it be larger than 0.23 for a positive adjustment. Again, from Figure 19, more adjustment is allowed if mixing ratio is small, and vice versa. In actual retrievals, it is found that this constraint is seldom used, which indicates the physical iteration is stable.

3.3 Validation

This section shows validation results of the improved clear-sky physical retrievals, with emphasis on the improvements over the legacy version (Ma et al., 1999) and the GFS forecast. Atmospheric moisture typically has more variability than temperature in both space and time. It is also more complicated than temperature in atmospheric thermodynamic processes due to latent heat. Over the CONUS, the GFS forecast has been found to predict the temperature well, but moisture less well. The validation in this section focuses on the moisture products, particularly the TPW which can accurately be measured from ground-based instruments.

3.3.1 Validation of TPW Retrievals against Microwave Measured TPW

Figure 2 shows the scatter plots between MWR measured and GOES-12 Sounder retrieved TPW using the MWR/GOES/GFS-ARM match-up database (see Chapter 2 for more details about the database). Both the legacy and the improved physical algorithm compare better than the first guess. The RMS is reduced after the physical retrieval. The legacy version (the GFS forecast was used as first guess) reduces RMS by 0.19 mm while bias is increased by 0.21 mm. The physical retrievals using regression as a first guess (PHYREG) reduces the bias by 1.14 mm and RMS by 0.64 mm, and the physical retrievals using GFS forecast as first guess (PHYFCST) reduces the bias by 0.21 mm and RMS by 0.55 mm. Although the two first guesses have about the same precision of 2.8 mm in RMS, the RMS of the improved physical retrievals (both PHYREG and PHYFCST) is about 0.4 mm smaller than the legacy retrievals. This indicates the improved physical algorithm performs better than the legacy version. Also, the improved physical retrieval shows a smaller bias (0.36 mm for PHYREG and -0.25 mm for PHYFCST) than the legacy retrievals (-0.67 mm), which again demonstrates the superiority of the improved physical algorithm.

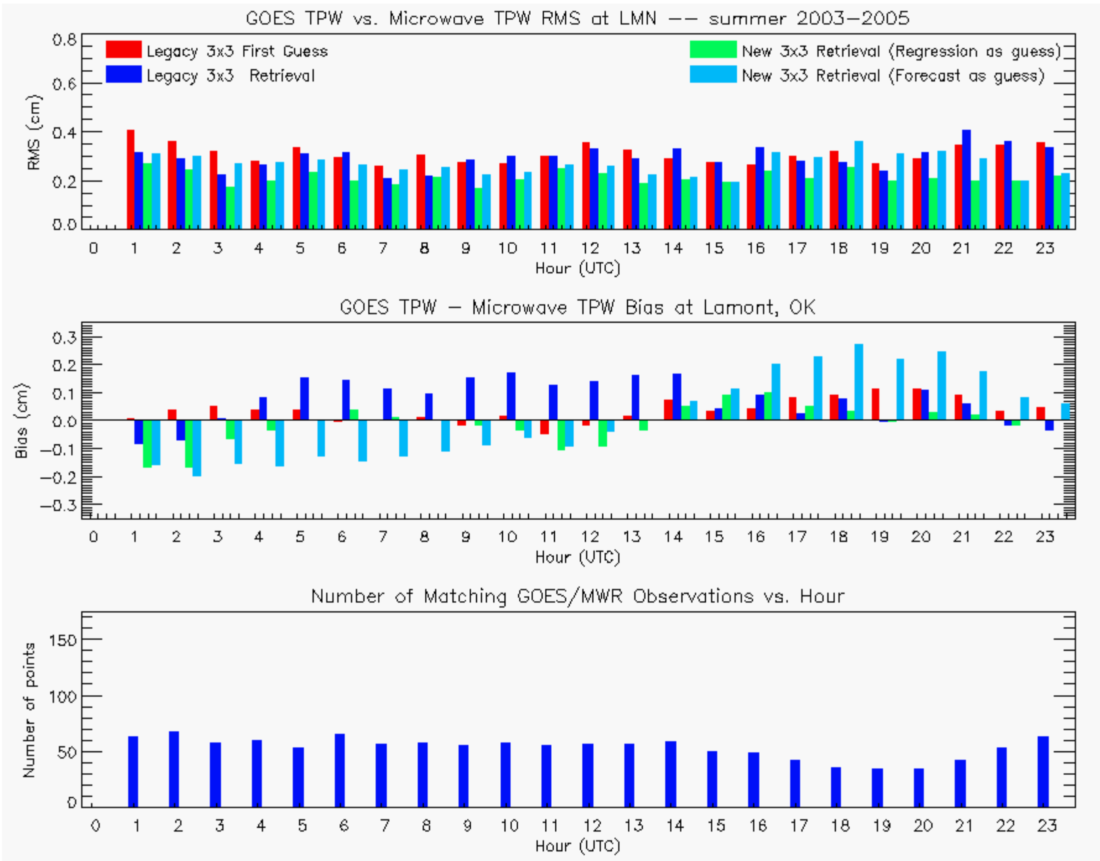

Figure 20. Comparison of TPW retrievals to microwave measured TPW at different UTC during summer time from June 2003 to May 2005 at the SGP CART site for (upper) RMS, (middle) bias, and (bottom) sample distribution. The red bar represents the first guess from the GFS forecast; the blue bar represents the legacy physical retrievals; the green bar represents PHYREG; and the light blue bar represents PHYFCST.

The regression retrieval has a much larger bias (1.50 mm) and slightly larger RMS (2.85 mm) than the forecast (-0.46 mm of bias and 2.80 mm of RMS) in Figure 2 (a). This is likely because of the failure to detect thin, low or broken clouds prior to the retrieval. The regression coefficients are derived under clear-sky conditions and are not suitable for cloudy situations. When the clouds are thick, the regression cannot provide a reasonable profile and the retrieval is flagged as a failure. However, when the clouds are thin, low or broken, the regression is able to return a reasonable profile albeit containing a bias, which increases the regression guess RMS. The larger bias and RMS do not affect the physical retrieval very much: PHYREG (2.21 mm) shows slightly better results than PHYFCST (2.25 mm) in terms of RMS.

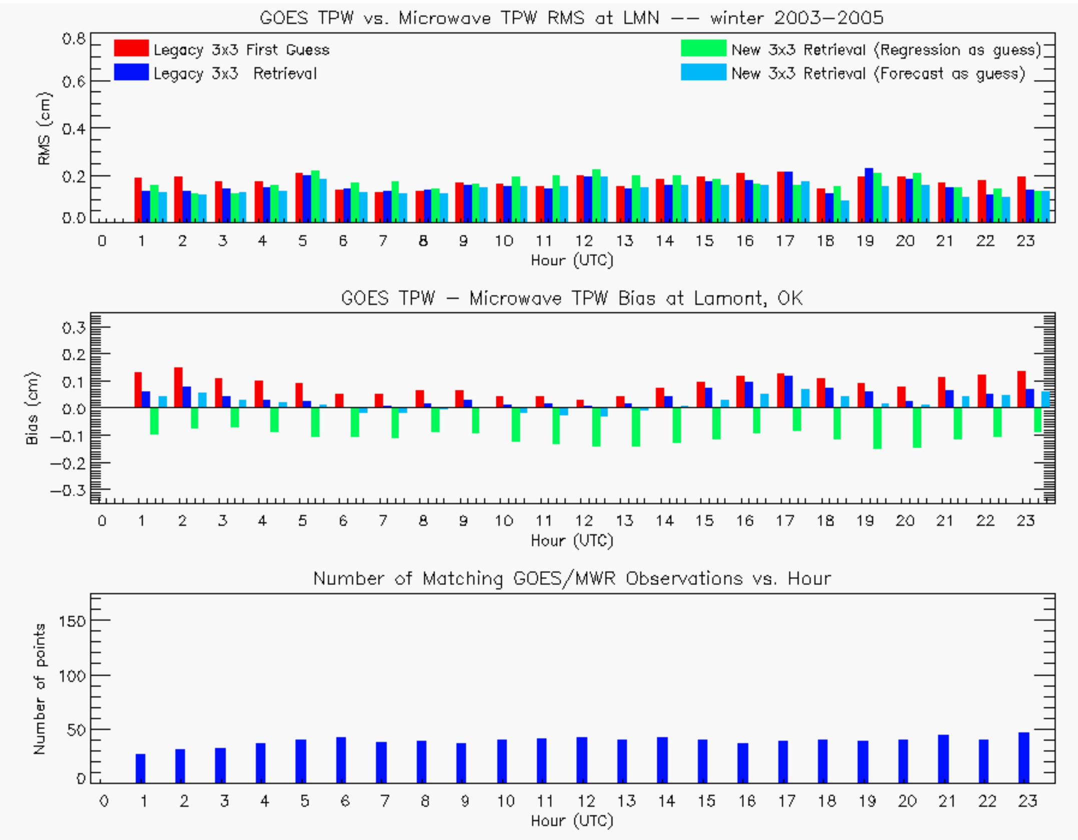

Figure 21. Same as Figure 20 except for winter time.

Figures 20 and 21 show the comparisons of TPW at different UTC times for summer and winter, respectively. For all UTC time in summer, the PHYREG retrievals show the smallest RMS of all. Most of time, PHYFCST show smaller RMS than the legacy retrievals. For bias, the PHYREG retrievals show much smaller bias than the legacy retrievals and the PHYFCST retrievals except for 1 and 2 UTC. For winter time, the PHYFCST retrievals show much better results than others; both the RMS and the bias are the smallest among them. Notice there are large negative biases in the PHYREG. The results in Figures 20 and 21 probably indicate that PHYREG is suitable for wet cases, while PHYFCST is suitable for dry cases.

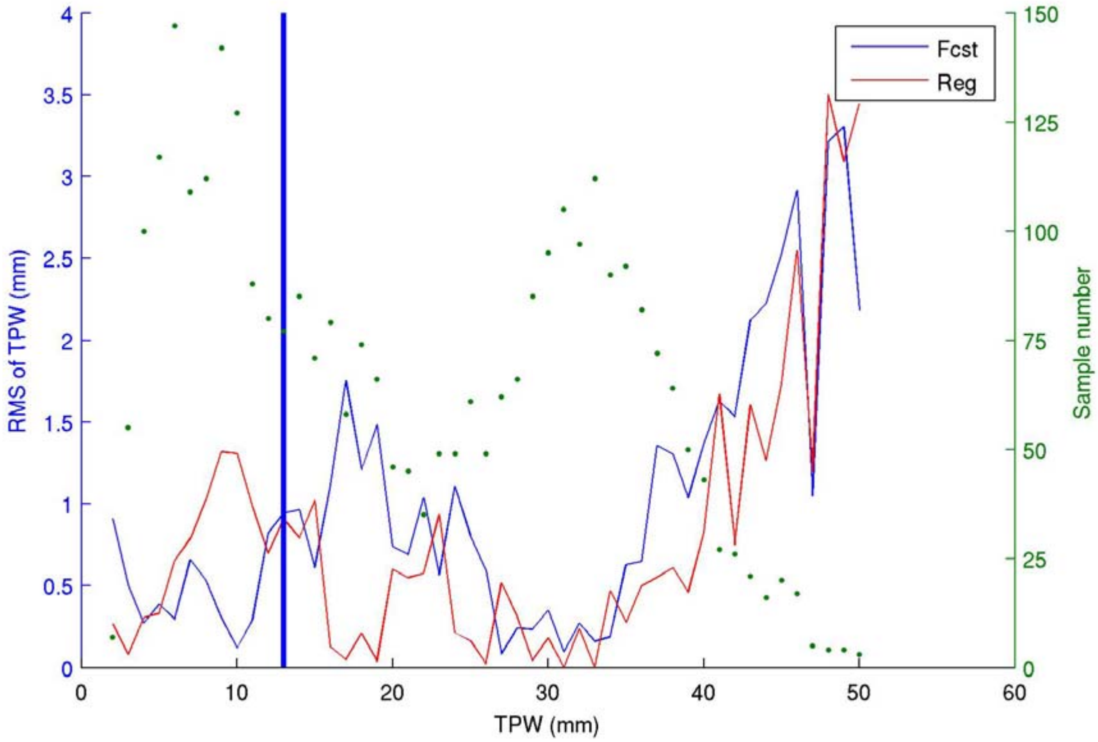

Figure 22. The RMS of the retrieved TPW with respect to different TPW values from June 2003 to May 2005 at the SGP CART site. The blue line show results from PHYFCST. The red line show results from PHYREG. The green dots show the sample distribution. TPW = 13 mm is the threshold to switch around.

To verify, the RMS is calculated with respect to different TPW values, and the results are shown in Figure 22. Clearly, the PHYREG performs better when TPW is large, while the PHYFCST performs better when TPW is small. The threshold is 13 mm (the blue spike) according to the statistics. Therefore, in the algorithm, the PHYREG is used for wet cases or the regression retrieved TPW is greater than 13 mm, and the PHYFCST is used for dry cases or the regression retrieved TPW is smaller than 13 mm.

3.3.2 GOES Moisture Retrieval Improvement with GPS TPW Measurements

To evaluate how the GPS retrieved TPW could help improve the moisture retrieval, a match-up database, containing GOES-12 Sounder radiances, the GFS forecast, the conventional RAOB and the GPS retrieved TPW, is constructed. The time period is from 00 UTC of 25 December 2005 to 00 UTC of 26 December 2005. Since the conventional RAOB is launched every 12 hours, there are only three times of RAOB observations. The GPS retrieves TPW every 30 minutes. The GPS and the RAOB are collocated within 30 minutes in time and 0.2 degree in space. After the collocation, there are 34 clear-sky samples. The retrievals of TPW with and without the help from GPS are compared with the RAOB, and the RMS are shown in Table 4.

The improvements by GPS are obvious. The RMS of regression retrievals is reduced from 1.67 to 1.29 mm. As a result, the physical retrieval using the regression retrievals as first guess is improved with RMS reduced from 1.45 to 1.21 mm. It is surprising to see the GPS could help the physical retrievals with GFS forecast as a first guess. This is because the first guess of the surface skin temperature is improved with the GPS TPW as an extra predictor in the regression algorithm. Table 4 also shows that, although the first guess of GFS forecast is not as good as the regression retrievals, PHYFCST shows smaller RMS than PHYFCST. This is because these are all dry cases. As discussed before, for dry cases, PHYFCST is better than PHYREG.

Table 4. The RMS of retrieved TPW (mm) compared with RAOB. "REG" represents the regression retrievals; "PHYREG" represents the physical retrievals using regression as a first guess; "FCST" represents the GFS forecast; and "PHYFCST" represents physical retrievals using GFS forecast as a first guess.

	REG	PHYREG	FCST	PHYFCST
Without GPS	1.67	1.45	2.13	1.20
With GPS	1.29	1.21	2.13	1.17

3.4 Applications to Short Term Severe Storms

For short-term severe storm nowcasting, the GOES Sounder derived product imagery (DPI) with hourly temporal resolution and nominal 10 km spatial resolution are useful (Menzel et al., 1998). Two supercell cases are presented to demonstrate how the GOES Sounder products available via the improved physical algorithm might assist the forecasters on short-term severe storm nowcasting. In the first tornadic storm, the LI is used to depict the potential convective environment surrounding a supercell before and during its development. In the second hailstorm case, different air masses around a supercell are identified, especially the one supplying low-level moisture into the supercell.

3.4.1 The Tornadic Storm at Eagle Pass, Texas on 24 April 2007

The lifted index (LI), a measurement of atmospheric instability, is the difference between the temperature at 500 hPa and the temperature an air parcel will have by lifting from the surface to 500 hPa. A positive value indicates a stable atmosphere, in which convection is unlikely. A LI of between 0 and -3 (degree Celsius) indicates that the air is **marginally unstable** and unlikely to lead to severe thunderstorms. Values between -3 and -6 indicate moderately **unstable** conditions. Values between -6 and –9 are found in **very unstable** regions. LI values less than -9 reflect **extreme instability**. The chances of a severe thunderstorm are best when LI is less than or equal to -6.

At approximately 00 UTC on 25 April 2007, a tornado that had originated in far northeast Mexico passed through the Eagle Pass area of Texas (the green X in Figure 23 (m), (n) and (o)). This EF-3 tornado killed 10 people in Mexico and the United States with another 120 injured. While forecasting such a fatal tornado remains challenging to forecasters and regional modelers, the GOES-12 Sounder DPI of LI could provide useful information to forecasters during such an event.

Figure 23 shows the time series of the derived LI imagery. Successfully retrieved areas are filled with LI values, with different colors representing different levels of severity. Unsuccessful areas are filled with 11 μm Tb; colder Tb are reflected in brighter grey shades. From the top to bottom is 20, 21, 22 and 23 UTC on April 24. The actual local scanning time is about 10 minutes after the label time. From the left to the right is GFS forecast, legacy physical retrieval and PHYREG.

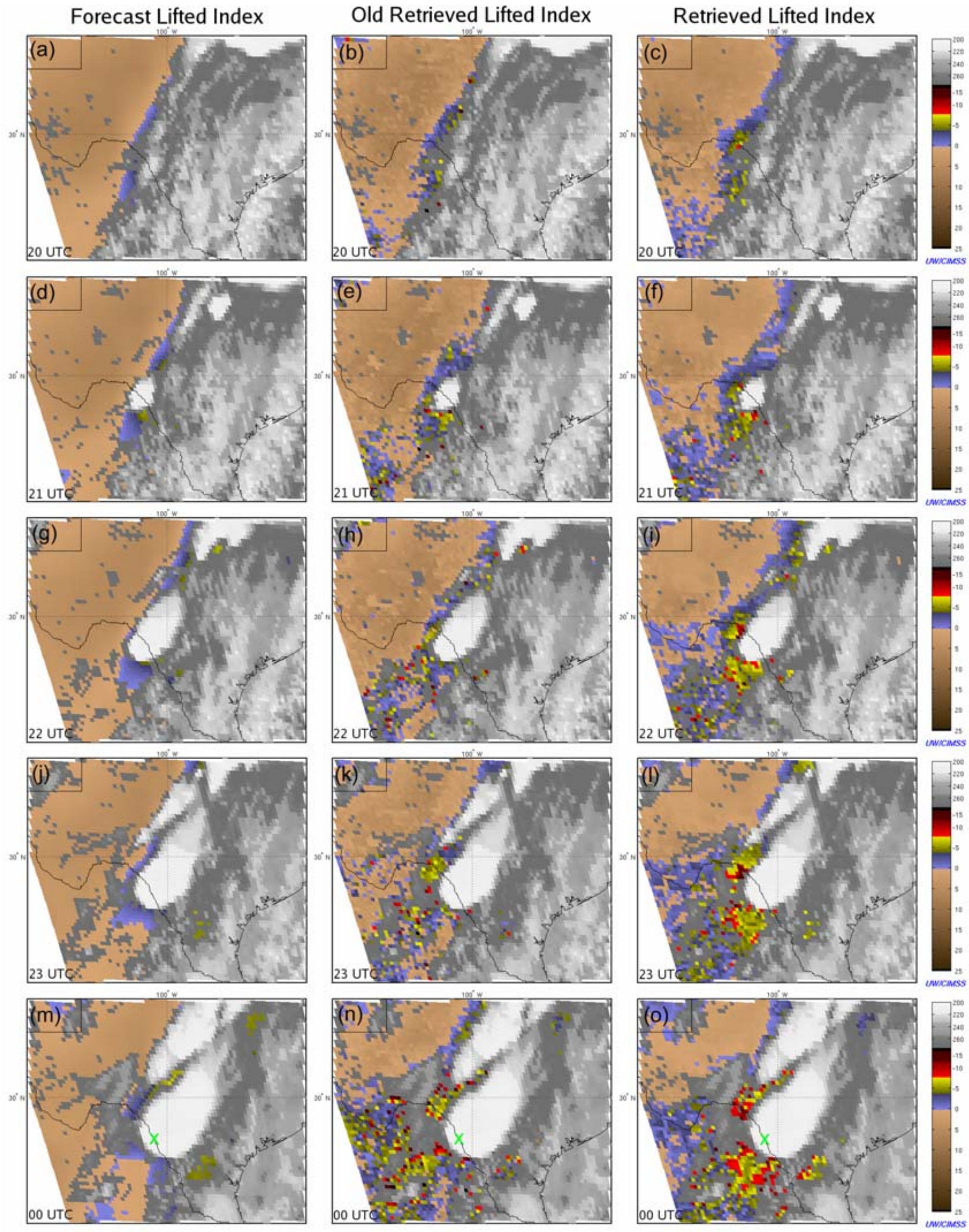

Figure 23. Time series of LI imagery on 24 April 2007. From top to bottom is 20, 21, 22, 23 and 00 UTC. From the left to the right is GFS forecast, the legacy retrieval and PHYREG. A tornado touched down near Eagle Pass, Texas (the green X along the Texas/Mexico border within the supercell in the bottom three panels) around 00 UTC.

One of the difficulties in forecasting such a supercell is the short lifetime of the whole system (typically just a few hours). It is very difficult for forecasters to predict where and when a supercell is going to form. In this case, it will be demonstrated that the LI values in the vicinity of weather systems are well correlated with the outbreak and the development of the systems. At around 19 UTC, neither the 11 μm imagery (no cold clouds) nor the LI DPI imagery (not shown here) indicate that a severe convective storm will be developing soon. However, one hour later, the LI DPI imagery (and hence the PHYREG retrievals) change dramatically from “marginally unstable” to “moderately unstable” and “very unstable” (the red region among the yellow area in Figure 23 (c). This indicates a more favorable pre-convective environment. The same degree of convective potential (in terms of coverage) is not seen on either the GFS forecast or legacy retrieval DPI imagery at 20 UTC (Figure 23 (a) and 23 (b)). The GOES Imager animation (http://www-angler.larc.nasa.gov/armsgp/g8usa.html/) shows the outbreak of the supercell occurring immediately prior to 20:15 UTC. Note that the cloud top Tb was less than 220 K in 11 μm at 21 UTC.

During the next several hours, the supercell grew rapidly, and the center of the cell moved southeast along the border. Compared with the GFS forecast, the legacy retrievals reveal increasing areas of instabilities surrounding the supercell; the improved retrievals are even more extended and pronounced. Figure 23 (o) shows three areas of large negative LI values. To the south of the supercell, the instabilities ensured the continuous growth of the supercell. To the northwest of the supercell, the instabilities initialized (between 22 and 23 UTC) and maintained another convective storm to the north of the supercell. To the west of the supercell, the instabilities initialized (between 01 and 02 UTC, not shown) and maintained the third convective storm. Not shown here are the instabilities that returned to normal values during the post-stage of the convective storms.

3.4.2 Wisconsin Hailstorm on 14 April, 2006

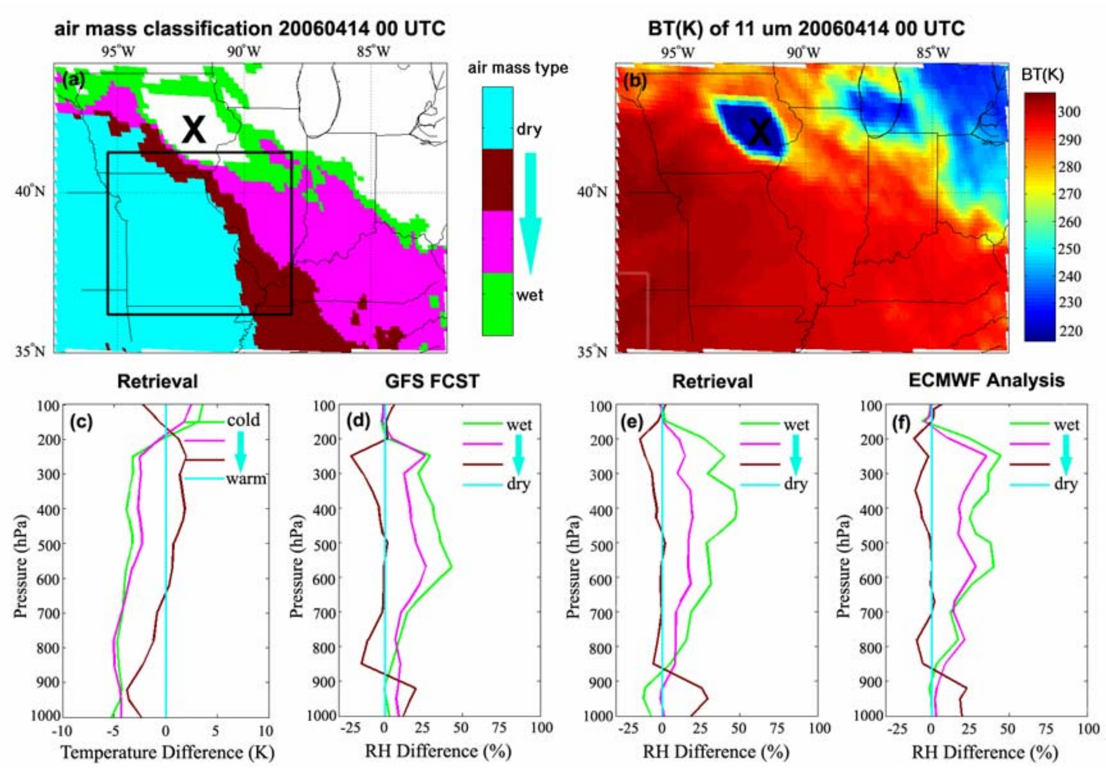

Figure 24. The GOES-12 Sounder classification of air masses and their associated moisture structures at 00 UTC 14 April 2006. a) the classification of air mass; b) 11 µm brightness temperature; c) profiles of temperature difference of different air masses compared with the light blue class; profiles of relative humidity differences compared with the light blue classes from d) the GFS forecast; e) the improved retrievals and f) the ECMWF analysis. Black X denotes the supercell, while the black rectangle encompasses the region used to compute the average of each class.

From approximately 01:40 UTC to 04:00 UTC on 14 April 2006, a severe thunderstorm moved across southern Wisconsin. The estimated loss of property was about 160 million dollars, most of which was caused by 1 to 4 inch diameter hail and downburst winds.

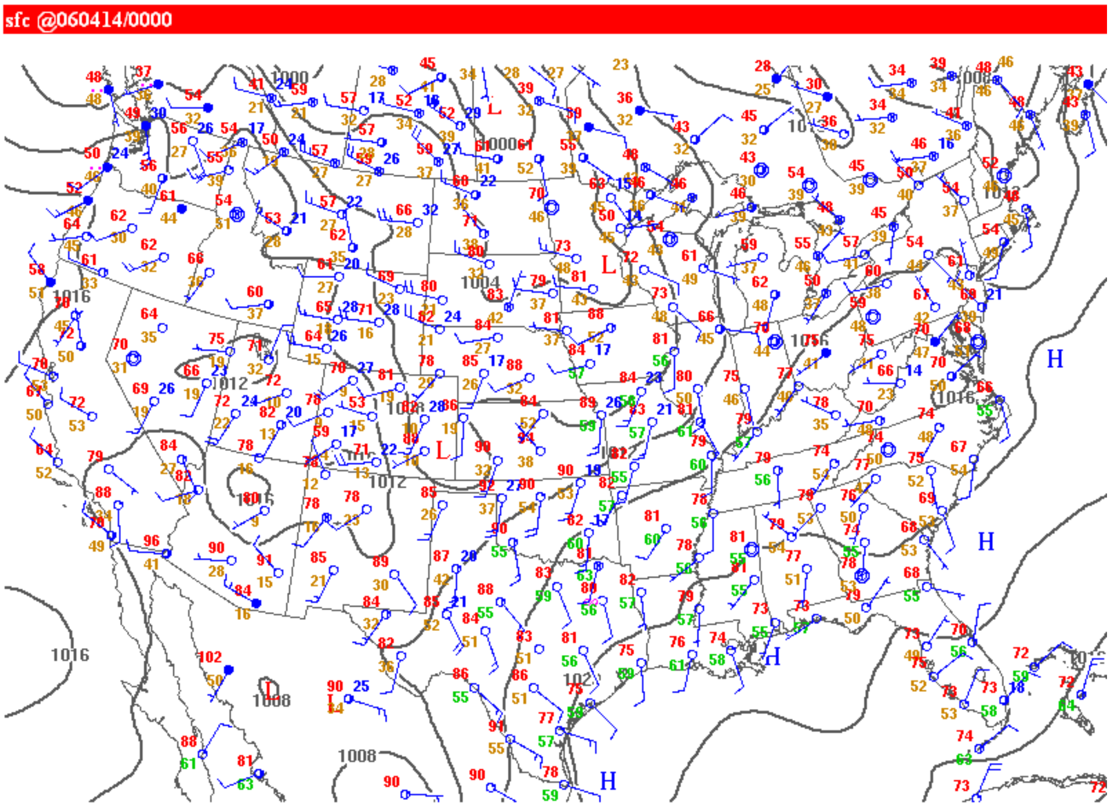

Figure 25. The surface weather map at 00 UTC on April 14 2006 from the National Weather Service Storm Prediction Center. Green numbers show moist areas. Winds over the moist areas are southerly.

The low level moisture is the fuel for severe storms in the Great Plain areas in springtime, and usually comes from the Gulf of Mexico. The southerly winds blow the moisture into supercell in the lower atmosphere. When meeting the supercell, updraft lifts the moisture air to its lifting condensation level (LCL). Then the latent heat boosts the supercell to keep growing.

In this case, the GOES sounding retrievals are used to identify the low-level moisture. We first separate the air mass into 10 different classes (only 4 clear-sky classes are shown in Figure 24 (a)) with a clustering method (Li et al., 2007) using the GOES-12 Sounder IR channels 1-15. Then the improved physical retrieval algorithm is performed on the clear-sky average of each class. The advantage of the average is an improved SNR. To represent the environment around the supercell, only FOVs close enough to the supercell are used. The black rectangle in Figure 24 (a) shows the area under consideration.

Figure 24 shows the results for 00 UTC, 2 hours after the outbreak in Iowa. This time was selected for two reasons: 1) the spatial distribution of the different air masses remained the same except for some eastward propagation; 2) the operational NOAA weather chart and the ECMWF analysis field from 00 UTC help evaluate the results. The supercell is clearly identified as the black X in Figure 24 (a) and 24 (b).

Figure 24 (d) – (f) are the RH difference profiles compared with the light blue class. All show the dry-to-wet gradient from west to east. However, they differ in the lower atmosphere between 900 and 1000 hPa; both the brown class from the retrieval (Figure 24 (e)) and ECMWF analysis (Figure 24 (f), 0.25 degree spatial resolution) are well separated from other classes (about 25 % more RH than others), perhaps indicating it is the main path of moisture transported into the growing supercell, as suggested by the southerly surface winds over this area shown by the surface weather map from the National Weather Service (NWS) Storm Prediction Center (SPC) (Figure 25). This 25 % RH difference along with the absolute values of RH as large as 80 % (not shown) ensures the quick and continuous growth of the supercell, while the

GFS forecast shows only an RH difference of about 10-15%.

The temperature gradients in the vicinity of the supercell are also important. Figure 24 (c) shows the profiles of the retrieved temperature differences compared to the light blue class. The temperatures below 650 hPa show a warm-to-cold gradient from west to east. This gradient, especially between the light blue and the brown, is a key factor for the supercell to grow. The dry and hot air mass between 700 and 900 hPa (see Figure 24 (c)) blows eastwardly (http://www.spc.noaa.gov/obswx/maps/), climbing up to the relative cool and moist air mass, forming a cap. This inversion cap inhibits the instability from being released until reaching the supercell, maintaining the low-level moisture path.

3.5 Time Continuity

There are only 15 IR bands used for GOES sounding retrievals. Radiances alone are not enough for precisely retrieving atmospheric parameter. Besides a reliable algorithm, one has to include other information as much as possible to assist the retrievals. The uniqueness of geostationary sounders compared with polar orbiting ones is high temporal resolution. For sounders on polar orbiting satellites, it usually takes more than 12 hours to observe the same location, depending on the orbit height and the scanning swath width of the satellites. On the contrary, the current GOES Sounders observe the atmosphere and surface every hour. The GOES Sounder’s temporal resolution not only provides hourly individual measurements and retrievals, but also an opportunity to extract more profile information. This could be done through the concept of the time continuity (TC).

3.5.1 The Concept of Time Continuity

The atmosphere is a smoothly changing system within a short period of time (several hours). Unless there is an air mass with different properties moving in/out of a region, both temperature and moisture do not change dramatically. This is especially true for upper troposphere (above 500hPa, excluding Jet and tropopause), where the effect of surface fluxes of heat and moisture is less significant and the gradients of temperature and moisture are small. Therefore, within a short time interval, there are very high temporal correlations between two atmospheric states. The previous observation, especially away from the surface, contains useful information for the next time. This is the concept of TC, and has not been fully exploited in the GOES analysis of atmospheric profiles.

In equation (7a), there are six variables in the right hand side. It is clear that the TC has no impacts on the covariance matrix of the background S_0, the weighting function K, the covariance matrix of measurements E and the calculated $R_c(x_i)$. In this study, the TC will focus to improve the first guess x_0 and measurements R_o. Two different methods will be tested to explore the potential of TC on profile retrievals.

In Method I, the retrievals from previous time are taken as the first guess for the current retrievals. The starting point t_0 is whenever the RAOB/analysis is available. The RAOB/analysis is taken as the retrievals at time t_0 to ensure a perfect starting point. Anytime later at t_i, the physical algorithm takes the retrievals from time t_{i-1}

as the first guess. The TC stops whenever the time difference between the previous and the current retrievals is too large (usually due to data loss) or when the radiance differences are too large (violation of the assumption of smooth atmosphere). When the TC is broken, the traditional non-TC (NTC) method (regression retrievals or the GFS forecast as first guess) is used. At 0, 6, 12 and 18 UTC, the RAOB/analysis is searched for a new starting point.

The Method II focuses on improving the measurements, especially reducing the radiance bias. The traditional way to do bias adjustment is to find linear relationship between the measured and the bias-free radiances (assume the RTM has zero bias). The same linear regression coefficients are used on all FOVs over the CONUS. However, the bias is a complicated variable. It is spatially varying and air-mass dependent (Eyre 1992). It also changes gradually with time as the instruments age. The linear regression is effective in removing time and air-masses dependent bias, but less effective on the spatially varying bias. The TC is useful on bias adjustment because the bias at the same location does not change dramatically during a short period of time when the assumption of the TC stands. For any location, the starting point is still when the RAOB/analysis is available. The bias is calculated using

$$\Delta = Tb_c(0) - Tb_o(0) \qquad (19)$$

where $Tb_c(0)$ is the calculated Tb at starting point, and $Tb_o(0)$ is the observed Tb at the starting point. Anytime later, the bias adjusted Tb is calculated using

$$Tb_c(i) = Tb_o(i) + \Delta \qquad (20)$$

TC stops and resumes in the same manner as Method I.

3.5.2 Results from Method I

To evaluate Method I, the improved physical iterative approach is used with the ECMWF analysis at 0 UTC on April 13 2006 as the starting point. For each hour thereafter, the first guesses come from previous hour physical retrievals except for 1 UTC, at which the ECMWF analysis from 0 UTC is used as previous retrievals. The algorithm is allowed to run for 24 hours. The results from 12 UTC on April 13 and 0 UTC on April 14 are compared with ECMWF analysis. Figure 26 shows the RMS and bias (both in unit of percentage) of the TPW, PW1 PW2 and PW3. At both 12 UTC (the dashed lines) and 0 UTC (the solid lines), both the TC and the NTC methods are effective on improving the GFS forecast; the RMS is reduced by 3 – 5 %, and the bias is reduced by 5 – 8 %. However, in Figure 26, the TC retrievals do not show better results than the NTC retrievals. Notice at 0 UTC, the NTC RMS is slightly smaller than the NTC RMS, although the NTC bias is larger than the TC bias.

The main reason why TC retrievals do not show better results than the NTC is due to the violation of the TC assumption. The atmosphere is not as smooth in the lower troposphere as in the upper troposphere. The GOES Sounder is not very sensitive to the lower troposphere. Within an hour, there could be dramatic changes of the temperature/moisture due to horizontal advection, vertical motion and surface fluxes in the lower troposphere. These changes are so dramatic that the TC assumption no long stands, and the retrievals from previous time are no longer good first guesses, which results in failed retrievals. However, the algorithm has difficulties to detect the violation of the TC assumption because the brightness temperature might not show such dramatic changes.

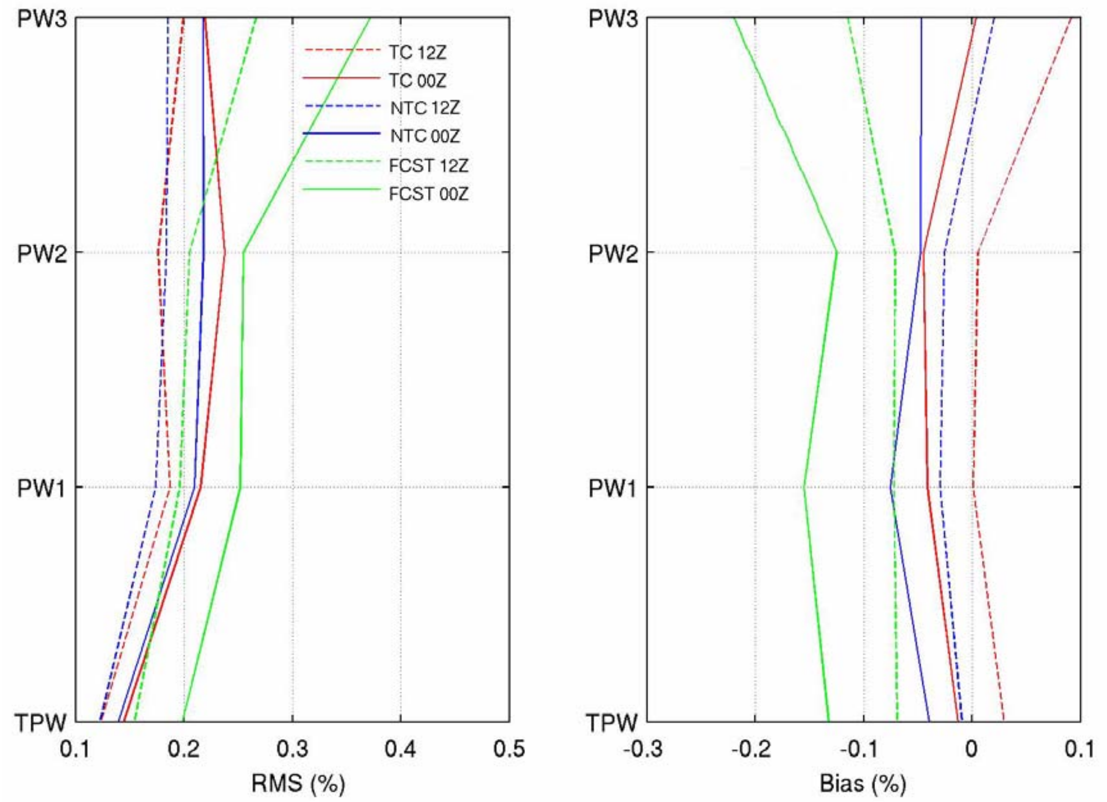

Figure 26. The RMS (left) and bias (right) of TPW, PW1, PW2, PW3 from TC retrievals (red lines), non-TC retrievals (blue lines) and GFS forecast (green lines) as compared with the ECMWF analysis at 12 UTC on 13 April 2006 (dashed lines) and 0 UTC on 14 April 2006 (solid lines). "TC" represents physical retrieval using the time continuity technique; "NTC" represent physical retrieval using either the GFS forecast or the regression as the first guess; and "FCST" represents GFS forecast. Both RMS and bias are in unit of percentage.

The Advanced Baseline Imager (ABI) aboard GOES-R (Schmit et al., 2005) will be used as the primary instrument for extracting legacy profile information. ABI will scan the full disk every 15 minutes and the CONUS every 5 minutes. The assumption of TC would be much better justified at the temporal resolution of 15 or 5 minutes. It is expected the TC concept will be better realized with future instruments with higher temporal resolution.

3.5.3 Results from Method II

To investigate how TC could help improve reducing the radiance biases, the RAOB/GOES/GFS-ARM database is used. The ARM RAOBs are excellent for TC purpose because of their high launch frequency (6 hours). Whenever a clear-sky RAOB is available, bias is calculated using equations (19). Two different bias adjustment schemes are applied to the next time when a clear-sky RAOB is available. The new TC technique uses equations (20) to do bias adjustment and the old one uses the traditional linear regression. The bias-adjusted Tb from both techniques are compared with the true Tb calculated from the RAOB. Figure 27 shows the results from both techniques. The values are the differences between the bias-adjusted Tb and the true (former minus latter). A good bias adjustment technique should have two characteristics: a) the bias of the differences is close to 0; b) the RMS of the differences is small.

The comparison in Figure 27 could be problematic in two situations. When the FOV is cloud contaminated and is misclassified as clear, both bias adjustment techniques might not be able to return reasonable values, in which the comparison becomes meaningless. The comparison could also fail when the RAOB is not a good representative of the whole FOV. The RAOB, as a spot measurement, can represent the whole FOV only if the atmosphere is horizontally homogeneous enough. To avoid these problematic FOVs, only FOVs with the differences of 11 µm Tb between the old bias-adjusted Tb and the calculated one smaller than 1.5 K are retained. The resulting sample size is 140.

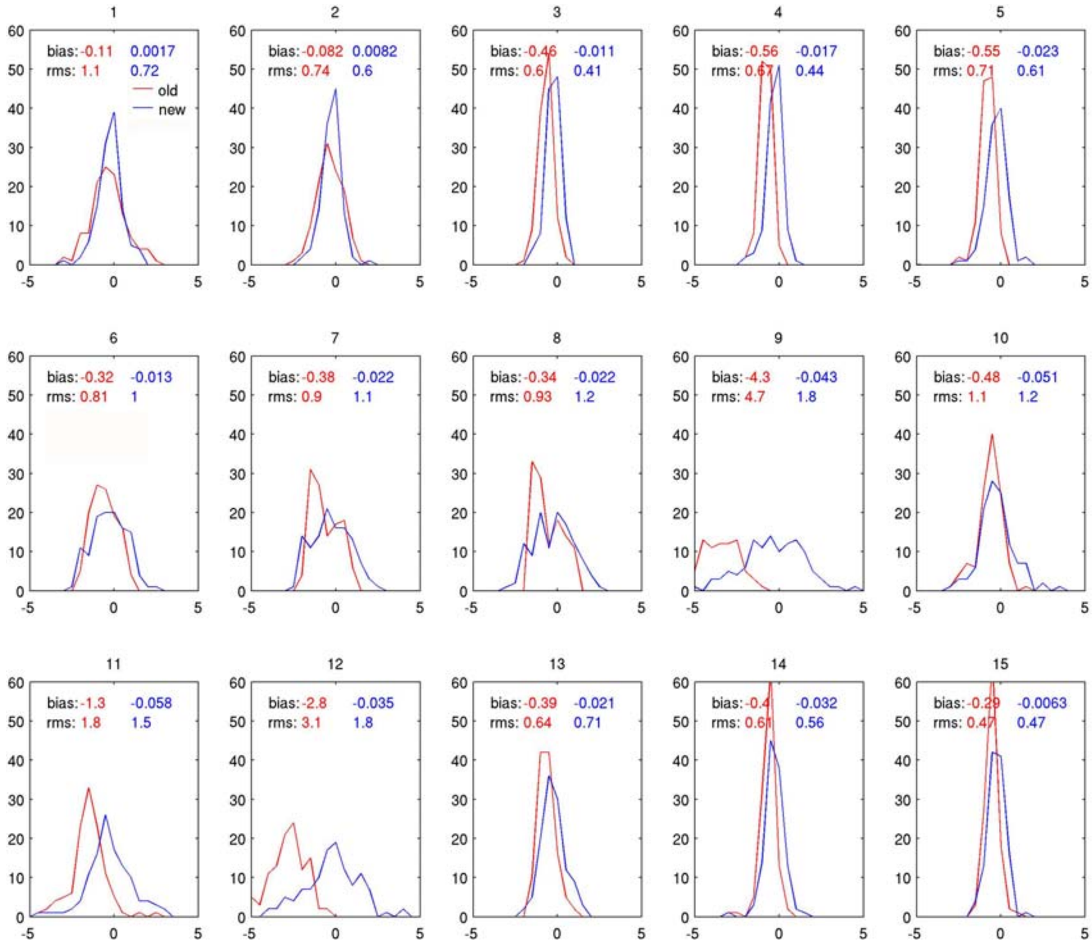

Figure 27. The histograms of differences between the bias-adjusted Tb and the calculated Tb for old regression (red) and new TC (blue) techniques. X-axis is the radiance biases with unit of K. Y-axis is the histogram with unit of number per 0.5 K. Also shown are the bias and RMS of the differences. The sample size is 140.

As seen in Figure 27, for temperature sensitive channels whose weighting functions peak away from the surface (channels 1 - 5 and 13 - 15), the new TC method is able to improve the bias adjustment. For channels 1 - 5, both the bias and the RMS of the differences from TC technique are significantly reduced compared with the old regression technique. For channels 13 - 15, the RMS is hard to reduce, but the bias is reduced and is close to zero (this is true for all the channels). For temperature channels whose weighting functions peak close to the surface (channels 6 - 8), the new TC bias adjustment technique fails to show any improvements. Although the bias is reduced to near 0, the RMS is increased.

Table 5. The RMS in percentage of retrieved TPW, PW1, PW2, PW3 as compared to RAOB. FCST represents the GFS forecast, which are used as the first guess for all physical retrievals. NTC refers to the physical retrievals using traditional linear regression radiance bias adjustment technique. TC refers to the physical retrievals using the new TC radiance bias adjustment technique. RAOB refers to the physical retrievals using bias free radiances as calculated from RAOB.

	TPW	PW1	PW2	PW3
FCST	.116	.163	.17	.339
NTC	.098	.148	.155	.18
TC	.092	.148	.147	.16
RAOB	.090	.147	.149	.14

There are five channels that are useful for moisture retrievals (channels 6 - 7 for the boundary layer moisture, channels 10 - 12 for the lower, middle and upper troposphere, respectively). As mentioned before, the new TC bias technique does not show improvements for channels 6 and 7. However, for the other three channels, the new TC bias technique not only reduces the bias to near 0, but also reduces the RMS, especially for channels 11 and 12. Thus, the improvement of moisture retrieval at middle and upper atmosphere is expected if the new bias adjustment technique is applied.

The results shown in Figure 27 are reasonable. The basic assumption for TC is that the atmosphere does not change dramatically during a short period of time. This is a good assumption for middle and upper troposphere. But for the lower atmosphere and the surface, both the temperature and moisture change dramatically. This is why the TC bias adjustment technique does not work well for those channels (channels 6 - 8). On the other hand, the old linear regression bias adjustment technique works fine for those channels. Therefore, in the algorithm testing the new TC bias adjustment technique, channels 6 – 8 still use the old linear regression bias adjustment technique.

Table 5 shows the RMS of physically retrieved TPW, PW1, PW2 and PW3. FCST represents the GFS forecast, which is used as the first guess for all physical retrievals. NTC refers to the physical retrievals using traditional linear regression technique to do bias adjustment. TC refers to the physical retrievals using the new TC technique to do bias adjustment. RAOB refers to the physical retrievals using bias free radiances as calculated from RAOB, which is considered as the best retrievals one may accomplish using the same physical retrieval algorithm. From Table 5, the TC retrievals show slightly better results than the NTC, both of which successfully improve the GFS forecast. Both PW2 and PW3 are slightly better improved by the TC retrievals than by the NTC retrievals. As a result, TPW is better improved by the TC retrievals. This is consistent with the fact that the TC bias adjustment technique is only applied to channels peaking away from the lower troposphere. In Table 5, the TC retrievals are not significantly better than the NTC retrievals. This is because the TC retrievals are already very close to the retrievals using bias free radiances.

These results indicate that the TC has some great potential to improve the sounding retrievals through improving the radiance bias adjustment. However, when applying on real-time data, cautions are needed as the TC radiance bias adjustment technique is prone to the imperfect starting point; any bias from the starting point will be transferred to later times (from such as cloud contamination and RAOB/analysis bias), causing retrieval biases in later times which typically do not exist if using the traditional NTC radiance bias adjustment technique.

3.6 Handling Surface Emissivity for Sounding Retrievals

The surface emissivity is retrieved using regression methods, and it is not updated in the physical iterations. The regression coefficients are trained using the SeeBor database (Borbas et al., 2005). When applying to real data, it is found there are artificial diurnal changes of surface emissivities. Figure 28 shows the GOES-12 Sounder 11 μm regression-retrieved surface emissivities from 15 UTC on 24 April 2007 to 14 UTC on 25 April 2007. All the clear-sky retrieved surface emissivities are averaged (see Figure 1 for spatial coverage). From Figure 28, the retrieval of surface emissivity is strongly affected by solar radiation in the morning and afternoon when the solar zenith angle is small. For other times, the retrievals still have discrepancies between the daytime and the nighttime, but rather stable. The reason of the false diurnal changes of the retrieved surface emissivity is that all the training data in the SeeBor database are at either 0 or 12 UTC. When applying these coefficients to other times, the diurnal changes of radiances introduce fake diurnal changes of the surface emissivity.

To examine how the biases in the retrieved surface emissivities affect the physical retrieval, the UW-Madison Baseline Fit database (Seemann et al., 2008; see Chapter 2 for more details about the database), are used to compare with the regression retrievals. Figure 29 (a) and (b) shows the differences of the surface emissivity at 12 and 11 μm between the Baseline Fit (BLF) database and the regression retrievals (the latter minus the former) on 20 UTC on 24 April 2007. The regression retrievals in this case are much smaller than the BLF database, especially over eastern New Mexico and western Texas, where the difference could be as large as -0.03. As a comparison, the false diurnal change in Figure 28 is only about 0.004 from 20 UTC to 01 UTC.

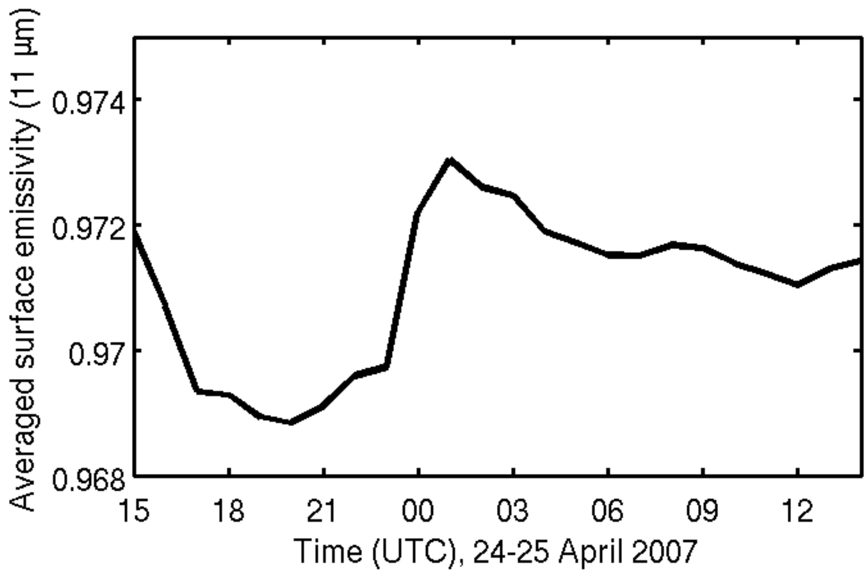

Figure 28. The averaged 11 μm regression-retrieved surface emissivities of GOES-12 Sounder from 15 UTC on April 24 2007 to 14 UTC on April 2007.

Figure 29 (c) shows the differences of the retrieved TPW. The difference is defined as the regression minus the BFL database. For most FOVs, the overall impacts of the surface emissivities on the TPW retrievals are small. The mean and the STD of the TPW differences in Figure 29 (c) are only -0.0013 cm and 0.0055 cm respectively, much smaller than the retrieval precision shown in Figure 2. There are a few areas where relatively large impacts are seen. Over eastern New Mexico and western Texas, the TPW differences are around 0.005 cm or 1 – 1.5 %; over Florida and central Illinois, the TPW differences are around -0.015 cm or -0.5 %. These are still much smaller than the TPW retrieval precision (around 12 % for GOES-12 Sounder).

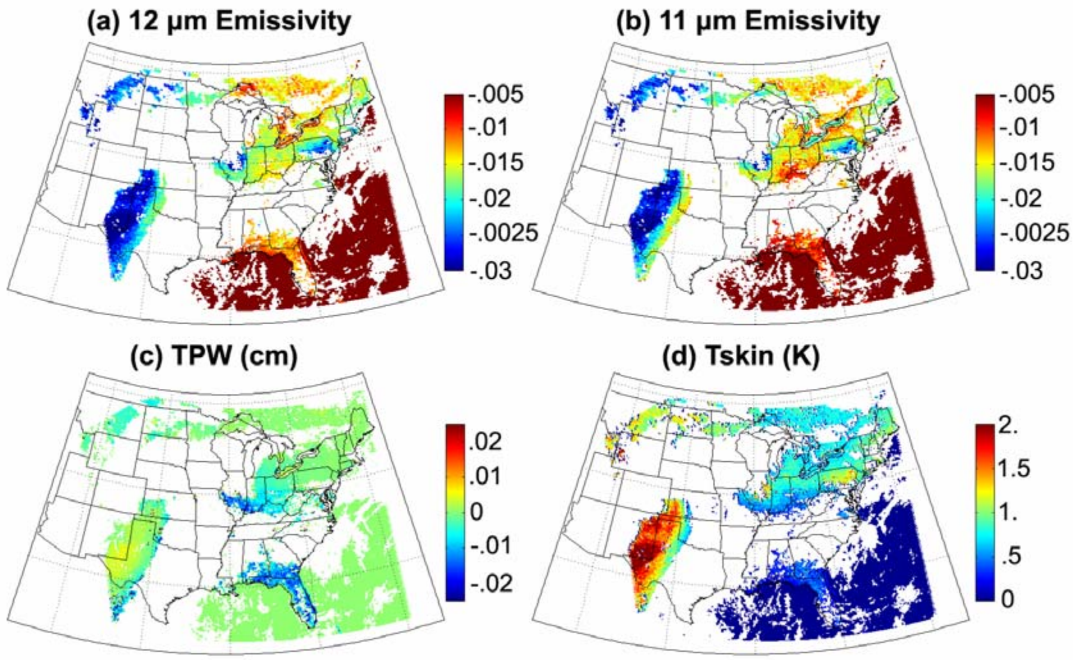

Figure 29. The surface emissivity differences of the GOES-12 Sounder a) channel 7 (12 µm) and b) channel 8 (11 µm) between the Baseline Fit database and the regression retrievals at 20 UTC on 24 April 24 2007. The differences of the retrieved clear-sky c) TPW and d) surface skin temperature using the two different surface emissivity schemes. The difference is defined as the regression minus the BLF.

On the other hand, the impacts of the surface emissivity on the surface skin temperature are large (Figure 29 (d)). Over the western Texas and eastern New Mexico, the large negative emissivity differences (as large as -0.03) results in large surface skin temperature differences (1.5 – 2 K). The results here are consistent with those pointed out by Susskind (1985); the retrieval of surface skin temperature is very sensitive to the accuracy of surface emissivity while the retrieval of profiles is less sensitive.

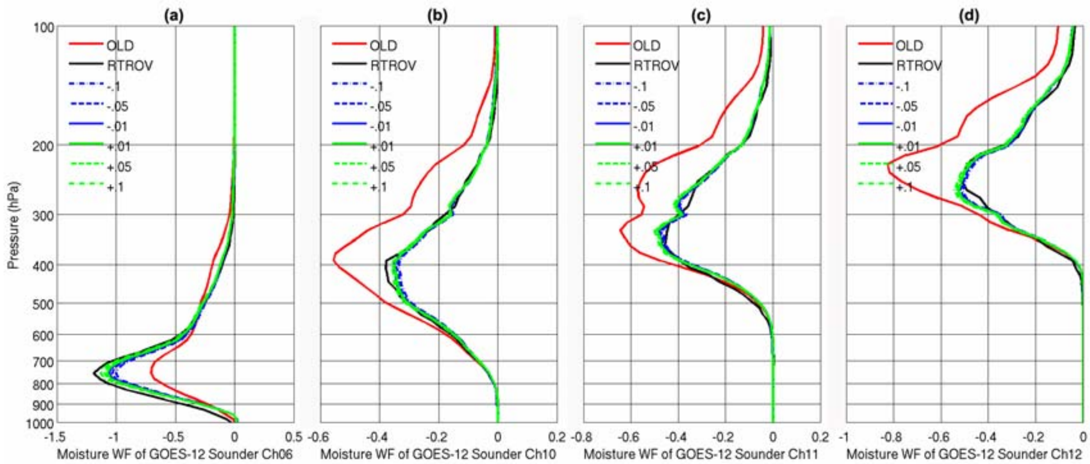

Figure 30. The GOES-12 Sounder moisture weighting functions of a) channel 6, b) channel 10, c) channel 11 and d) channel 12 using the RAOB at the ARM SGP CART site at Lamont, OK (C1, 36°37' N, 97°30' W) at 0 UTC on 8 August 2006. "OLD" represents the analytical approximation method. "RTTOV" represents calculation by the RTTOV-9.1. The blue and green lines represent the calculation using the perturbation method. Different number represents different magnitude of perturbation.

3.7 Weighting Functions on Sounding Retrievals

One basic assumption of the analytical approximation (Zeng 1974; Li 1994) is that the moisture absorption coefficients do not change with pressure, temperature and moisture, which clearly is not realistic. In this section, the impacts of the weighting functions on the retrievals will be investigated.

Figure 30 shows the moisture weighting functions calculated by three different methods. The green and blue lines represent the results using the perturbation method. The number indicates the magnitude of the perturbation. All the four channels have consistent weighting functions by using different perturbations. Notice the smallest perturbations (±0.01) did not introduce obvious numerical errors. Therefore, the weighting functions calculated by the perturbation method could be used as true to evaluate other methods. From Figure 30, the analytical approximation method significantly underestimates the moisture weighting functions for channel 6, and overestimates for channels 10, 11 and 12. The black lines in Figure 30 are the moisture weighting functions calculated with the Radiative Transfer for TOVS (RTTOV-9.1; Saunders et al., 1999). Clearly, the RTTOV weighting functions agree much better with the perturbation results than the analytical approximation method. However, the analytical approximation method has its own advantage; the calculation is much faster than the other two methods. The time needed to calculate weighting functions for the three different methods is, perturbation method >> RTTOV >> analytical approximation.

To examine whether the RTTOV weighting functions could further improve the physical retrievals, the RAOB/GOES/GFS-ARM match-up database (see Chapter 2 for more details about the database) are used. Figure 31 shows the RMS and bias of the RH profile and the 3 layer PWs as compared with the RAOB. For the RH error profiles, the RTTOV weighting functions (the blue lines) do not show much superiority over the approximation method in terms of RMS. But there are slight improvements between 300 and 700 hPa in terms of bias. As a result, PW3 are slightly improved; the RMS is reduced by 1.7 % and the bias is reduced by 2.5 %. As for PW2 and PW1, there is no obvious improvement at all. It should be emphasized that, in the physical retrieval algorithm using RTTOV weighting functions, only three moisture channels (10, 11 and 12) are replaced by the RTTOV weighting functions. Others are still calculated from the analytical approximation method. It is empirically found that this use of RTTOV weighting functions generate the best retrieval.

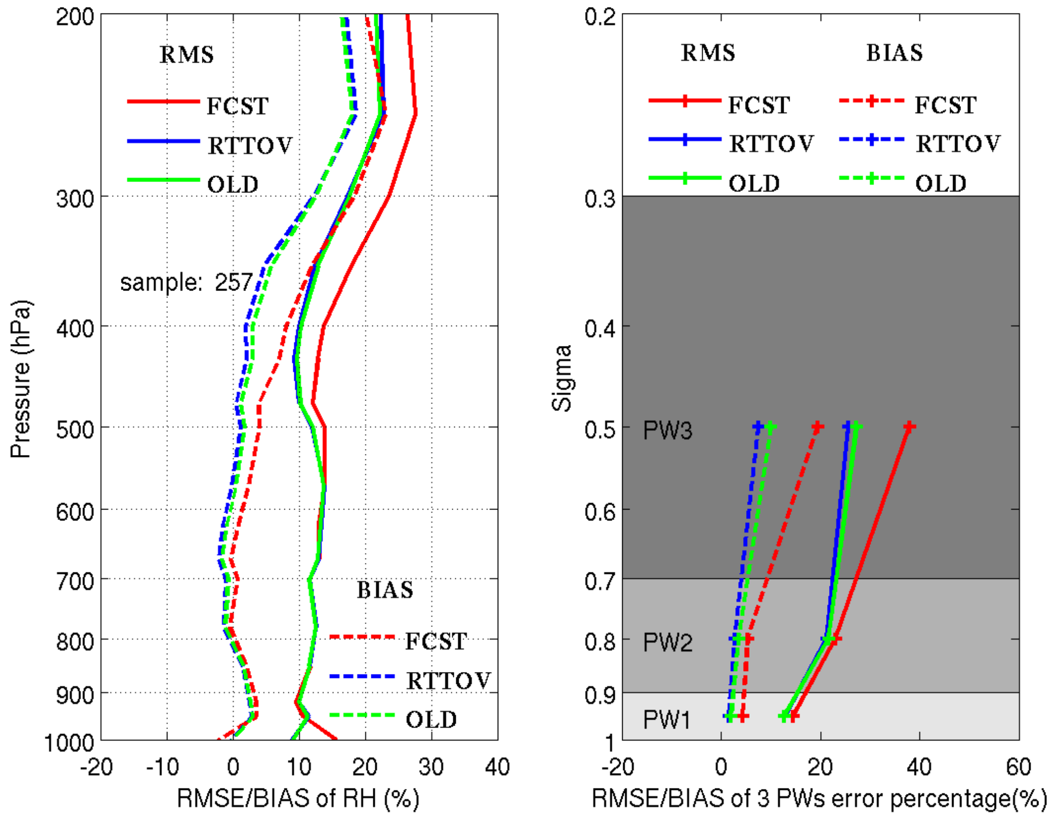

Figure 31. Comparison of physical retrievals using different weighting functions. The left panel is the relative humidity error profiles; the right panel is the 3 PW relative error profiles. The red lines are the GFS forecast, the green lines are physical retrievals using old weighting functions, and the blue lines are physical retrievals using RTTOV weighting functions.

3.8 Summary

In this chapter, an improved version of the clear-sky physical retrieval algorithm is developed. By using a realistic background error covariance matrix of retrieval parameters, an improved fast forward RTM, a radiance bias adjustment scheme, inverted cone clear-sky observed radiance averaging, a first guess from regression, and an improved surface emissivity scheme, the improved physical retrieval algorithm is able to generate better retrievals of temperature and moisture profiles from GOES-12 Sounder radiances than the previous legacy algorithm, which is currently used in CIMSS routine GOES Sounder data processing. The improved physical retrieval algorithm betters TPW retrievals by 0.4 mm over the old legacy version when the retrievals are compared with SGP CART site microwave radiometer TPW measurements.

A case study of a deadly tornadic supercell at Eagle Pass, Texas on 24 April 2007 reveals that the improved physical retrieval is able to identify the pre-convective environment while the GFS forecast fails to do so. Another supercell case on 14 April 2006 demonstrates that the improved physical algorithm is able to detect the low-level moisture better than the GFS forecast. These hourly products provide information that should help forecasters estimate the further development of the current weather system.

Two methods are advocated to explore the application of the time continuity to the GOES sounding retrievals. In the first method, the retrievals from previous time are taken as the first guess for the current time. Comparisons with the ECMWF analysis show the time continuity technique does not generate better sounding retrievals than the traditional technique, which uses regression or forecast as the first guess. It is expected the time continuity could be better realized with the future instrument with more frequent measurements. In the second method, the time continuity is used to improve the radiance biases. Comparisons with the RAOB at the ARM site show that the time continuity has great potential to improve the sounding retrievals, albeit caution is needed to prevent bias introduced by the imperfect starting point.

An independent land surface emissivity database, the UW-Madison Baseline Fit database is used to study the impacts of the surface emissivity on the physical retrieval. It is found the bias in the surface emissivity could result in the bias in the retrievals of TPW and the surface skin temperature. However, the impact on the surface skin temperature is much more significant than on the TPW.

The moisture weighting functions provided by the RTTOV-9.1 are compared with those calculated by the analytical approximation method, which is used in the improved physical retrieval algorithm. It is found the moisture retrievals could be improved slightly in the upper troposphere by using the RTTOV moisture weighting functions of channels 10, 11 and 12.

Chapter 4 Extending Sounding Retrievals to Cloudy Regions

The GOES Sounder measured IR radiances are typically not used for sounding retrievals under cloudy conditions because of the strong absorption by the clouds. However, the chance for a GOES Sounder FOV to be clear-sky is only about 1/3. To extend the sounding retrievals from clear sky to cloudy regions,, a cloudy retrieval algorithm is developed to explore the GOES Sounder's performance under thin and low thick cloud conditions. In this section, thin clouds are defined as having retrieved COT smaller than 2.0 and low thick clouds are defined as having retrieved CTP larger than 850 hPa and retrieved COT larger than 2.0.

4.1 The GOES Cloudy Sounding Retrieval Algorithm

Unlike the physical retrieval algorithm for clear skies (Li et al., 2008), the GOES SFOV cloudy sounding algorithm starts with a statistical linear synthetic regression technique (Seemann et al., 2003; Li et al., 2009; check section 3.2.1 for more details on the regression algorithm). The GOES-12 Sounder IR measurements are simulated radiances calculated from the PFAAST (Hannon et al., 1996). The predictors for the linear regression algorithm include 1) the brightness temperature (Tb) and the quadratic terms (Tb^2) of the first 15 IR channels; 2) the surface pressure; 3) the local zenith angle; 4) the observed surface air temperature and moisture if available (following the work by Smith et al., 1985; Smith and Woolf, 1988; Ma et al., 1999; Li et al., 2000); and 5) the forecast profiles of temperature and moisture (Li et al., 2008). The predictants include 1) the profiles of temperature, moisture and ozone; 2) the surface skin temperature; 3) the cloud optical thickness (COT) at 0.55 μm; and 4) the cloud top pressure (CTP). Separate sets of regression coefficients are generated for water and ice clouds. More details about the predictors and predictants are given in the following sections.

4.1.1 The Training Database and Cloud Top Determination

In the training process, the GOES IR radiances are calculated with given profiles of temperature, moisture and ozone, sensor's view angle, surface skin temperature, surface pressure, surface emissivities, CTP, 0.55 μm COT, and effective particle size, using the equation for radiative transfer (Zhou et al., 2007)

$$R = R_0 F_T \tau_{tc} + R_c \tau_{tc} + R_1 + R_1^{\downarrow} F_R \tau_{tc} \qquad (21)$$

where R is exiting radiance at the top of the atmosphere. R_0, R_c, R_1, and $R_1^{\downarrow}$ are upwelling emission below the cloud, emission from the cloud, upwelling emission from the atmosphere above the cloud, and downwelling emission from the atmosphere above the cloud, respectively. F_T and F_R are the cloud transmissive and reflective functions. τ_{tc} is the transmittance between the cloud and the top of the atmosphere. The upwelling emission R_0 includes the surface emission, the atmospheric upwelling emission below the cloud, and the downwelling emissions by the cloud and the atmosphere (both above and below the cloud), which are reflected back to the space by the surface.

In the SeeBor training database (Borbas et al., 2005), most profiles are from clear sky conditions. In order to generate the cloudy profiles, clouds are added at a selected level. Figure 32 (a) shows the thresholds of relative humidity (RH) used to select the level where clouds are added. Working from the top to the surface, clouds are added at a level when the RH is larger than the given threshold. The purpose of these thresholds is to distribute the clouds evenly at all heights. In our approach, ice clouds are added between 100 and 500 hPa; water clouds are added between 400 hPa and the surface. Figure 32 (b) and (c) show the histograms of the CTP assigned to the cloudy profiles in training datasets for ice and water clouds, respectively.

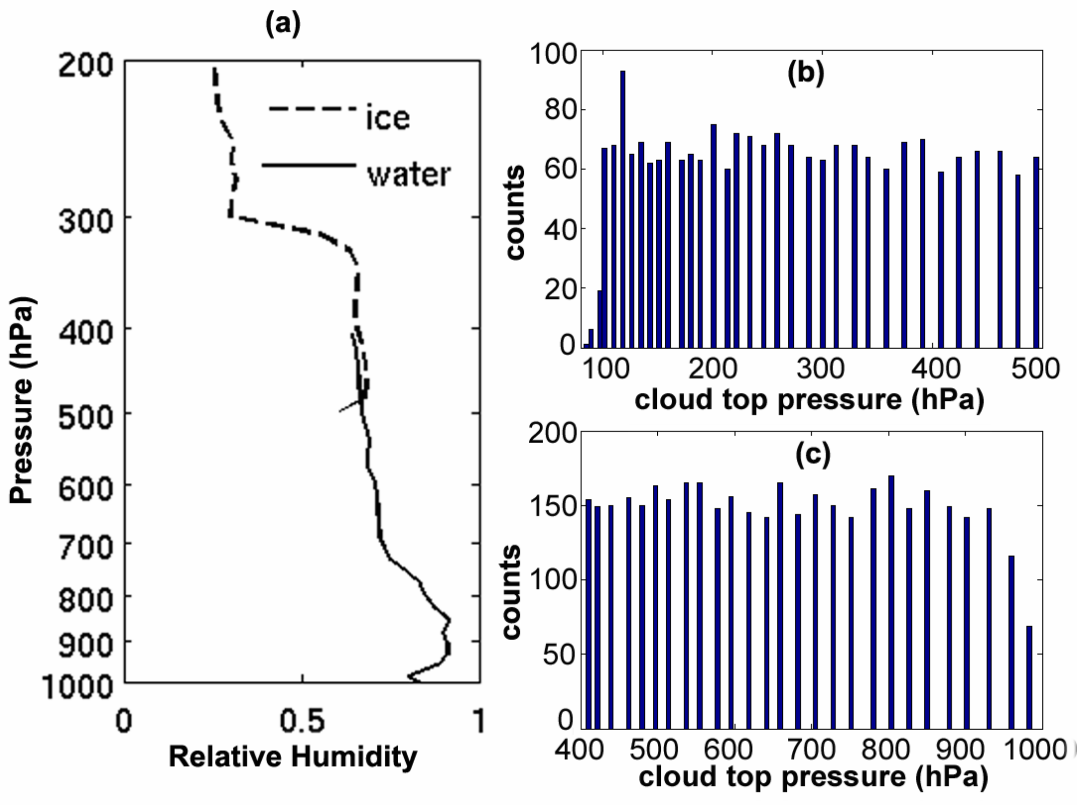

Figure 32. a) The profiles of RH threshold to determine where to add clouds; b) the histogram of ice cloud top pressure; c) the histogram of water cloud top pressure

Among the 15000 profiles, 2162 suitable profiles are found where ice clouds can be added and 4017 for water clouds. The clouds are added with a random value of COT from [0.01, 0.1, 0.2, 0.5, 1.0, 1.5, 2.0, 3.0, 4.5, 6.5, and 10.0]. The training set is classified into 10 different satellite view angles (note this is not local zenith angle) classes appropriate for the GOES-12 Sounder [3.5, 4.0, 4.5, 5.0, 5.5, 6.0, 6.5, 7.0, 7.5, and 8.0]. For each view angle, random values between x - 0.25 º and x + 0.25 º are assigned. For ice clouds, the effective particle size in diameter (De) is obtained using (Heymsfield et al., 2003)

$$De = \frac{A \cdot \tau^{\alpha}}{\tau - B \cdot \tau^{\alpha}}, A = 18.7652, B = 0.32522, \alpha = 1.1905 \qquad (22)$$

where τ is COT at 0.55 µm. As suggested by Li et al. (2005), a 10 % random variation is added to De, and the final value is restricted to be between 10 and 50 µm. For water clouds, sensitivity studies by Li et al., (2005) show that De could be randomly assigned between 5 and 35 µm, with a mean of 30 µm, and an STD of 10 µm.

4.1.2 The Radiative Transfer Model

The cloudy radiances are calculated by coupling the clear-sky optical thickness from PFAAST (Hannon et al., 1996) with the associated COT at 0.55 µm. The COT is calculated with a fast radiative transfer cloud model developed by University of Wisconsin-Madison (UW) and Texas A&M University (Wei et al., 2004). The original model, designed for hyperspectral IR sounders, is adapted to the GOES-12 Sounder. In this model, the bulk single-scattering properties of ice crystals are calculated by assuming aggregates for large particles (>300 µm), hexagonal geometries for moderate particles (50–300 μm) and droxtals for small particles (0–50 μm); the water cloud droplet is assumed to be spherical and the classical Lorenz-Mie theory is used to calculate the single-scattering properties.

The surface IR emissivities are assumed to be 0.98 in cloudy skies.

4.1.3 Constructing Forecast Error Profile

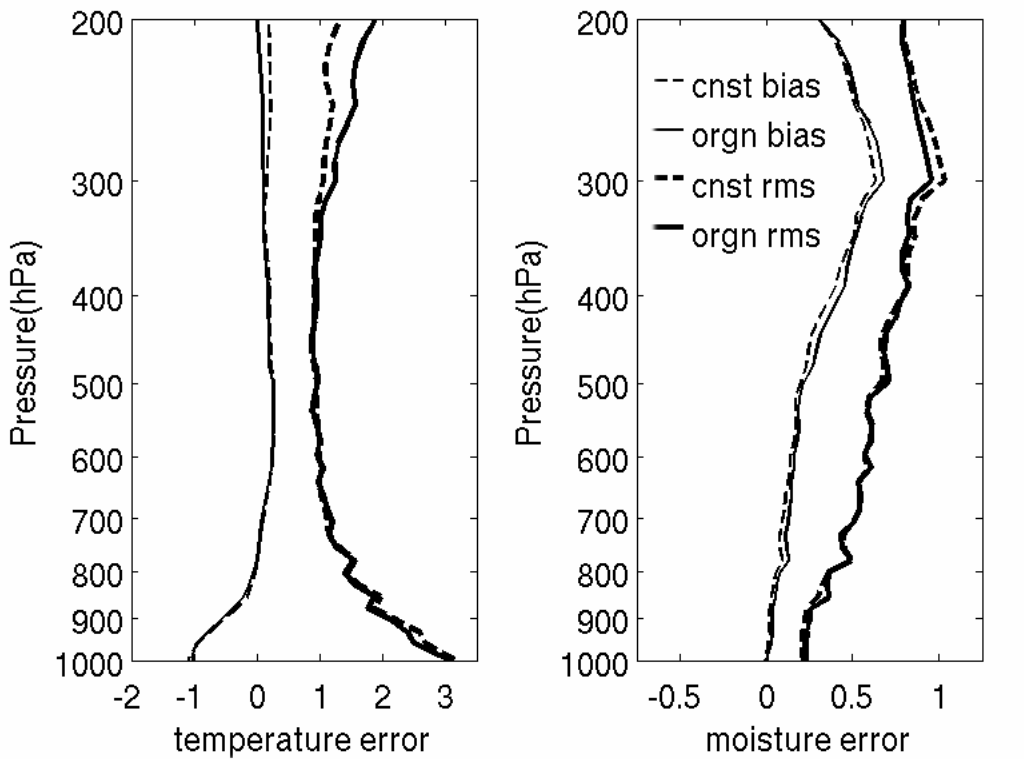

Figure 33. The original and constructed bias and RMS of forecast error. The temperature is in unit of K, and the moisture in unit of logarithm of mixing ratio (g/Kg). The thin dotted line is the constructed bias profile; the thin solid line is the original bias profile; the thick dotted line is the constructed RMS profile; and the thick solid line is the original RMS profile.

The forecast temperature and moisture profiles are used as predictors for the retrievals by providing extra profile information (Li et al., 2008). Since there are no forecast data in the SeeBor database (Borbas et al., 2005), the forecast error profiles have to be constructed to simulate the forecast data over CONUS and nearby oceans.

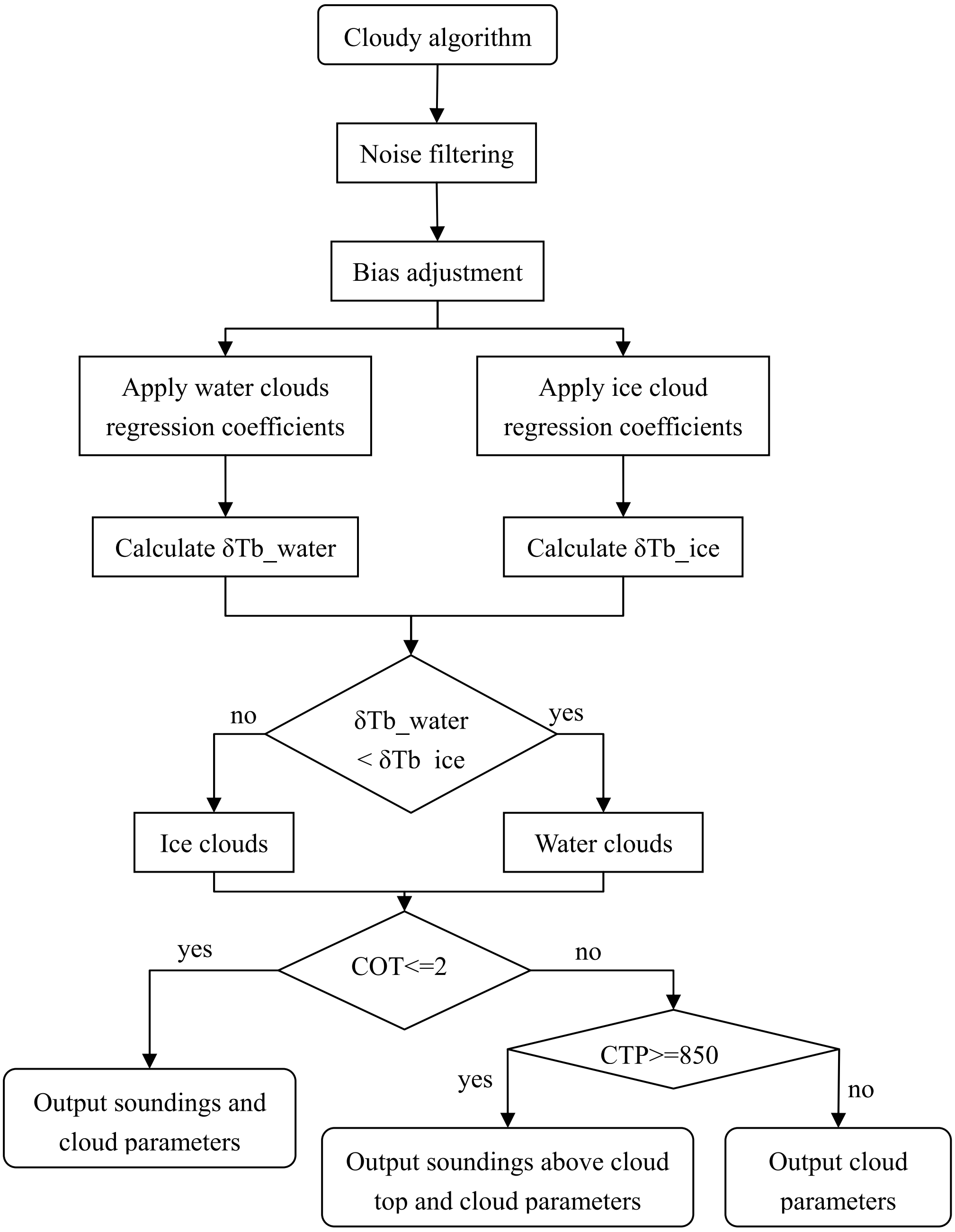

Figure 34. The flow chart of the cloudy sounding retrieval algorithm

The RAOB/GOES/GFS-2003 match-up database is used to derive the forecast error profile. One difficulty in constructing a forecast error profile is that temperature/moisture at one level is highly correlated with those from nearby levels. In order to characterize the correlation in the error profiles, a principle component analysis (PCA) is applied.

From the match-up database, a set of forecast error profiles U are obtained. Then the PCA is performed on U

$U = E \times \Lambda$ (23)

where $E = \begin{bmatrix} E_1 & E_2 & \cdots & E_m \end{bmatrix}$ represents the eigenvectors, and m is the number of eigenvectors. Λ is the matrix set of eigenvalues. For each error profile U_i (i=1, n, where n is the number of profiles), we have

$U_i = E \times \Lambda_i$ (24)

where $\Lambda_i = \begin{bmatrix} \Lambda_{i1} \\ \Lambda_{i2} \\ \vdots \\ \Lambda_{im} \end{bmatrix}$ are the eigenvalues for the ith error profile. The jth eigenvalue Λ_{ij} corresponds to the jth eigenvector E_j. Both the eigenvectors and the eigenvalues are arranged in the order of relative importance with the most important eigen-value/vector as the first one. Statistical analysis is performed on all the eigenvalues to get the mean and the STD, which are used to generate random numbers as eigenvalues, which in turn are used to simulate the forecast error profiles. Because the nearby levels are correlated, it is not necessary to have all the eigenvalues and vectors to reconstruct each profile. From the PCA analysis, 15 temperature and 9 moisture eigenvectors are sufficient to construct 95 % of the variance of the forecast error profiles (see Figure 33). Except around 200 hPa, where the temperature is highly variable near the tropopause, the constructed error profiles have similar bias and RMS as the original ones.

4.1.4 Cloud Phase Determination

For each FOV, two sets of Tb are calculated, one with ice and the other with water cloud regression coefficients. The Tb closer to the observed Tb (smaller residuals) is chosen and cloud phase is assigned accordingly. See Figure 34 for the retrieval algorithm flow chart.

4.1.5 Noise Reduction and Bias Adjustment

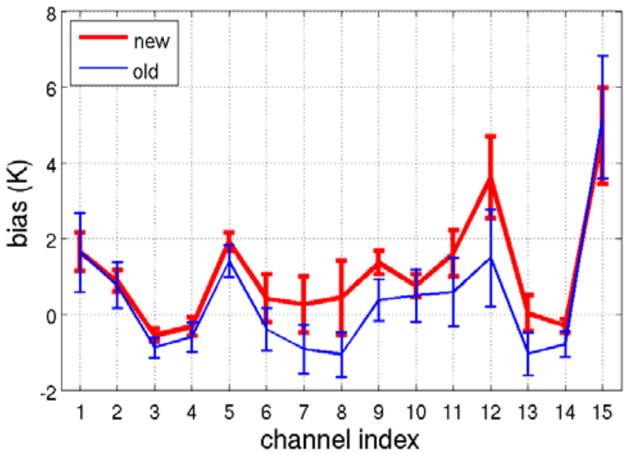

Figure 35. The averaged bias for GOES Sounder's first 15 IR channel. The old bias (thin blue line) is from June 2003 to September 2004. The new bias (thick red line) is from August 2006 to May 2007. The bar at each point represents the standard deviation of the bias.

Noise reduction is done differently under cloudy than clear sky conditions. In the case of clear sky, the inverted cone method (Li et al., 2008; Plokhenko and Menzel, 2001) is used, where more opaque spectral band radiances are averaged over larger areas to reduce noise. Under cloudy conditions, due to (1) the large radiance contrast between clear and cloudy regions and (2) the non-homogeneousness of cloud tops, a 3 by 3 FOV averaging method is used to reduce the radiance noise:

$$\overline{R}(m,n) = \frac{\sum_{j=-1}^{1} \sum_{i=-1}^{1} R(m+i,n+j) \cdot K(m+i,n+j)}{\sum_{j=-1}^{1} \sum_{i=-1}^{1} K(m+i,n+j)} \qquad (25)$$

where $\overline{R}(m,n)$ is the averaged radiance at location (*m, n*), $R(m+i,n+j)$ is the measured radiance at location (*m+i, n+j*), and $K(m+i,n+j)$ equals 1 if the FOV is cloudy or 0 if it is clear.

A radiance bias adjustment is also necessary. Radiance biases are the result of changes in radiometer performance and calibration, and uncertainty of radiative transfer model. Changes over time in bias are caused by radiometer performance drift. Figure 35 shows how the GOES-12 Sounder's biases have changed with time. For June 2003 to September 2004, most channels have biases less than 2.0 K except channel 15, which has a bias of about 5 K. For August 2006 to May 2007, biases calculated from clear cases in the RAOB/GOES/GFS-ARM database (see Chapter 2 for more details about the database) are somewhat larger. In this section, the biases are simply removed by deducting the averaged biases. Note for channels 1, 2, 10, 11, 12, 14 and 15, the STD of the 2006 - 2007 bias is smaller than the 2003-2004 bias. This is because the inverted cone method is used to reduce the noise in the newer match-up database for the clear cases; the simple 3 by 3 radiance averaging is used in the older one. Although the noise reduction does not reduce the average of the biases, it reduces the STD of the biases.

4.2 Validation of Cloudy Soundings

Two different data sets of temperature and moisture profiles are used for validation. The first one is the RAOB/GOES/GFS-ARM match-up database, and the second as the RAOB/GOES/GFS-2007 match-up database (see Chapter 2 for more details about the database). In the first database, 765 collocated samples have been obtained, in which 362 are cloudy. In the second database, 53037 collocated samples have been obtained, in which 21607 are cloudy.

The ARM RAOB data in the first database are listed separately from the conventional RAOB in the second database because they are more frequent (4 times a day), and have better overall quality than the conventional RAOB (Turner et al., 2003). The sampling rate is 2 seconds through the flight. For each sample output, details about time in seconds and quality flag are provided. Experiences at the Cooperative Institute for Meteorological Satellite Studies (CIMSS)/UW have shown that the GOES sounding retrievals agree with ARM RAOB better than with the conventional RAOB (Miloshevich et al., 2006). Therefore, the RAOB/GOES/GFS-ARM match-up database will be used as the primary database for validation. However, validation against conventional RAOB is also presented because it is the only way to demonstrate that the algorithm works under different weather and surface conditions. Figure 3 shows the station location and monthly sample distribution of the collected conventional RAOB.

4.2.1 Determination of Thin Clouds

Sounding retrievals below optically thick clouds are not attempted because there is little information from beneath the clouds. A threshold COT of 2.0 has been set and clouds with COT larger than 2.0 are not considered for profile retrieval except for low thick clouds, for which sounding retrievals above cloud top are performed.

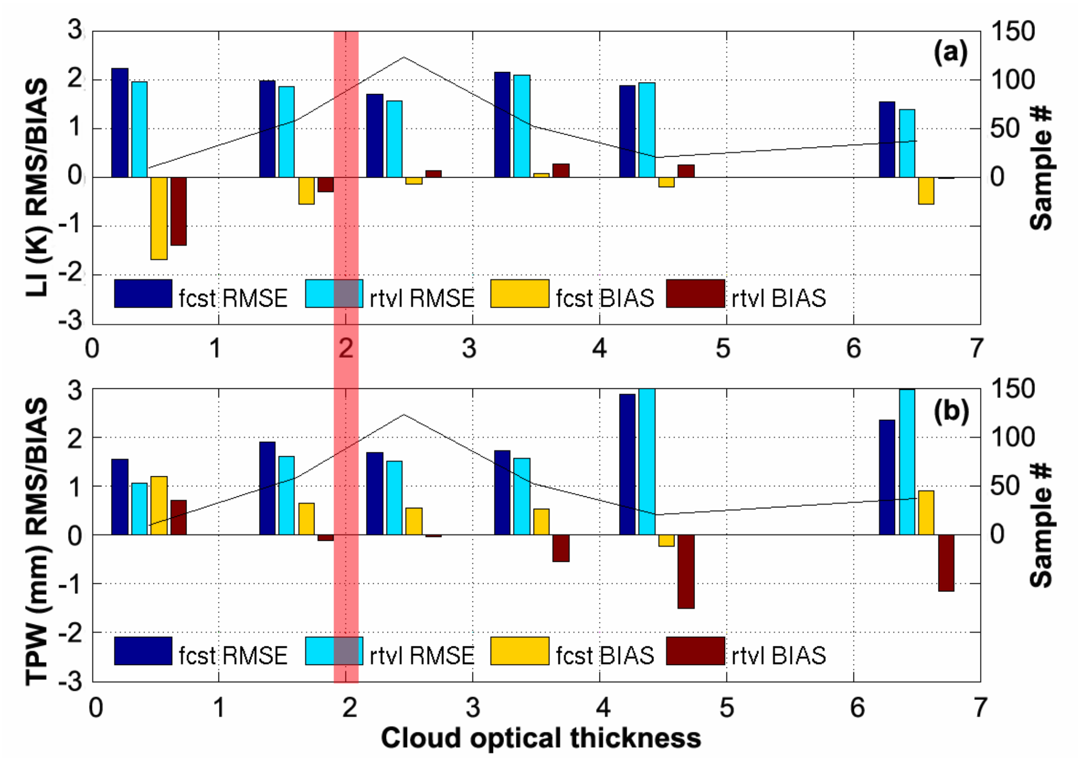

Figure 36. Validation of LI (upper) and TPW (bottom) against RAOB for different cloud optical thickness. Thin clouds are better improved than thick clouds. The black solid line shows the sample distribution of cloud optical thickness (right axis). The red strip is where the suggested COT threshold for thin clouds.

Figure 36 shows how the RMS and bias of retrieved total precipitable water (TPW) and the lifted index (LI) change with the COT using the RAOB/GOES/GFS-ARM match-up database. As the clouds get thinner, the retrieval improvement over forecast, as shown by the RMS and bias, gets more significant. In this study, the COT of 2.0 was selected for the threshold to determine soundings under thin cloud conditions, which has 61 samples in Figure 36 (or 17 % of cloudy FOVs). One might argue that 2.5 even 3.0 is still a good threshold from Figure 36, and a larger threshold will ensure more cloudy retrievals. But the main reason 2.0 is chosen is because low water clouds with the same COT are more difficult to retrieve than high ice clouds. Whether the retrieval algorithm is sensitive to cloud parameters depends on the derivative of the radiance to the COT. A large value indicates large sensitivity and promises better retrievals. Low clouds typically exhibit little temperature contrast between the surface and the cloud top. Therefore, with the same COT, low clouds introduce more retrieval errors than ice clouds.

4.2.2 Validation of Cloudy Soundings using ARM RAOB

Our validation focuses on moisture, especially the RH profile and 3-layer PW. The 3 layer PW is integrated precipitable water in sigma coordinates. PW1 is from the surface to 0.9 (roughly 900 hPa), PW2 is from 0.9 to 0.7 (roughly 900 to 700 hPa), and PW3 is from 0.7 to 0.3 (roughly 700 to 300 hPa). In other words, the 3-layer PW depicts the moisture in the lower, middle and upper troposphere.

Thin Clouds

A typical NCEP GFS forecast RH error profile (Divakarla et al., 2006) has smaller error in the lower troposphere (RMS is around 20 %) than the middle troposphere (RMS is around 35 %) and the upper troposphere (RMS is around 50 %) as compared with RAOB. There is little bias for pressure greater than 400 hPa, and less than 15 % for pressure less than 400 hPa.

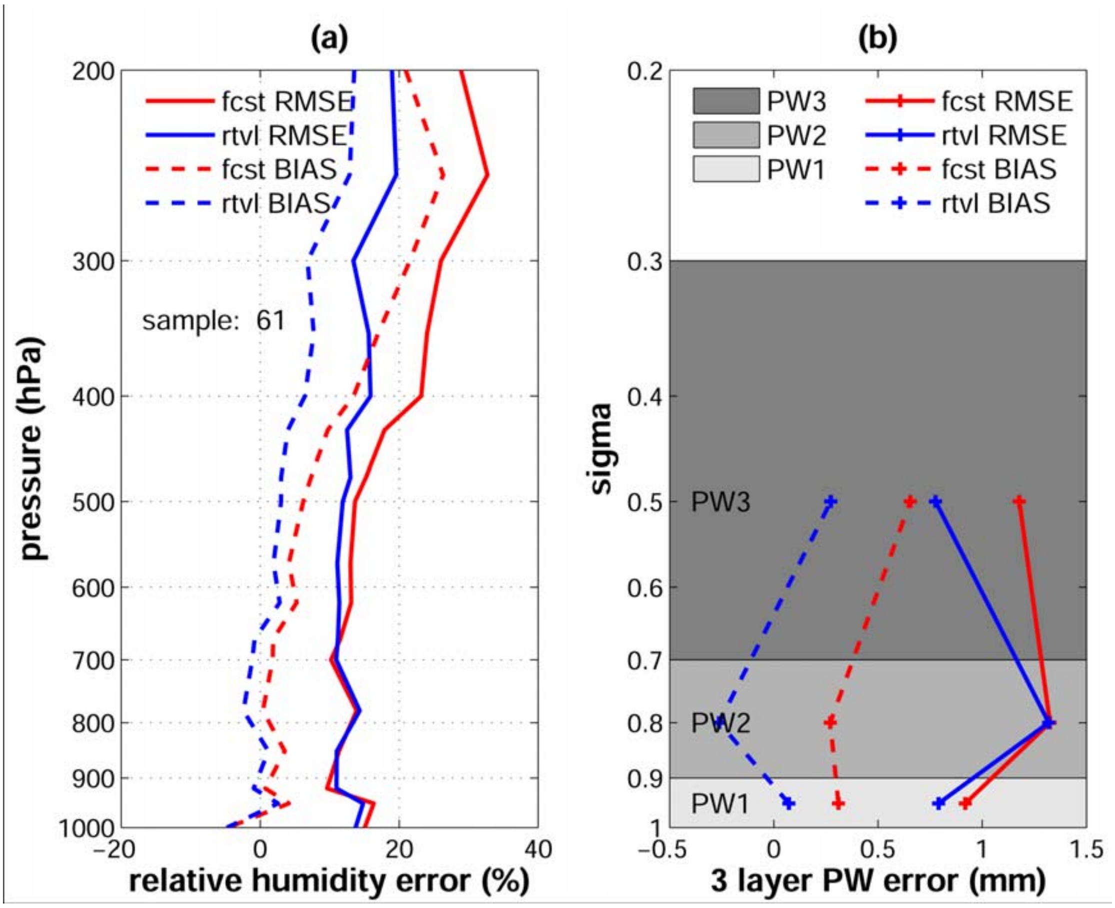

Figure 37. Error profiles of (a) RH and (b) 3-layer PW for thin clouds with retrieved COT less than 2.0

Figure 37 (a) shows the RH error profile under thin cloud conditions. At the ARM SGP site, the GFS forecast has an RMS of 15 % in the lower troposphere (pressure greater than 500 hPa), and 35 % in the upper troposphere. After the retrieval, all RMS magnitudes decrease. Around 250 hPa, the improvement by the cloudy retrieval algorithm is the largest; the RMS is reduced to about 20 %. Going closer to the surface, the improvement is smaller. From 700 to 1000 hPa, it is hard to see any improvement. Figure 37 (b) shows the 3-layer PW in sigma coordinate. As expected, PW3 is improved significantly; the RMS is reduced by 0.4 mm and the bias is reduced by 0.38 mm. PW1 has some improvements although not as much as PW3. PW2 is not improved in RMS or bias.

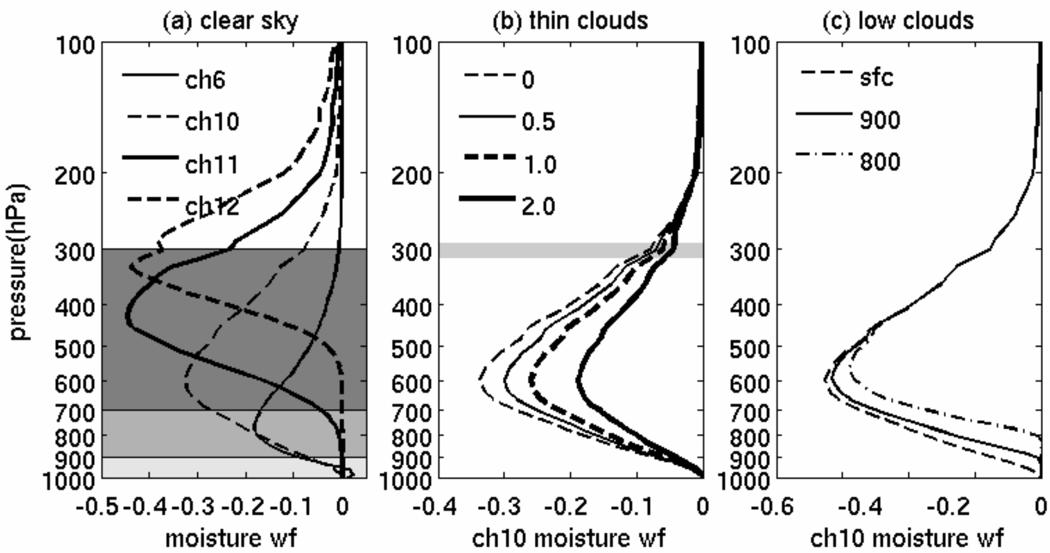

Figure 38. GOES-12 Sounder's moisture weighting functions for a) channel 6, 10, 11 and 12 under clear skies; b) channel 10 under thin clouds with different cloud optical thickness; c) channel 10 under opaque clouds with different cloud top pressure. The shaded areas in (a) corresponds to the coverage of 3 layer PWs (see Figure 37). The shaded line in (b) is where the cloud top relies. (The US standard Atmosphere 1976)

There are only four significant moisture sensitive channels (channel 6, 10, 11 and 12) on the GOES-12 Sounder (see Table 1). Figure 38 (a) shows the moisture weighting functions (which show the relative contributions to the radiance measurements by different layer of moisture) of the four channels calculated for the US Standard Atmosphere 1976; channel 6 (12.66 μm) peaks around 800 hPa, channel 10 (7.43 μm) around 600 hPa, channel 11 (7.02 μm) around 400 hPa, and channel 12 (6.51 μm) around 300 hPa. Thus, channel 10, 11 and 12 are likely to influence PW3 which allows the largest improvement. Only channels 6 and 10 have some influence on PW2. PW2 has some improvement depending on the location of the weighting functions; if the atmosphere becomes wet, the moisture weighting functions move upward, and PW2 is unlikely to be improved. Semi-transparent clouds also affect the amplitude of the weighting functions, hence the influence in thin clouds of channel 10 on PW2 retrieval (as shown in Figure 38 (b)). In thin clouds there is less improvement in PW2. Channel 6, together with channel 7 (not shown), contain PW1 boundary layer moisture information. But more importantly, the hourly surface observations, used as the predictors, account for most of the improvement in the PW1 retrieval.

Low Thick Clouds

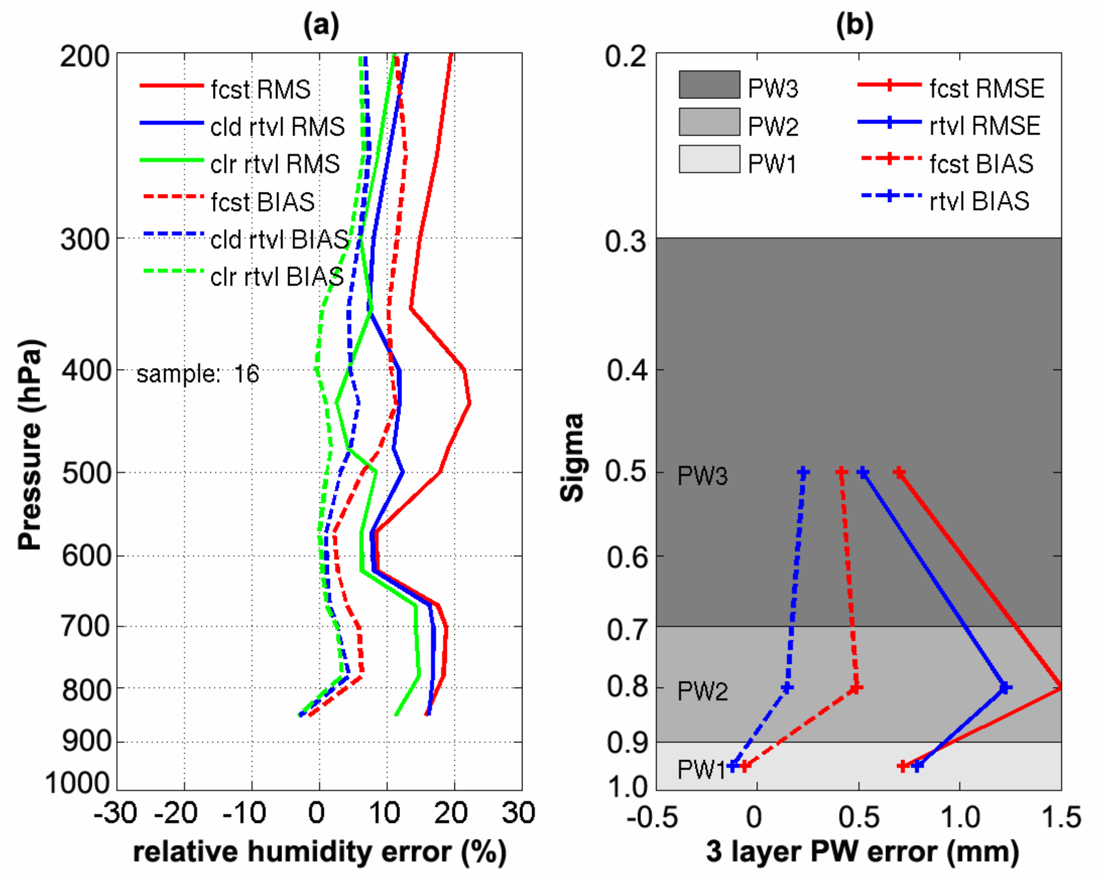

Figure 39. Same as Figure 37 except for low clouds with retrieved CTP larger than 850 hPa and COT larger than 2.0. The green lines show the clear-sky physical retrieval results with surface at the effective cloud top.

Under low thick cloud conditions (defined as retrieved CTP greater than 850 hPa and retrieved COT greater than 2.0), the NCEP GFS forecast performs very well (see Figure 39 (a)); the RH RMS is less than 10 % between 500 and 600 hPa, and less than 20 % from 850 to 200 hPa. Closer to the surface, the effect of the low thick clouds becomes more significant. Figure 39 (a) shows that the retrieval algorithm is able to improve the forecast moisture profile above the cloud top. Again, larger improvement is found in the upper troposphere than in the lower troposphere. In Figure 39 (b), PW3 (RMS is improved by 0.21 mm) and PW2 (RMS is improved by 0.38 mm) have significant improvement; but PW1, even with surface observations, does not show any improvement at all.

In this study, the difference between the low thick clouds and the thin clouds is that the former could be regarded as thick in the spectrum of IR. Radiation from below the clouds is negligible. It is like the surface is being lifted to the height of the effective cloud top (referred to as the lifted surface assumption in this thesis). This has the largest impact on channel 6 and 10. Figure 38 (c) shows the moisture weighting function of channel 10 by using the lifted surface assumption (channel 6 should see the same effect). Although the magnitude decreases a little above the cloud top, the disappearance below the clouds sharpens the weighting function, which actually increases the sensitivity above the clouds. Thus the retrieval of PW2 and PW3 can be expected to show improvement.

To explore the lifted surface assumption, the clear-sky physical retrieval algorithm (Li et al., 2008) is performed for low thick cloud conditions by placing the surface at the height of CTP, which has been retrieved from the cloudy retrieval algorithm. The GFS forecast is used as first guess. The green lines in Figure 39 (a) show the clear-sky retrievals with surface at CTP are a little better (roughly 5% RH improvement below 400 hPa) than the cloudy ones. This suggests another viable approach to extract profile information above the low thick clouds would be to use clear retrievals with the surface lifted to the CTP.

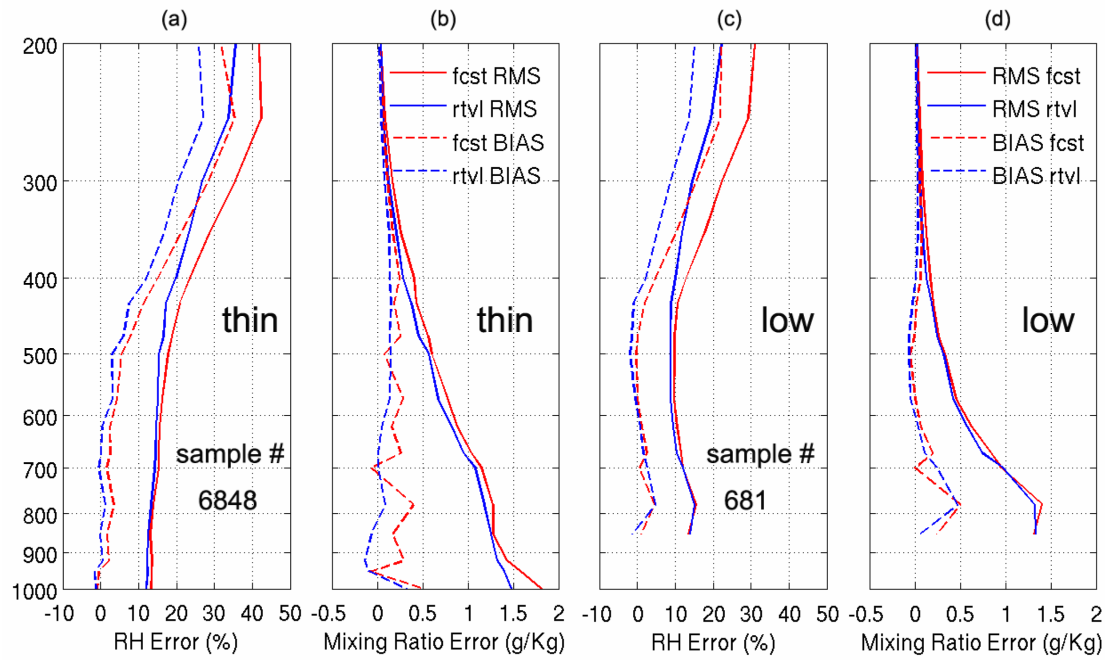

Figure 40. Validation of moisture profiles using RAOB/GOES/GFS-2007 match-up database: a) relative humidity under thin clouds conditions, b) mixing ratio under thin clouds conditions, c) relative humidity under low thick clouds conditions, d) mixing ratio under low thick clouds conditions. The blue lines represent retrievals, and the red lines represent the NCEP GFS forecast. The dashed lines represent the biases, and the solid lines represent the RMS.

4.2.3 Validation of Cloudy Soundings using Conventional RAOB Network

Previous validations were from RAOBs at one location. In this section, the validations include many locations using the RAOB/GOES/GFS-2007 match-up database. Figure 40 shows the bias and RMS differences of the moisture profiles as compared with RAOB. The results here are very similar to those in Figure 37 (a) and Figure 39 (a). Under the thin cloud conditions, the largest improvements over forecast are in the upper troposphere; both the RH and the mixing ratio show significant improvements. In the middle troposphere, the improvements are small with respect to RH, but substantial with respect to mixing ratio. In the lower troposphere, the improvements become more substantial, especially with respect to the mixing ratio. In the case of low thick clouds, the largest improvements are in the upper troposphere too. And the improvements become less significant in the lower troposphere, as the impacts by the clouds become more significant.

Statistical comparisons of other sounding derived products are shown in Table 6. For each product, four statistical parameters are shown: the correlation coefficient (R), the RMS, the bias and the STD. The samples are categorized into 3 groups of conditions: “clear” represents all the successfully retrieved clear-sky samples, “low” represents all the successfully retrieved cloudy samples with retrieved CTP larger than 850 hPa and retrieved COT larger than 2.0; “thin” represents all the successfully retrieved cloudy samples with the retrieved COT less than 2.0. LI, TPW and PW1 retrievals in low thick clouds are not attempted.

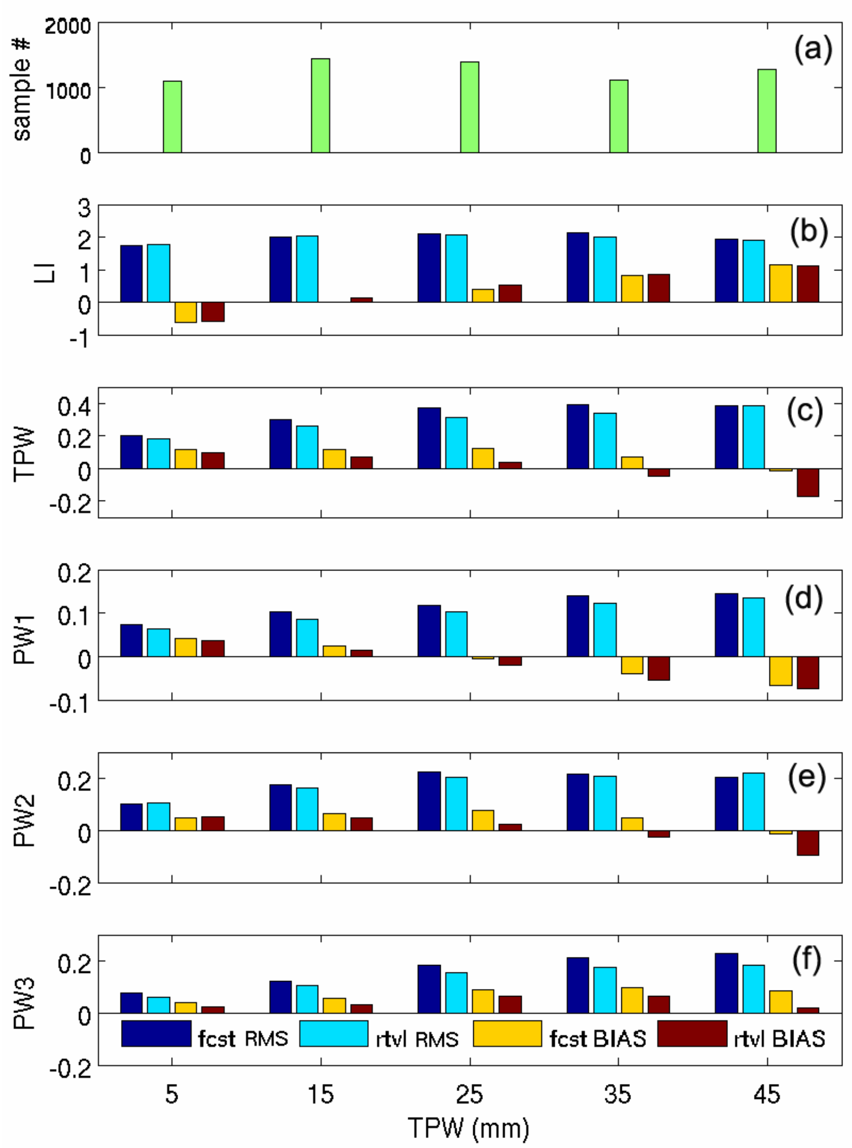

Figure 41. Validation of moisture products under the thin cloud conditions at different TPW level using RAOB/GOES/GFS-2007 match-up database. a) the sample distribution; b) LI; c) TPW; d) PW1; e) PW2; and f) PW3. The dark and light blue bars represent the RMS of the forecast and the cloudy retrievals respectively. The yellow and dark red bars represent the bias of the forecast and the cloudy retrievals respectively.

Columns 5 and 6 in Table 6 show the results of TPW. Under both clear-sky and thin cloud conditions, the retrievals show better TPW products than the GFS forecast. The correlation coefficients increase. The STD, RMS and bias decrease.

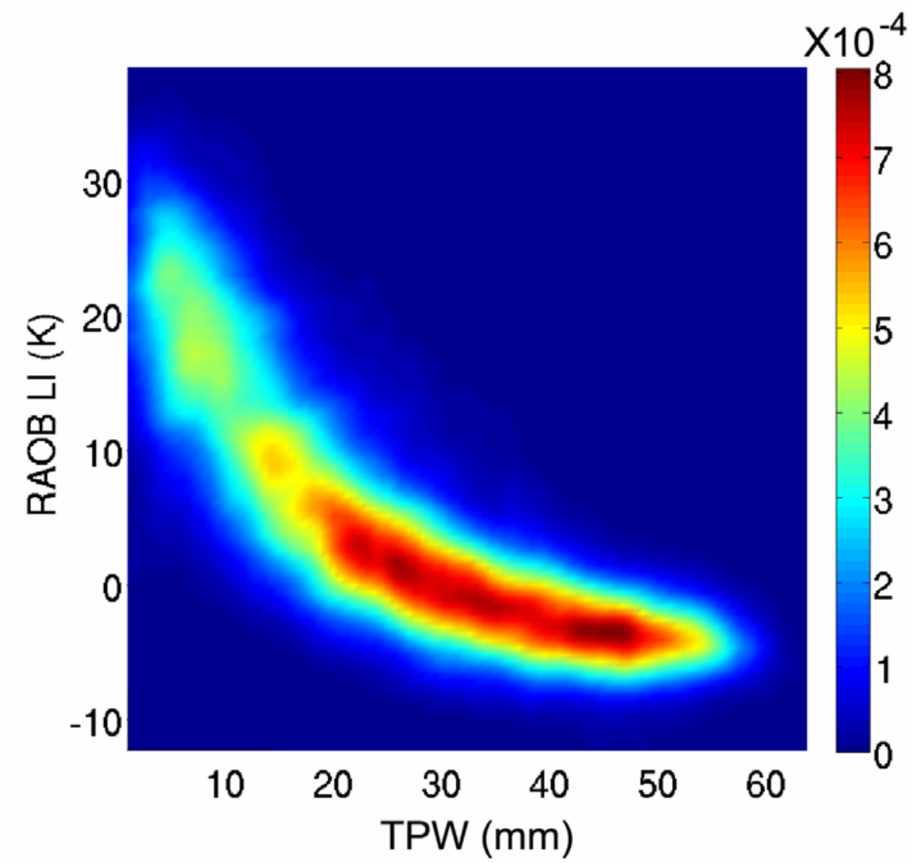

Figure 42. The scatter plot of density between TPW and LI calculated from RAOBs in RAOB/GOES/GFS match-up database. Notice LI is almost always greater than 0 when TPW is smaller than 20 mm.

Columns 7 - 12 show the statistical results of PW1, PW2 and PW3. Again, the results are similar to those in Figure 37 (b) and Figure 39 (b). The improvements of moisture decrease from the upper troposphere to the lower troposphere. Near the surface, the surface observations improve the retrieval. It is interesting that PW2 gets improved in terms of RMS under all the three conditions. However, this improvement is not substantial considering the correlation coefficients do not increase and the STD does not decrease much. The reason that the STD of low thick clouds has the largest decrease of 0.05 mm is because the atmosphere tends to be dry in low thick cloud conditions over land (TPW smaller than 30 mm, not shown). As noted before, less moisture results in more PW2 improvement.

Table 6. Correlation coefficient (R), RMS, Bias and standard deviation (STD) of LI, TPW, PW1, PW2 and PW3 under different conditions as compared with the conventional RAOB using the RAOB/GOES/GFS-2007 match-up database from January 2007 to November 2008. "Clear" represents all the successful retrievals under clear skies; "Low" represents all the successful cloudy retrievals with the retrieved CTP larger than 850 hPa and COT larger than 2.0; "Thin" represents all the successful cloudy retrievals with the retrieved COT less than 2.0.

		LI		TPW		PW1		PW2		PW3	
		GFS	RTVL	GFS	RTVL	GFS	RTVL	GFS	RTVL	GFS	RTVL
R	Clear	0.974	0.977	0.972	0.974	0.969	0.973	0.959	0.959	0.919	0.926
	Low	N/A	N/A	N/A	N/A	N/A	N/A	0.884	0.882	0.460	0.471
	Thin	0.977	0.979	0.973	0.975	0.969	0.974	0.959	0.959	0.925	0.933
RMS	Clear	2.08	1.95	3.19	3.05	1.26	1.17	1.79	1.76	1.43	1.28
	Low	N/A	N/A	N/A	N/A	N/A	N/A	2.08	2.00	1.31	1.24
	Thin	2.10	2.06	3.51	3.24	1.25	1.22	1.93	1.89	1.79	1.47
BIAS	Clear	0.568	0.565	0.418	0.220	-0.241	-0.116	0.293	0.229	0.550	0.391
	Low	N/A	N/A	N/A	N/A	N/A	N/A	0.425	0.297	0.078	-0.066
	Thin	0.574	0.662	0.839	-0.090	-0.201	-0.335	0.414	-0.006	0.840	0.462
STD	Clear	2.01	1.87	3.16	3.05	1.24	1.16	1.76	1.75	1.32	1.22
	Low	N/A	N/A	N/A	N/A	N/A	N/A	2.03	1.98	1.31	1.24
	Thin	2.02	1.95	3.41	3.24	1.24	1.17	1.89	1.89	1.58	1.40

Columns 3 and 4 show the results of LI. In both clear-sky and thin cloud conditions, the algorithm is able to produce better LI than the GFS forecast; the correlation coefficients increase; the STD and the RMS decrease. But the algorithm fails to decrease the bias under the thin cloud conditions; the reason for this is still under investigation.

Previous analysis shows the overall performance by the retrieval algorithm. To study the performance under different weather conditions, Figure 41 shows how the

RMS and the bias of the moisture products change with the TPW under the thin cloud conditions. Only the thin cloud cases are shown here because the low thick cloud cases are limited (less than 4 % of the cloud cases). From Figure 41 (d) and (f), the retrieval of PW1 and PW3 is not significantly affected by the total moisture content; the retrieval algorithm improves the first guess no matter what TPW is. For PW2 (Figure 41 (e)), if the atmosphere is dry or TPW is smaller than 30 mm, the retrieval algorithm improves the first guess. But, if the atmosphere is wet or TPW is larger than 40 mm, the retrieval algorithm fails to improve the first guess. This is consistent with the discussion in section 4.2.2 for thin clouds.

Figure 41 (b) shows how the RMS and the bias of the LI change with the TPW. It is interesting that the algorithm fails to improve LI when TPW is less than 20 mm. However, this is probably not significant for severe storm nowcasting, because most of the severe storms happen in the vicinity of areas with large TPW. Figure 42 shows the scatter plot of the density between the TPW and the LI, both of which are calculated from RAOB. When TPW is smaller than 20 mm, LI is almost always greater than 0. Although the improvement of LI is not significant, the increased coverage is of more importance.

4.2.4 Analysis of Retrieved Cloud Parameters

The cloudy algorithm retrieves not only the profile information in cloudy regions, but also the cloud parameters. In this section, an example of retrieved cloud parameters will be shown and interpreted with the help from the false RGB composite image. It should be noted that this section is not an attempt to validate CTP or phase product, as done by Hollars et al. (2004) and Hawkinson et al. (2005). More quantitative comparisons will be presented in the next section.

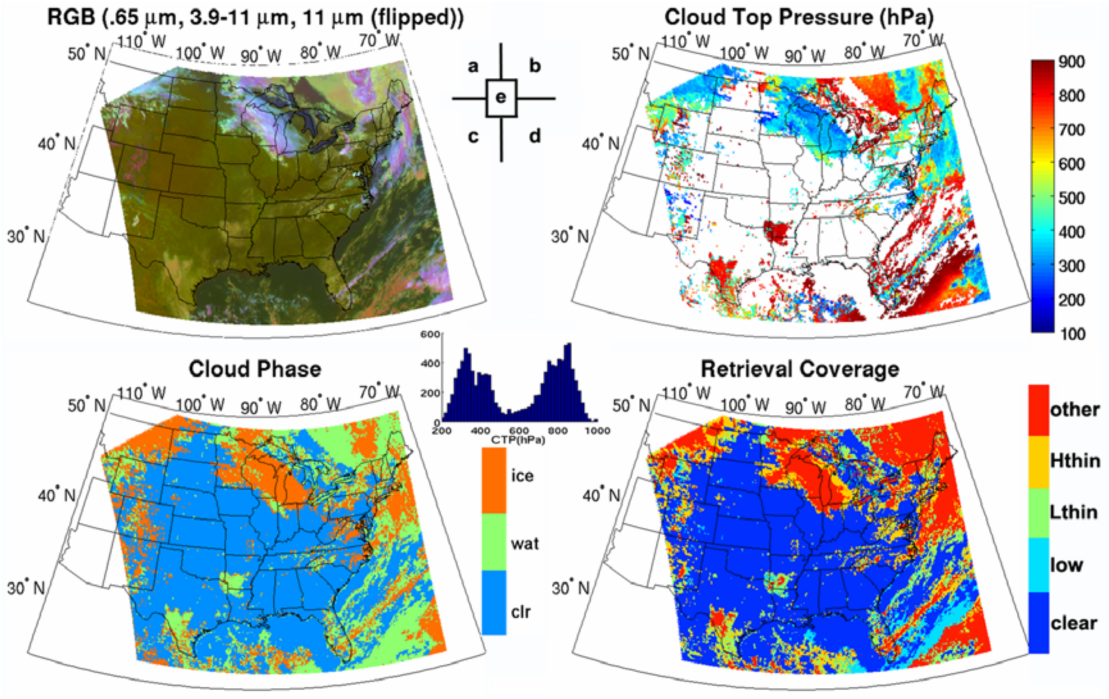

Figure 43. DPI of the retrieved cloud parameters at 18 UTC on 13 April 2006. a) The false color RGB image (R=0.65 μm, G=3.9-11 μm and B=11 μm flipped); b) the cloud top pressure; c) the cloud phase; d) the retrieval coverage; and e) the histogram of CTP of thin clouds. Lthin indicates thin clouds with CTP larger than 500 hPa, and Hthin indicates thin clouds with CTP smaller than 500 hPa.

Figure 43 shows the DPI of the retrieved cloud parameters at 18 UTC on 13 April 2006, or 4 hours before the outbreak of a severe thunderstorm with large hail and damaging downburst winds. Figure 43 (a) is the false RGB image using R = 0.65 μm, G = 3.9 - 11 μm and B = 11 μm flipped (note this is a daytime case). The clear sky is green with the water darker (sea) or bluer (great lakes) than the land. The orange or light yellow regions are low clouds. The pink or white areas are high clouds.

Figure 43 (b) shows the retrieved CTP. The high clouds appear blue while low clouds appear red in the image. The CTP values agree qualitatively with the RGB image. The thin cirrus clouds over the New Mexico, west Minnesota and central Michigan are retrieved with CTP less than 400 hPa. Some high clouds on top of the low clouds over the sea (Gulf of Mexico and to the east of Florida) are also identified correctly. Most of the low clouds have CTP larger than 700 hPa. There are two large low cumulus cloud regions over south Texas and southwest Arkansas; most have CTP greater than 700 hPa, but some appear to be well developed with CTP less than 500 hPa.

Most of the cloud phase (Figure 43 (c)) also agrees with the RGB image. But the algorithm underestimates the coverage by ice clouds. For example, both the RGB and the CTP show there is a cirrus cloud band extending from Florida to the east of Bahamas, but the cloud phase image shows it being ice clouds mixed with water clouds. The cloud phase determination is difficult in two situations. If the clouds are mixed phase or the ice (water) clouds are too low (high), the water and ice cloud retrieval might have comparable residuals, making it hard to determine the phase. If there are multiple-layer clouds and the cirrus clouds on the top are too thin, the algorithm will not be able to identify the thin cirrus clouds either.

Figure 43 (d) shows the additional coverage accomplished with cloudy soundings, reducing the non-retrieval area by 57 %. The low thick cloud retrievals (light blue) are those with the retrieved CTP larger than 850 hPa and the retrieved COT larger than 2.0. Most of them are over the sea. The thin cloud retrievals are those with the retrieved COT less than 2.0. The green color represents the low thin (Lthin) clouds with CTP larger than 500 hPa, and the yellow color represents the high thin (Hthin) clouds with CTP less than 500 hPa. Figure 43 (e) shows the histogram of these thin clouds. About half of them are Hthin (mostly thin cirrus clouds) with CTP less than 500 hPa. Others are mostly low clouds with CTP greater than 700 hPa. These clouds are mostly low broken clouds. As a result, they appear more scattered than the Hthin in Figure 43 (d). The “other” category in Figure 43 (d) includes clouds with COT larger than 2.0 and CTP less than 850 hPa, moisture retrievals in these cloud conditions were not validated in this study.

4.2.5 Comparison of GOES Sounder CTH with CALIPSO

In this section, the retrieved cloud top height (CTH), which is calculated from the CTP, is compared with the Cloud-Aerosol Lidar and Infrared Pathfinder Satellite Observations (CALIPSO) measurements. The operational CTP, which is derived using the CO_2-slicing method, is one of the GOES Sounder products assimilated into the RUC model.

The CALIPSO satellite (McGill et al., 2007; Winker et al., 2007) is one of the five satellites of NASA’s “A-train” constellation (Stephens et al., 2004). Leading by the Aqua satellite, the remaining A-train satellites include CloudSat, CALIPSO, PARASOL and Aura. The CloudSat lags Aqua by less than 120 seconds; the CALIPSO lags the CloudSat by 15 ± 2.5 seconds; the PARASOL lags CALIPSO by around 2 minutes; and AURA lags the PARASOL by 15 minutes. The A-train satellites fly in a 705 km Sun-synchronous orbit with a 1330 local time crossing equator, providing both active and passive measurements of the atmosphere and the earth surface.

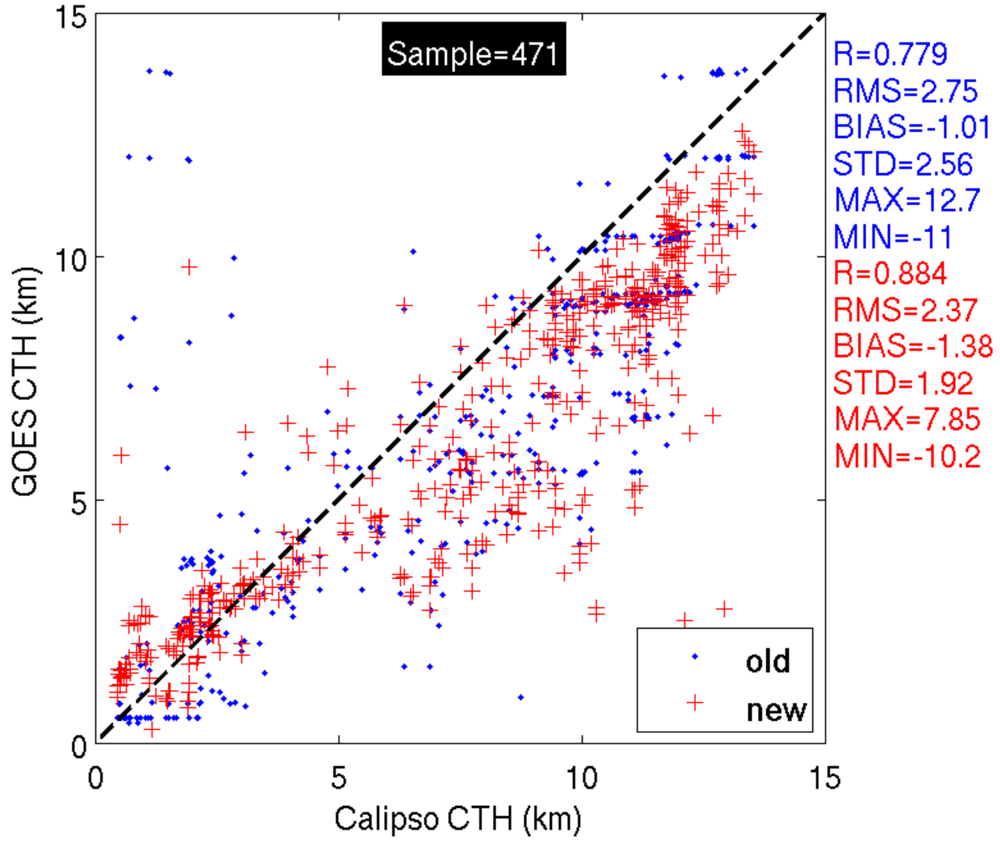

Figure 44. The scatter plots of the retrieved CTH from GOES-12 Sounder over the CONUS compared with the CALIPSO CTH, collected from 00 UTC of 13 April 2007 to 23 UTC of 14 April 2007. The blue dots are the old retrieved CTH, which is routinely run at CIMSS, and the red pluses are the new regression-based retrievals.

The CALIPSO satellite was launched on 28 April 2006 (Winker et al., 2007), and became operational on 7 June 2006. The primary payload aboard is the Cloud-Aerosol Lidar with Orthogonal Polarization (CALIOP), which is a dual wavelength (532 and 1064 nm), polarization-sensitive backscatter lidar that measures vertical profiles of clouds and aerosols. The backscattering signals provide information about optical properties of clouds and aerosols, and the depolarization measurements are used to determine the cloud phase. In this study, the lidar instrument refers to CALIOP on CALIPSO.

Both CALIPSO and CloudSat provide measurements of clouds. The lidar is more sensitive to small particles, and thus is able to detect thin cirrus clouds, tenuous cloud tops and aerosols. On the other hand, the Cloud Profile Radar (CPR) aboard CloudSat is able to penetrate the non-precipitating clouds, but has little sensitivity to thin cirrus. Therefore, a space borne lidar is able to provide vertical information through thin cirrus clouds and cloud tops of opaque clouds. Study shows that the CPR shows lower cloud tops than CALIPSO for thin cirrus clouds (Weisz et al., 2007). Similar as space borne lidars, the GOES Sounder, working at IR wavelength, is able to provide information about cloud tops, but has limited information about the vertical structure of the clouds.

The routinely produced CTP at CIMSS (Schreiner et al., 2001) is included in the comparison, and is referred as the old CTP. The old CTP is retrieved using the CO_2-slicing technique (Menzel et al., 1992; Menzel and Purdom 1994). The regression-generated CTP is referred as the new CTP. The CTP is converted to CTH using the NCEP GFS forecast temperature and moisture profiles. Figure 44 shows the scatter plots of the retrieved CTH as compared with the CALIPSO measured CTH, which is CALIPSO level-2 (version V2.01) products with 5 km horizontal resolution, from 0 UTC of 13 April 2007 to 23 UTC of 14 April 2007. Seven CALIPSO tracks are found within the GOES-12 Sounder viewing area. Totally, 1056 collocated samples are found, among which 471 are detected to be cloudy by both the GOES-12 Sounder and the CALIPSO.

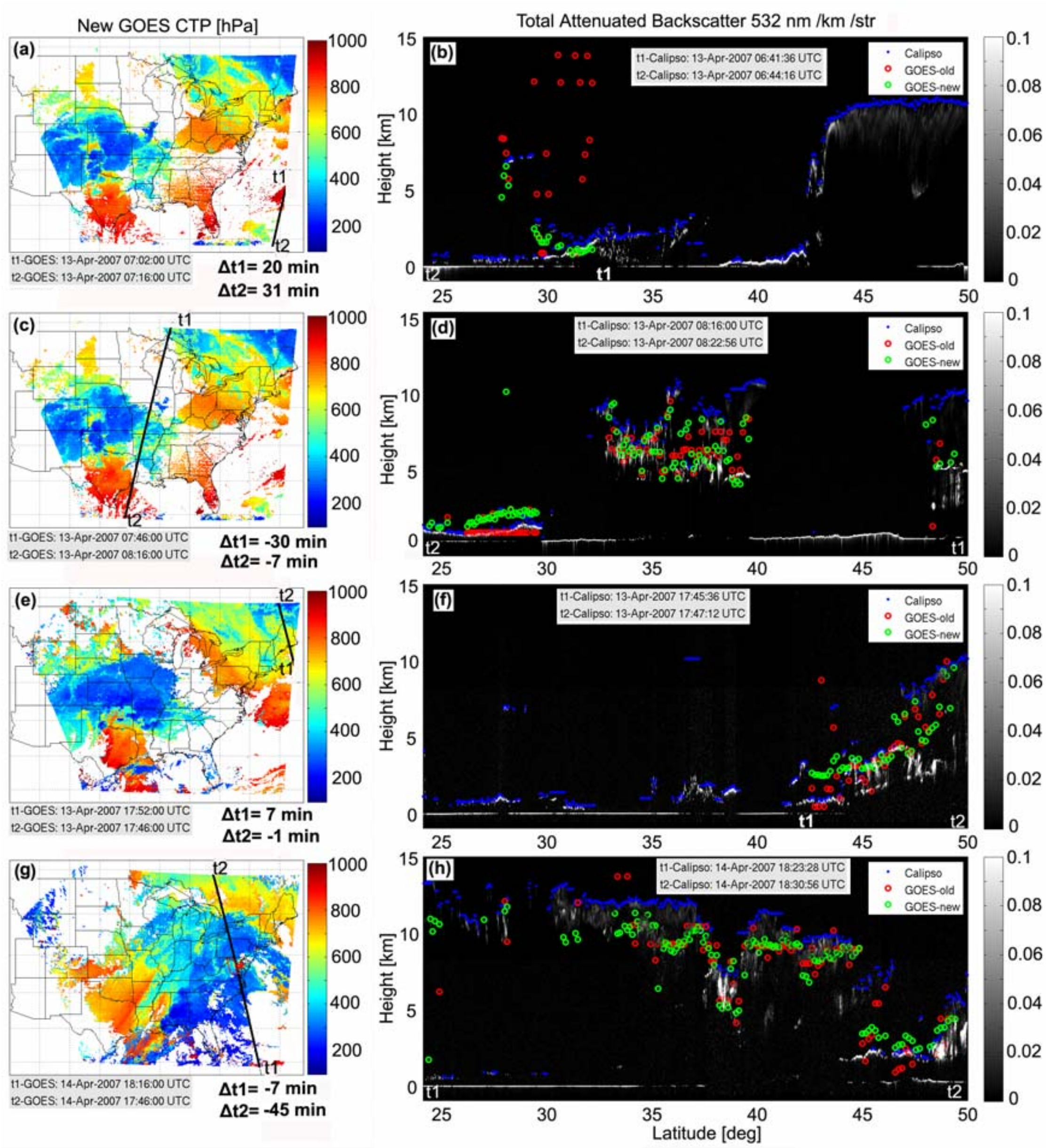

Figure 45. (left) The GOES-12 Sounder regression-retrieved CTP over the CONUS for (a) 07 UTC, (c) 08 UTC, (e) 18 UTC of 13 April 2007, and 18 UTC of 14 April 2007 with CALIPSO track (the black lines). (right) The corresponding CALIPSO 532 nm total attenuated backscatter /km/steradian with overlapped CTH from the CALIPSO (blue dots), the old GOES retrievals (red circles), and the new GOES retrievals (green circles).

"t1" refers to the starting point, and "t2" refers to the ending point. The approximate scanning time of GOES-12 Sounder and CALIPSO are provided. Δt is the approximate time difference and is defined as GOES scanning time minus CALIPSO scanning time.

From Figure 44, both the old and the new methods agree with CALIPSO measurements well. It appears the new retrievals show slightly better results than the old retrievals; the correlation coefficient is increased from 0.779 to 0.884; the RMS is reduced from 2.75 km to 2.37 km; and the STD is reduced from 2.56 km to 1.92 km. The results here are similar, if not better, to the study by Weisz et al., (2007). In their study, the AIRS retrieved CTH has an STD of 2.9 km, and the MODIS retrieval has an STD of 3.2 km, as compared with CALIPSO. It is noted that AIRS has much better spectral resolution and MODIS has much better spatial resolution than the GOES Sounder. More importantly, the temporal difference between AIRS/MODIS and CALIPSO is less than 3 minutes. It will be shown later that the temporal difference sometimes has significant impacts on the comparison.

Although the results in Figure 44 are encouraging, there are still many FOVs that either the old or the new method has difficulty to quantify the CTH. Most of the low clouds (defined as CTH smaller than 5 km) are retrieved with CTH within 3 km difference from the CALIPSO, but some of them are misidentified as high-level clouds with CTH much larger than 5 km, especially by the CO_2-slicing technique. The difficulty of retrieving low-level clouds relies on the fact that the presence of low clouds does not affect the IR radiance too much due to the small temperature contrast between the cloud top and the surface. Most of the high clouds (defined as CTH larger than 5 km in this section) are retrieved with CTH lower than the CALIPSO. This is mainly because CALIPSO is more sensitive to small particles, and the GOES Sounder has much less sensitivity. Therefore, cirrus clouds are usually retrieved with CTH lower than those measured by airborne lidars (Weisz et al., 2007; Hawkinson et al., 2005). For clouds with CTH higher than 12 km, the retrievals show much better agreement, although still lower CTH, with the CALIPSO measurements.

There are a few other reasons that could cause the discrepancies between the retrieved CTH and the CALIPSO. First, both the regression algorithm and the CO_2-slicing are based on the assumption of single-layer cloud, and their performances on two or more layers of clouds are limited. When there are two layers of clouds, the received radiance has information from both layers. Depending on the optical thickness of the two layers, the retrieved CTH reflects the effective cloud-top and could be close to top layer cloud top, or the lower-level cloud top or somewhere in between. In Figure 45 (d) between 48° N and 50° N, there are very thin cirrus clouds (very weak signals in the total attenuated backscatter) on top of the thick lower-layer clouds; the retrieved CTH is close to the lower-level cloud top. When the thin cirrus clouds are on the top of another layer of thin clouds, the lower-level clouds have fewer impacts on the CTH retrieval, and the retrieved CTH is close to the top cirrus cloud top (Figure 45 (f) 49° – 50° N and Figure 45 (h) 44° – 45° N).

One of the more difficult situations of multi-layer clouds is in Figure 45 (b) in 29° – 32° N. The lower-layer clouds are well identified by the total attenuated backscatter. The CALIPSO CTH shows there are another level of clouds on top of the low clouds.

Some of them could be recognized by the total attenuated backscatter, while others are hard to see. While the new retrieval method successfully finds the CTH between the top cloud top and the lower cloud top, the old CO_2-slicing method misidentifies these clouds as high clouds. This is the main reason the new retrievals show slightly better RMS, STD and correlation coefficient than the old retrievals in Figure 44. In fact, if removing these FOVs from the comparison, the STD is 1.78 km and 1.84 km for the old and the new retrievals. Therefore, it is concluded that the new regression method is comparable to the old CO_2-slicing method in terms of CTH retrieval.

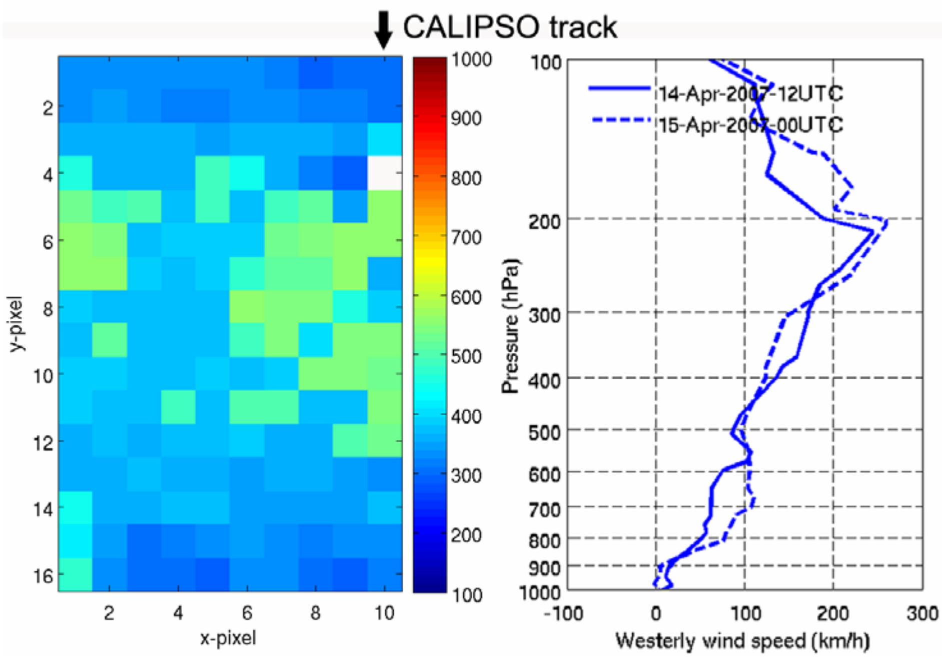

Figure 46. (left) The retrieved cloud top pressure of zoom-in of the red rectangle in Figure 45 (g). The right end column is the collocated CALIPSO track. (right) The RAOB westerly wind speed from 12 UTC of April 24 and 00 UTC of April 25 2007.

Secondly, the scanning time difference between the GOES-12 Sounder and the CALIPSO could cause large discrepancies between the retrieved CTH and the CALIPSO. In Figure 45 for each case, the approximate starting (t1) and ending (t2) time of GOES-12 Sounder and CALIPSO are provided. The time differences at the starting (Δt1) and the ending (Δt2) points are also shown (GOES minus CALIPSO); positive time difference indicates CALIPSO measures earlier than the GOES-12 Sounder. For cases shown in Figure 45, the time difference could be as large as 45 minutes. Since cloud tops are highly variable horizontally, vertically and temporally, large time difference may cause large discrepancies between the retrieved CTH and the CALIPSO unless the clouds are horizontally homogeneous, at least along the wind direction.

In Figure 45 (h), most of the CTH are reasonably retrieved except for the clouds around the latitude of 38° N. For these thick clouds (because of the strong total attenuated backscatter), the retrieval algorithm should be able to quantify the CTH. However, some of the CTH retrievals from both the new and the old method are much lower than the CALIPSO CTH. This large discrepancy is actually because of the time difference between CALIPSO and GOES-12 Sounder. Around this location (the red rectangle area in Figure 45 (g)), the time difference is about -30 minutes, which means the CALIPSO observation is 30 minutes later than the GOES-12 Sounder. A zoom-in image of the red rectangle area is shown in Figure 46 (a). The right-end column (x-pixel = 10) is the CALIPSO track. There are 6 (2+4) FOVs with the retrieved CTP larger than 500 hPa. These are the FOVs with the retrieved CTH much lower than the CALIPSO around the latitude of 38° N in Figure 46 (h).

The prevailing winds around this area are westerly. Figure 46 (b) shows the westerly wind speed from RAOB (the red star in Figure 46 (g) denotes the RAOB location) at 12 UTC of 14 April 2007 and 00 UTC of 15 April 2007. The wind speed is around 140 km/h between 300 and 400 hPa, and around 100 km/h between 400 and 600 hPa. Most clouds in Figure 46 (a) are between 300 and 600 hPa. For 30 minutes (the CALIPSO observation is 30 minutes later than the GOES-12 Sounder), these clouds could move eastwardly for 50 - 70 km or 5 – 7 FOVs. Therefore, the clouds that the CALIPSO observed should be originally from the 5 – 7 FOVs away from the west or from FOVs with x-pixel between 3 and 5. In Figure 46 (a), these clouds have CTP 350 - 400 hPa or CTH 7.5 – 8 km, and are the actual clouds observed by the CALIPSO. This is consistent with the CALIPSO measurements in Figure 45 (h). In this case, clouds do not have much vertical variation, which typically will cause the problem more complicated. The time difference between the CALIPSO and the GOES-12 Sounder is not important if cloud tops are homogeneous zonally or along the wind direction.

4.3 Applications to Short-term Severe Storms

In this section, two cases will be presented to demonstrate how the GOES cloudy soundings and the derived products could be useful in short-term severe storm nowcasting. The first one, or the Texas tornado case, is used to demonstrate how the cloudy soundings and the derived products can help provide early warnings to forecasters. In the second case, the GOES derived products will be used to help avoid a severe storm forecast bust.

4.3.1 The Tornadic Storm at Eagle Pass, Texas on 24 April 2007

The GOES-12 Sounder IR imagery around Eagle Pass, Texas on 24 April 2007 reveal three individual storms within six hours. The first storm, a supercell, initialized around 2015 UTC; the second storm happened between 2200 and 2300 UTC to the north of the supercell; and the third storm (not shown) happened between 0100 and 0200 UTC of the next day to the west of the supercell. A tornado was observed within the supercell around 00 UTC on 25 April 2007 at Eagle Pass, Texas. This EF-3 tornado killed 10 people in Mexico and the United States with another 120 injured. Li et al., 2008 demonstrated that clear-sky GOES soundings improve the first guess of the GFS forecast for this storm.

Figure 47 shows the results of the time sequence of the lifted index (LI) retrieved from clear and some cloudy FOVs. From the top to bottom are LI images at 20, 21, 22 and 23 UTC (Figure 47 (1) – (4)). From the left to right are LI images from NCEP GFS forecast, the Rapid Update Cycle (RUC, Benjamin et al., 2004) 6-hour forecast, GOES-12 clear-sky retrievals and GOES-12 clear plus cloudy retrievals (Figure 47 (a) – (d)). The retrievals are indicated by LI values, with different colors representing different values. Otherwise, 11 μm Tb values are shown, most of which are in cloudy regions with COT greater than 2.

The regional model, RUC, performs better than the coarse global model, GFS, on this severe storm case. During the 4 hours, the GFS forecast model failed to predict the convective instability surrounding the supercell, while the RUC successfully did so. The locations of the convective instability are to the southeast or southwest of the convective storms, as expected from the prevailing wind flow.

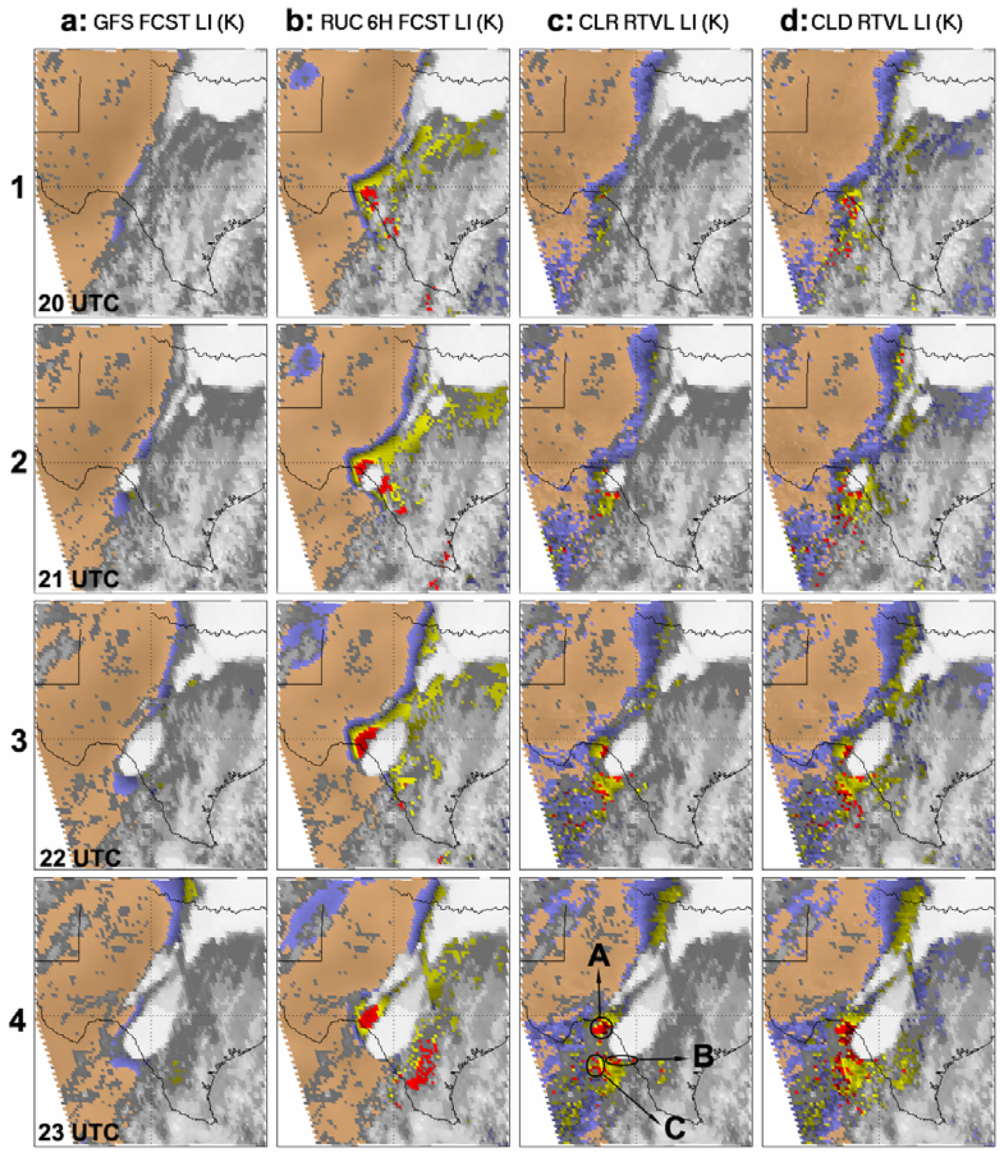

Figure 47. Time series of LI imagery on 24 April 2007. From top to bottom are 1) 20 UTC, 2) 21 UTC, 3) 22 UTC and 4) 23 UTC. From the left to the right are a) the GFS forecast, b) the RUC 6-hour forecast, c) GOES-12 clear-sky retrievals and d) GOES-12 clear plus cloudy retrievals. Note the two areas A and B are each associated with an individual convective storms. The area C will trigger and support the third storm between 01 and 02 UTC on 25 April 2007.

The clear-sky retrievals (Figure 47 (c)) successfully identify three large areas of instabilities. As shown in Figure 47 (4c), area A is located to the northwest of the supercell, area B is located to the south of the supercell, and area C is located to the southwest of the supercell. Each of these areas is associated with convective activity. The clear plus cloudy retrievals (Figure 47 (d)) have better coverage than the clear-sky retrievals; more convective instability is found in areas B and C. More importantly, before the clear-sky retrievals indicate any large instability areas, the cloudy retrievals have identified some areas in the cloudy regions. The earliest convective instability revealed by the clear plus cloudy retrievals was around 19 UTC or about 75 minutes before the super cell outbreak.

The RUC 6-hour forecast appears to have a similar performance as the clear plus cloudy retrievals (comparing Figure 47 (b) with (d)); both reveal the convective instability in area A. These instabilities are associated with the second convective storm. Careful examination reveals that the RUC differs from the clear plus cloudy retrievals to the south of the supercell. Both the clear and the cloudy retrievals identify areas B and C consistently and continuously. The RUC picks up area B at 20 and 21 UTC, but it fails completely at 22 UTC in Figure 47 (3b). And the instabilities at 23 UTC in Figure 47 (4b) are too far away from the supercell. The RUC completely misses area C, which is associated with the third convective storm. It is not until the outbreak of the third convective storm that the RUC picks up area C (not shown). The GOES-12 Sounder provides additional useful information beyond the RUC for the forecasters in this severe storm case. According to Benjamin et al. (2004), high-frequency moisture observations above the surface used in the RUC analysis are

TPW (and CTP) from satellites (such as GOES Sounder, Special Sensor Microwave Imager and GPS). The disadvantage of these observations is lack of vertical information. As a result, it is hard for RUC to predict when and where a storm is likely to form.

4.3.2 A Busted Forecast in Texas on 13 April 2007

At 12 UTC on 13 April 2007, the NWS SPC issued a moderate (MDT) risk of severe weather over portions of North Central, Northeast Texas, Southern Arkansas and Northern Louisiana (area covered by the red line in Figure 48). At 20 UTC, the moderate risk is upgraded to high risk (HIGH) (area covered by the pink line in Figure 48).

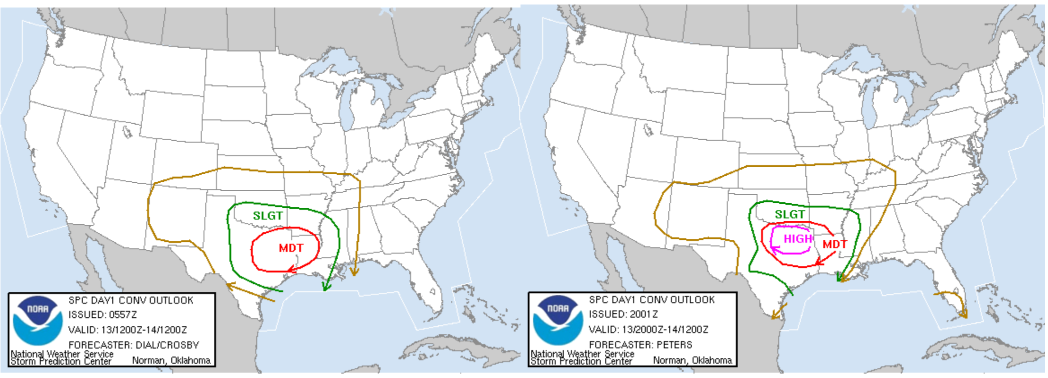

Figure 48. The convective outlook issued by NWS SPC at (left) 12 UTC on 13 April 2007 and (right) 20 UTC on 13 April 2007.

According to SPC, there are three categories of severe storms. A slight risk (SLGT) implies well-organized severe thunderstorms are expected, but in small numbers and/or low coverage. Depending on the size of the area, approximately 5 - 25 reports of 3/4 inch of larger hail, and/or 5 - 25 wind events, and/or 1 - 5 tornadoes would be possible. A MDT risk indicates a potential for a greater concentration of severe thunderstorms than the slight risk, and in most situations, greater magnitude of the severe weather. A HIGH risk area suggests a major severe weather outbreak is expected, with a high concentration of severe weather reports and an enhanced likelihood of extreme severe (i.e., violent tornadoes or very damaging convective wind events occurring across a large area). In a high risk, the potential exists for 20 or more tornadoes, some possibly F2 or stronger, or an extreme derecho potentially causing widespread wind damage and higher end wind gusts (80+ mph) that may result in structural damage.

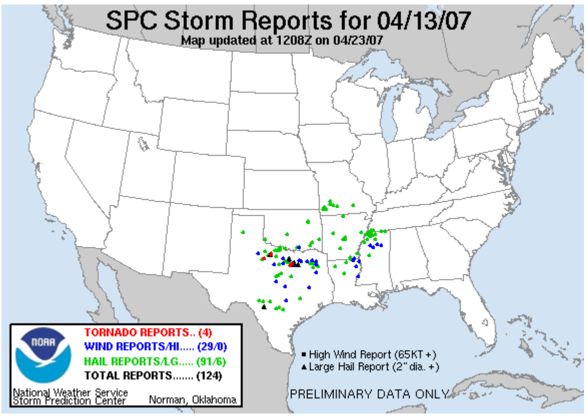

Figure 49. Storm reports on 13 April 2007 from NWS SPC

Figure 49 shows the storm reports provided by SPC. There are only 4 confirmed tornado reports and no single report of wind speed larger than 130 km/h (http://www.spc.noaa.gov/climo/online/). These reports indicate that the previous high risk of severe storm forecast was wrong. In this case, the derived LI and TPW from the GOES-12 sounding retrievals will be compared with the RUC 6-hour forecast and GFS forecast to show how the GOES sounding retrievals and the derived products could be useful in such a situation.

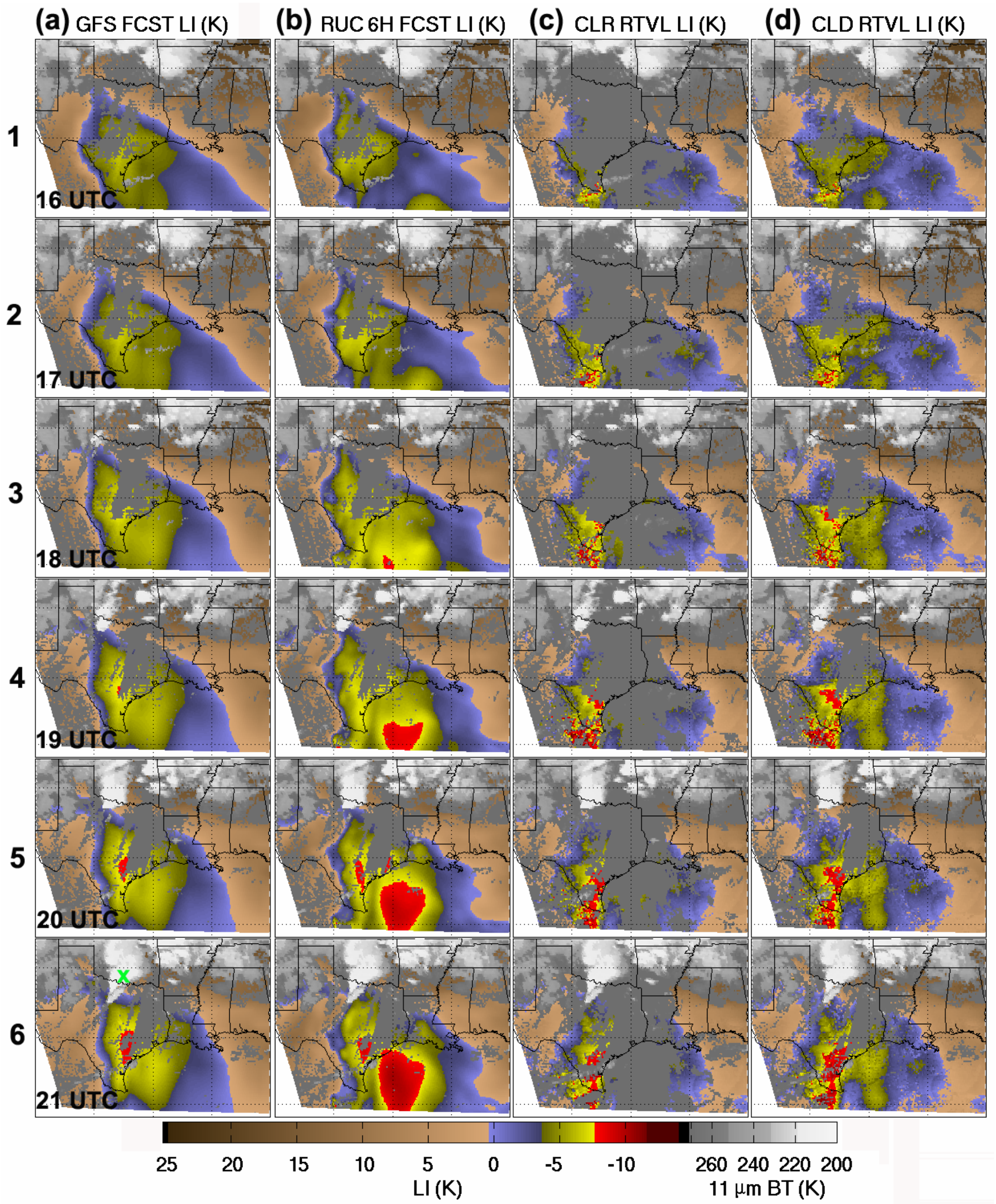

Figure 50. Time series of LI imagery on 13 April 2007. From top to bottom are 1) 16 UTC, 2) 17 UTC, 3) 18 UTC, 4) 19 UTC, 5) 20 UTC and 6) 21 UTC. From the left to the right are a) the GFS forecast, b) the RUC 6-hour forecast, c) GOES-12 clear-sky retrievals and d) GOES-12 clear plus cloudy retrievals.

Figure 50 shows the time sequence of the LI imagery. From the top to bottom are LI images at 16, 17, 18, 19, 20 and 21 UTC (Figure 50 (1) – (6)). From the left to right are LI images from NCEP GFS forecast, the RUC (Benjamin et al., 2004) 6-hour forecast, GOES-12 clear-sky retrievals and GOES-12 clear plus cloudy retrievals (Figure 50 (a) – (d)). The retrievals are indicated by LI values, with different colors representing different values. Otherwise, 11 μm Tb values are shown, most of which are in cloudy regions with COT greater than 2.

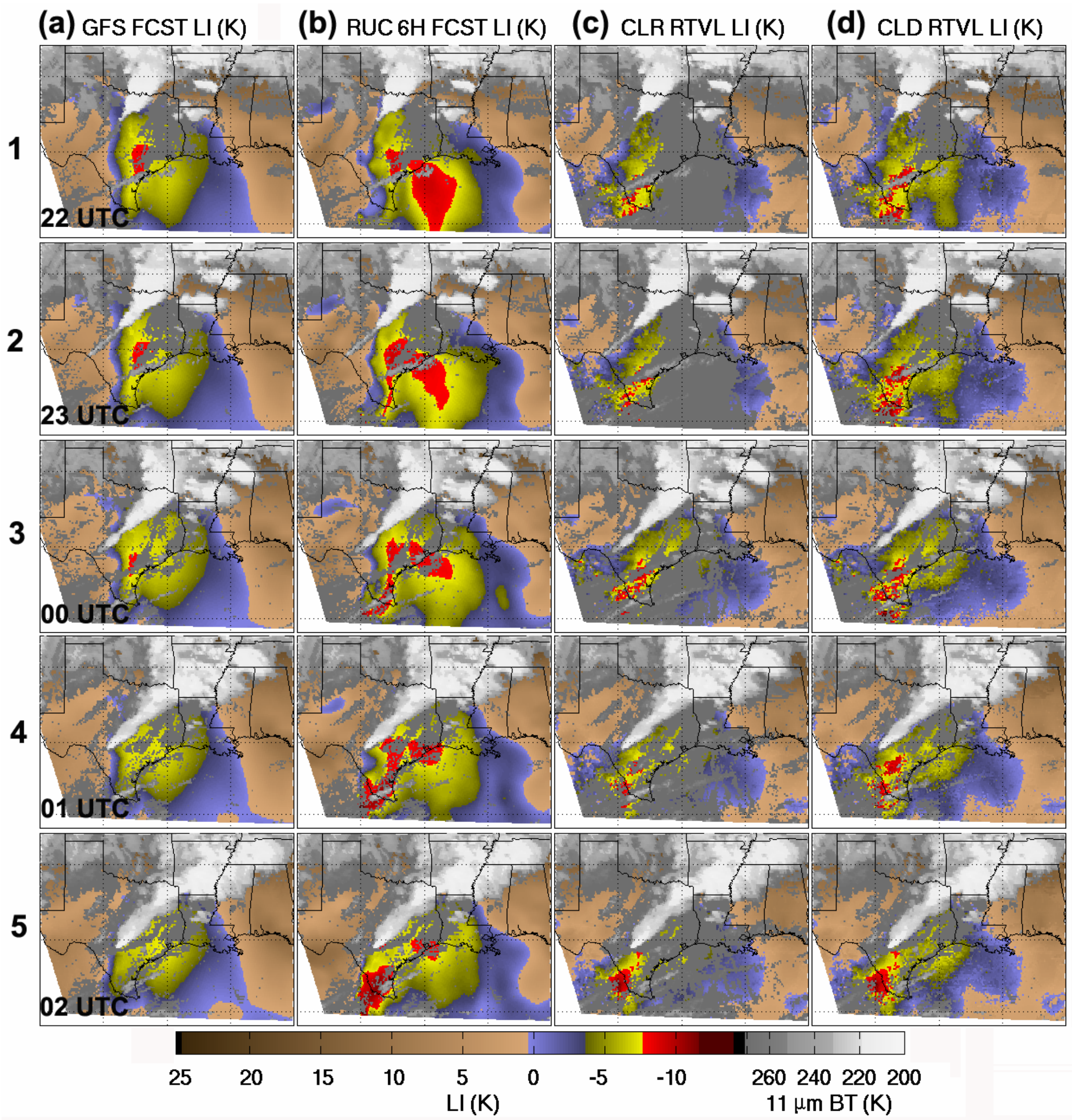

Figure 51. Same as Figure 50 except for 22, 23, 00, 01 and 02 UTC.

In this case, the GOES sounding retrievals again show earlier warning than the RUC 6 hour forecast and the GFS forecast. Large instabilities smaller than -7.5 K (reds) are revealed at 16 and 17 UTC. The GOES Imager animation (http://www-angler.larc.nasa.gov/armsgp/g8usa.html/) shows the outbreak of the storm occurring around 18 UTC. That gave two hours of early warning compared with GFS forecast and RUC 6-hour forecast. Although the GOES cloudy sounding retrievals do not reveal more large instabilities than the clear-sky ones during the first two hours, it does so in the later times. More importantly, the cloudy sounding retrievals significantly increase the coverage of the GOES-12 sounding products.

After the outbreak of the storm (the green X in Figure 50 (6a) along the boundary between Texas and Oklahoma) around 18 UTC, the RUC successfully predicted the large instabilities to the south of the storm. During the next two hours (20 and 21 UTC), both the RUC 6-hour forecast and the GOES sounding retrievals reveal that the large instabilities (reds) are to the south of the storm and are about 300 km away from the storm.

Figure 51 shows the time sequence of the LI imagery from 22 UTC to 02 UTC. During these five hours, the RUC 6-hour forecast reveals more instabilities than the GOES sounding retrievals. And the RUC instabilities are much closer to the storm. These instability differences probably are associated with the weak development of the storm. The weather map (not shown) at 00 UTC on 14 April 2007 shows the wind speed in the lower troposphere (850 hPa) around the instabilities in Figure 51 (d) is only 15 – 32 km/h. Therefore, these instabilities only have limited impact on the development of the storm.

Figure 52 shows the time sequence of the TPW imagery from 16 UTC to 21 UTC.

From the top to bottom are TPW images at 16, 17, 18, 19, 20 and 21 UTC (Figure 52 (1) – (6)). From the left to right are TPW images from NCEP GFS forecast, the RUC 6-hour forecast, the GOES-12 Sounder clear plus cloudy retrievals, and the difference between the GOES-12 Sounder retrievals and the RUC 6-hour forecast (former minus latter) (Figure 52 (a) – (d)). The retrievals are indicated by TPW values, with different colors representing different values. Otherwise, 11 μm Tb values are shown, most of which are in cloudy regions with COT greater than 2.

From Figure 52 (a, b and c), the moisture path associated with the storm is from the south (the Gulf of Mexico) to the north (southeast Texas), and the dryline relies in the middle of Texas parallel and to the west of the moisture path. Although the three TPW products look similar in both spatial distribution and magnitude, careful examination reveals that the GOES-12 sounding retrievals show weaker moisture gradients than the RUC forecast in the vicinity of dryline environment. This is even more significant in Figure 52 d. Throughout the 6 hours, the GOES-12 sounding retrievals show more moisture than the RUC forecast to the west of the dryline (see the vertical color bar). Differences as large as 5 mm are widely observed. In some areas, the differences are over 7.5 mm. To the east of the dryline within the moisture path, the retrievals show less moisture than the RUC forecast. Except around 17, 18 and 19 UTC over the Gulf of Mexico, where the retrievals show slightly more moisture (about 0-4 mm) than the RUC forecast, in other areas within the moisture path, the retrievals show less moisture than the RUC forecast. Especially in areas close to the storm, differences as large as 7.5 mm are found. In some area, the differences are over 10 mm.

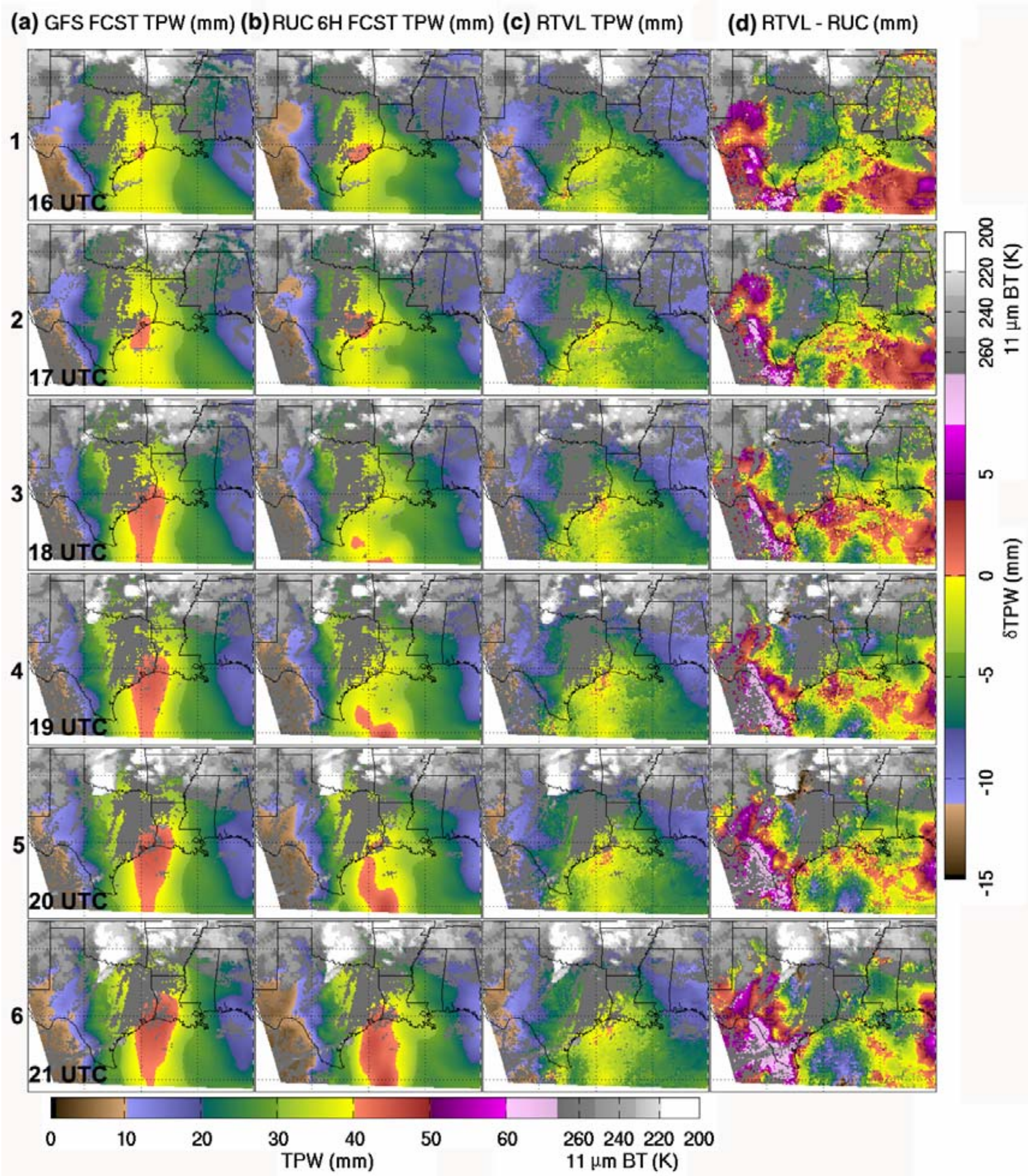

Figure 52. Time series of TPW imagery on 13 April 2007. From top to bottom are TPW images at 1) 16 UTC, 2) 17 UTC, 3) 18 UTC, 4) 19 UTC, 5) 20 UTC and 6) 21 UTC. From the left to the right are TPW images from a) the GFS forecast, b) the RUC 6-hour forecast, c) GOES-12 clear plus cloudy retrievals and d) the difference between (c) and (b) (c-b). The horizontal color bar is for (a), (b) and (c). The vertical color bar is for (d).

More moisture to the west and less moisture to the east of the dryline indicate the weaker moisture gradients along the dryline. Considering the TPW retrieval error is about 2.4 mm, these differences between the GOES-12 sounding retrievals and the RUC forecast are strong signals indicating a possibly weak development of the storm. Additionally, less moisture in the moisture path (much less moisture closer to the storm) as revealed by the GOES-12 sounding retrievals results in less moisture transported into the storm. All of the differences between the RUC forecast and the GOES-12 sounding products indicate the storm might not be able to develop to a high risk severe storm.

4.4 Summary

The large probability that a GOES Sounder measurement is affected by clouds prompted this study to extend the clear-sky retrievals to cloudy regions. A synthetic regression-based cloudy retrieval algorithm is developed and applied to GOES-12 Sounder radiance measurements. To complement the limited profile information from GOES-12 Sounder's first 15 IR channels, the GFS forecast profiles, and hourly surface observations are included as predictors.

Cloudy retrievals are attempted in a) thin clouds, defined as having cloud optical thickness (COT) <= 2.0, and b) low thick clouds, defined as having cloud top pressure (CTP) >= 850 and COT >=2.0.

Comparisons with the RAOBs at the ARM SGP site from August 2006 to May 2007 and the conventional RAOBs from January 2007 to November 2008 show that under thin cloud conditions moisture retrievals are of similar quality to clear-sky retrievals. The largest improvements are found in the upper atmosphere; the RMS is reduced by 0.4 mm. Going down to the middle troposphere, the improvements diminish. However, in the boundary layer, the moisture retrieval is usually improved with the help from the surface observations.

The low thick clouds have a different impact. The opaqueness of low thick clouds blocks the radiation from below the clouds. As a result, the boundary layer moisture is hardly improved, even with the help of hourly surface observations. However, the weighting functions above the cloud top are sharpened. Together with the fact that the atmosphere is usually dry under the low thick cloud conditions, both the middle and upper troposphere moisture retrievals are improved; the RMS is reduced by 0.21 mm for PW3, and by 0.38 mm for PW2.

The retrieved cloud parameters compare well with the false RGB (0.65 μm, 3.9 - 11 μm and 11 μm flipped) image; the high clouds have small CTP and are classified as ice clouds and the low clouds have large CTP and are classified as water clouds. The additional sounding retrievals in low thick clouds and thin clouds reduce the non-retrieval area by 57 % in the selected case.

The regression retrieved CTH from 00 UTC on 13 April 2007 to 23 UTC on 14 April 2007, together with the routinely produced CTH using the CO_2-slicing technique, is compared with CALIPSO measurements. The regression technique shows a comparable performance to the CO_2-slicing technique, both of which agree well (within +/- 2.75 Km) with the CALIPSO measurements.

The cloudy retrieval algorithm was applied to a tornadic severe storm case on 24

April 2007; the cloudy retrievals were especially useful during the early stages of the storms, when the nearby clouds were usually broken/low/thin clouds. There are three areas of convective instability in this case, which are associated with subsequent activity. The clear-sky retrievals are able to identify the three areas, but the additional cloudy retrievals improve the early identification with more pronounced and extensive instability in the three areas. These earlier and stronger warnings should be important for forecasters.

While the Rapid Update Cycle (RUC) forecast model reveals more convective instability than the GFS model on this severe storm case, the retrievals, both in clear and cloudy skies, locate the convective instability more accurately to the south (or southeast/southwest) of the individual storms. These results are especially encouraging considering that some of the operational GOES Sounder products (clear-sky TPW and CTP) are already assimilated into the RUC.

At 20 UTC on 13 April 2007, a high risk of severe weather was issued by the NWS SPC. It turned out to be a forecast bust; the storms never developed as severely as expected. The GOES-12 sounding retrievals again show an earlier warning of about two hours than the GFS and the RUC 6 hour forecast before the initial storm outbreak. After the outbreak, comparisons show that the retrievals reveal fewer storm related instabilities than the RUC 6 hour forecast, and these instabilities are too far away from the storm to have significant impact. In addition, the GOES sounding retrievals show weaker moisture gradients along the dryline, and less moisture in the moisture path than the RUC forecast. All of these differences between retrievals and forecast are useful information for forecasters regarding the weak development of the storms.

Overall, the results presented in this section promising. For forecasters, the new cloudy retrievals can provide nowcasting products with better coverage for monitoring weather development. For modelers, the retrieved cloud parameters, as well as the profile information, should be additional useful input to NWP models.

Chapter 5 Conclusions and Future Perspectives

A unique feature of the GOES Sounder over the POES sounders is that it observes the atmosphere and the surface on an hourly basis with a nominal spatial resolution of 10 km. The temporally and spatially dense observations are of great importance for short-term severe storm forecasting. In this thesis, an improved clear-sky physical retrieval algorithm for atmospheric temperature and moisture is applied to the GOES-12 Sounder.

A comparison with the microwave radiometer measured TPW at the Southern Great Plains (SGP) Cloud and Radiation Testbed (CART) site from June 2003 to May 2005 shows that the clear sky TPW retrievals are improved by 0.4 mm over the legacy GOES Sounder TPW product. The derived lifted index (LI) product from the improved soundings better depicts the pre-convective environment surrounding a tornadic supercell at Eagle Pass, Texas on 24 April 2007. Application to the severe storm case of 13 April 2006 demonstrates that the improved physical algorithm successfully detects low-level moisture. Both cases show that the new retrievals along with the derived products could help the forecasters with short-term severe storm nowcasting.

The use of the GOES Sounder is usually limited to clear skies to avoid cloud contamination. However, the chance for a GOES Sounder FOV to be clear is only about 34 %. Until the advent of a microwave sounder in geostationary orbit, the search for viable soundings in cloudy conditions will continue. In an effort to extend the high temporal resolution GOES sounding retrievals from clear to cloudy skies, a synthetic regression-based cloudy sounding retrieval algorithm has been developed. This thesis presents some successful soundings in thin as well as low thick clouds.

Comparisons against radiosondes at SGP CART site from August 2006 to May 2007 and the conventional radiosonde network over the Continental United States (CONUS) from January 2007 to November 2008 both show the retrievals of moisture under thin cloud conditions perform as well as those with the clear sky conditions. The largest improvement to the GFS first guess is found in the upper level (roughly 300 – 700 hPa) integrated precipitable water vapor (PW) or PW3; the RMS is reduced by 0.4 mm. Also in the case of low thick clouds, PW3 is usually improved significantly (the improvement of RMS is about 0.21 mm). In addition, the retrieved cloud parameters are consistent with the false RGB composite image for the selected case. The retrieved CTH from 0 UTC on 13 April 2007 to 23 UTC on 14 April 2007 shows a good agreement with the CALIPSO measurements. With the addition of the soundings under thin cloud as well as low thick cloud conditions, the area without soundings is reduced by 57 % in the selected case.

The application to a tornadic storm on 24 April 2007 reveals that the GOES cloudy sounding retrievals are more useful during the early stage of the storm development, when nearby clouds are considered thin or broken. The GOES cloudy sounding algorithm reveals more pronounced and extensive convective instability, and it does so earlier than the clear-sky only results. In a busted forecast for a high risk of severe weather for 13 - 14 April 2007, the storm reports by SPC show much less severity than expected. The GOES sounding retrievals, as compared with the RUC 6-hour forecast, reveal much weaker moisture gradients along the dryline. The instabilities are found far away from the storms, and the moisture path is found to be much weaker than the RUC 6-hour forecast. With these derived products from the GOES-12 Sounder, the forecasters should be able to improve the forecast in such a situation.

The results presented in this study demonstrate that the hourly measurements from the current GOES Sounder with 10 km nominal spatial resolution can improve short term weather forecast. However, there is considerable room for additional improvement because of the limited vertical resolution and slow scan rate. Hyperspectral IR sounders, such as AIRS and the Infrared Atmospheric Sounding Interferometer (IASI) onboard METOP-A (Phulpin et al., 2007) are an advancement over the traditional broad band IR sounders with much finer spectral resolution and more complete spectral coverage. Both increase the vertical resolving power for deriving temperature and moisture profiles (Wang et al., 2007). But, the polar-orbiting hyperspectral IR sounders do not have the temporal resolution necessary for severe storm nowcasting. A geostationary advanced IR sounder is needed for regional model forecasting, severe storm forecasting and nowcasting. Simulation studies have shown that the temperature and moisture retrievals with a geostationary hyperspectral sounder far exceed those from the current low spectral resolution GOES Sounder (Schmit et al., 2009). It is therefore expected that future geostationary hyperspectral sounders will further improve the short term weather forecasting.

References

Benjamin, S.G., D. Devenyi, S.S. Weygandt, K.J. Brundage, J.M. Brown, G.A. Grell, D. Kim, B.E. Schwartz, T.G. Smirnova, T.L. Smith, and G.S. Manikin, 2004: An Hourly Assimilation-Forecast Cycle: The RUC, Monthly Weather Review, 132, 2, 495-518.

Bevis, M., S. Businger, T. A. Herring, C. Rocken, R. A. Anthes, and R. H. Ware, 1992: GPS meteorology: Remote sensing of atmospheric water vapor using the global positioning system. Journal of Geophysical Research, D.Atmospheres 97, 15 787–15 801.

Birkenheuer, D., and S. Gutman, 2005: A comparison of the GOES moisture-derived product and GPS-IPW during IHOP. Journal of Atmospheric and Oceanic Technology. 22, 1838-1845.

Borbas, E., S., Seemann, H.-L. Huang, J. Li, and W. P. Menzel, 2005: Global profile training database for satellite regression retrievals with estimates of skin temperature and emissivity, 14th International ATOVS Study Conference, NASA, Beijing.

Carrier, M., X. Zou, and W. M. Lapenta, 2007: Identifying Cloud-Uncontaminated AIRS Spectra from Cloudy FOV Based on Cloud-Top Pressure and Weighting Functions, Monthly Weather Review, 135, 6, 2278-2294.

Chang, F. and Z. Li, 2005: A Near-Global Climatology of Single-Layer and Overlapped Clouds and Their Optical Properties Retrieved from Terra/MODIS Data Using a New Algorithm, Journal of Climate, 18, 22, 4752-4771.

Chevallier, F., P. Bauer, J.-F. Mahfouf, and J.-J. Morcrette, 2002: Variational retrieval of cloud profile from ATOVS observations, Quarterly Journal of the Royal Meteorological Society, 128, 585, 2511-2525.

Cho, C. and D.H. Staelin, 2006: Cloud clearing of Atmospheric Infrared Sounder hyperspectral infrared radiances using stochastic methods, Journal of Geophysical Research.D.Atmospheres, 111, D9.

Claud, C., N.A. Scott, A. Chedin, and J. Gascard,, 1991: Assessment of the accuracy of atmospheric temperature profiles retrieved from TOVS observations by the 3I method in the European Arctic; application for mesoscale weather analysis, Journal of Geophysical Research, Washington, DC, 96, D2, 2875-2887.

Clough, S.A. and M.J. Iacono, 1995: Line-by-line calculations of atmospheric fluxes and cooling rates. 2: Applications to carbon dioxide, ozone, methane, nitrous oxide and the halocarbons. Journal of Geophysical Research, 100, 16519-16535.

Divakarla, M.G., C.D. Barnet, M.D. Goldberg, L.M. McMillin, E. Maddy, W. Wolf, L. Zhou, and X. Liu, 2006: Validation of Atmospheric Infrared Sounder temperature and water vapor retrievals with matched radiosonde measurements and forecasts, Journal of Geophysical Research.D.Atmospheres, 111, D9.

Dostalek, J.F. and T.J. Schmit, 2001: Total Precipitable Water Measurements from GOES Sounder Derived Product Imagery, Weather and Forecasting, 16, 5, 573-587.

Duan, J., M. Bevis, P. Fang, Y. Bock, S. Chiswell, S. Businger, C. Rocken, F. Solheim, T. van Hove, R. Ware, S. McClusky, T.A. Herring, and R.W. King, 1996: GPS meteorology: direct estimation of the absolute value of precipitable water, Journal of Applied Meteorology, Boston, MA, 35, 6, 830-838.

English, S.J., R.J. Renshaw, P.C. Dibben, A.J. Smith, P.J. Rayer, C. Poulsen, F.W. Saunders, and J.R. Eyre, 2000: A comparison of the impact of TOVS and ATOVS satellite sounding data on the accuracy of numerical weather forecasts, Quarterly Journal of the Royal Meteorological Society, Berkshire, England, 126, 569, 2911-2931.A

Eyre, J.R., 1992: A bias correction scheme for simulated TOVS brightness temperatures. ECMWF Tech. Mem., 186.

Eyre, J. R., G. A. Kelly, A. P. McNally, E. Andersson, and A. Persson, 1993: Assimilation of TOVS radiance information through one-dimensional variational analysis. Quarterly Journal of the Royal Meteorological Society, 119, 1427–1463.

Hannon, S., L.L. Strow, and W.W. McMillan, 1996: Atmospheric infrared fast transmittance models: A comparison of two approaches, Proceedings of SPIE Conference 2830, Optical Spectroscopic Techniques and Instrumentation for Atmospheric and Space Research II (12pp.)

Hawkinson, J.A., W. Feltz, and S.A. Ackerman, 2005: A Comparison of GOES Sounder- and Cloud Lidar- and Radar-Retrieved Cloud-Top Heights, Journal of Applied Meteorology, 44, 8, 1234-1242.

Heymsfield, A. J., S. Matrosov, and B. Baum, 2003: Ice water path – optical depth relationships for cirrus and deep stratiform ice cloud layers, Journal of Applied Meteorology, 42, 1369– 1390.

Hollars, S., Q. Fu, J. Comstock, and T. Ackerman, 2004: Comparison of cloud-top height retrievals from ground-based 35 GHz MMCR and GMS-5 satellite observations at ARM TWP Manus site, Atmospheric Research, 72, 1-4, 169-186.

Huang, H.-L., and W. L. Smith, 1986: An extension of the simultaneous TOVS retrieval algorithm—The inclusion of cloud parameters. Tech. Proc. Third Int. TOVS Study Conf., Madison, WI, NOAA/Int. Assoc. Meteor. and Atmos. Physics, 118–130.

Huang, H.-L. and W. L. Smith, 2004: Apperception of clouds in AIRS data, in Proc. ECMWF Workshop on Assimilation of High Spectral Resolution Sounders in NWP, pp. 155–169.

Jin, Xin, J. Li, T.J. Schmit, J. Li, M.D. Goldberg, and J.J. Gurka, 2008: Retrieving Clear Sky Atmospheric Parameters from SEVIRI and ABI infrared radiances. Journal of Geophysical Research.D.Atmospheres, 113, D15310, DOI:10.1029/2008JD010040

Jin, Xin, J. Li, C. C. Schmidt, T.J. Schmit, and J. Li, 2008: Retrieval of total column ozone from Imagers onboard a Geostationary Satellite, IEEE Transactions on Geoscience and Remote Sensing, 46 (2), 479 – 488, DOI: 10.1109/TGRS.2007.910222

Joiner, J. and L. Rokke, 2000: Variational cloud-clearing with TOVS data, Quarterly Journal of the Royal Meteorological Society, Berkshire, England, 126, 563, 725-748.

Levenberg, K., 1944: A method for the solution of certain non-linear problems in least squares. Quarterly of Applied Mathematics, 2, 164–168.

Li, J., 1994: Temperature and water vapor weighting functions from radiative transfer equation with surface emissivity and solar reflectivity. Advances in Atmospheric Sciences, 11, 421 - 426.

Li, J., and H.-L. Huang, 1999: Retrieval of atmospheric profiles from satellite sounder measurements by use of the discrepancy principle, Applied Optics, 38, 6, 916-923.

Li, J., W. Wolf, W. P. Menzel, W. Zhang, H.-L. Huang, and T. H. Achtor, 2000: Global soundings of the atmosphere from ATOVS measurements: The algorithm and validation, Journal of Applied Meteorology, 39, 1248 - 1268.

Li, J., W.P. Menzel, and A.J. Schreiner, 2001: Variational Retrieval of Cloud Parameters from GOES Sounder Longwave Cloudy Radiance Measurements, Journal of Applied Meteorology, 40, 3, 312-330.

Li, J., C. Y. Liu, H.-L. Huang, T. J. Schmit, W. P. Menzel, and J. Gurka, 2005: Optimal cloud-clearing for AIRS radiances using MODIS. IEEE Transactions on Geoscience and Remote Sensing, 43, 1266 - 1278.

Li, J., C. Y. Liu, H.-L. Huang, T. J. Schmit, W. P. Menzel, and J. Gurka, 2005: Optimal cloud-clearing for AIRS radiances using MODIS. IEEE Transactions on Geoscience and Remote Sensing, 43, 1266 - 1278.

Li, Z., J. Li, W.P. Menzel, T.J. Schmit, and S.A. Ackerman, 2007: Comparison between current and future environmental satellite imagers on cloud classification using MODIS, Remote Sensing of Environment, 108, 3, 311-326.

Li, Z., J. Li, W. P. Menzel, T. J. Schmit, J. P. Nelson, III, J. Daniels, and S. A. Ackerman, 2008: GOES sounding improvement and applications to severe storm nowcasting, Geophysical Research Letters, 35, L03806, doi:10.1029/2007GL032797.

Li, Z., J. Li, W. P. Menzel, J. P. Nelson III, T. J. Schmit, Elisabeth Weisz, and S. A. Ackerman, 2009: Forecasting and nowcasting improvement in cloudy regions with high temporal GOES Sounder infrared radiance measurements, Journal of Geophysical Research.D.Atmospheres, in press.

Ma, X.L., T.J Schmit, and W.L. Smith, 1999: A nonlinear physical retrieval algorithm —its application to the GOES-8 /9 sounder, Journal of Applied Meteorology, 38, 5, 501-513.

Marquardt, D. W., 1963: An algorithm for least-squares estimation of nonlinear parameters. Journal of the Society for Industrial and Applied Mathematics, 11, 431–441.

McGill, M.J., M.A. Vaughan, C.R. Trepte, W.D. Hart, D.L. Hlavka, D.M. Winker, and R. Kuehn, 2007: Airborne validation of spatial properties measured by the CALIPSO lidar, Journal of Geophysical Research.D.Atmospheres, 112, D20.

McNally, A.P., 2002: A note on the occurrence of cloud in meteorologically sensitive areas and the implications for advanced infrared sounders, Quarterly Journal of the Royal Meteorological Society, 128, 585, 2551-2556.

McNally, A.P. and P.D. Watts, 2003: A cloud detection algorithm for high-spectral-resolution infrared sounders, Quarterly Journal of the Royal Meteorological Society, 129, 595, 3411-3423.

McNally, A.P., P.D. Watts, J.A. Smith, R. Engelen, G.A. Kelly, J.N. Thepaut, and M. Matricardi, 2006: The assimilation of AIRS radiance data at ECMWF, Quarterly

Journal of the Royal Meteorological Society, 132, 616, 935-957.

McPherson, R. M., 1999: The future of the North American radiosonde network. Third Symposium on Integrated Observing Systems, 10-15 January, 1999. Dallas, Texas. pp 14-17.

Menzel, W.P., D. P. Wylie, and K. I. Strabala, 1992: Seasonal and diurnal changes in cirrus clouds as seen in four years of observations with the VAS. Journal of Applied Meteorology, 31, 370–385.

Menzel, W.P. and J.F.W. Purdom, 1994: Introducing GOES-I: the first of a new generation of geostationary operational environmental satellites, Bulletin of the American Meteorological Society, Boston, MA, 75, 5, 757-781.

Menzel, W.P., F.C. Holt, T.J. Schmit, R.M. Aune, A.J. Schreiner, G.S. Wade, and D.G. Gray, 1998: Application of GOES-8/9 soundings to weather forecasting and nowcasting, Bulletin of the American Meteorological Society, Boston, MA, 79, 10, 2059-2077.

Miloshevich, L.M., H. Voemel, D.N. Whiteman, B.M. Lesht, F.J. Schmidlin, and F. Russo, 2006: Absolute accuracy of water vapor measurements from six operational radiosonde types launched during AWEX-G and implications for AIRS validation, Journal of Geophysical Research.D.Atmospheres, 111, D9.

Phulpin, T., D. Blumstein, F. Prel, B. Tournier, P. Prunet, and P. Schl¨ussel, 2007: Applications of IASI on MetOp-A: first results and illustration of potential use for meteorology, climate monitoring, and atmospheric chemistry, Proc. SPIE, 6684, 66840F, doi:10.1117/12.736816, 2007.

Plokhenko, Y. and W.P. Menzel, 2001: Mathematical Aspects in Meteorological Processing of Infrared Spectral Measurements from the GOES Sounder. Part I: Constructing the Measurement Estimate Using Spatial Smoothing, Journal of Applied Meteorology, 40, 3, 556-567.

Plokhenko, Y., W.P. Menzel, G. Bayler, and T.J. Schmit, 2003: Mathematical Aspects in Meteorological Processing of Infrared Spectral Measurements from the GOES Sounder. Part II: Analysis of Spatial and Temporal Continuity of Spectral Measurements from the GOES-8 Sounder, Journal of Applied Meteorology, 42, 6, 671-685.

Plokhenko, Y. and W.P. Menzel, 2003: Mathematical Aspects of the Meteorological Processing of Infrared Spectral Measurements from the GOES Sounder. Part III: Emissivity Estimation in Solving the Inverse Problem of Atmospheric Remote Sensing, Journal of Applied Meteorology, 42, 11, 1533-1546.

Press, W., B. Flannery, S. Teukolsky, and W. Vetterling, 1990: Numerical Recipes in C. Cambridge University Press.

Press, W. H., S.A. Teukolsky, W.T. Vetterling, and B.P. Flannery, 1992: Numerical Recipes, 2nd edition. Cambridge: Cambridge University Press.

Rothman, L.S. R.R. Gamache, R.H. Tipping, C.P. Rinsland, M.A.H. Smith, D.C. Benner, V.M. Devi, J.-M. Flaud, C. Camy-Peyret, A. Perrin, 1992: The HITRAN Molecular Database: Editions of 1991 and 1992, Journal of Quantitative Spectroscopy and Radiative Transfer, 48, 469-507.

Saunders, R., M. Matricardi, and P. Brunel, 1999: An improved fast radiative transfer model for assimilation of satellite radiance observations, Quarterly Journal of the Royal Meteorological Society, Berkshire, England, 125, 556, 1407-1425.

Schmit, T. J., 1996: Sounder bias correction of the east–west radiance gradient. Proc. SPIE, 2812, 630–637.

Schmit, T.J., W.F. Feltz, W.P. Menzel, J. Jung, A.P. Noel, J.N. Heil, J.P. Nelson III and G.S. Wade, 2002: Validation and Use of GOES Sounder Moisture Information, Weather and Forecasting, 17, 1, 139-154.

Schmit, T.J., M.M. Gunshor, W.P. Menzel, J.J. Gurka, J. Li, and A.S. Bachmeier, 2005: Introducing the Next-Generation Advanced Baseline Imager On Goes-R, Bulletin of the American Meteorological Society, 86, 8, 1079-1096.

Schmit, T.J., J. Li, S.A. Ackerman and J.J. Gurka, 2009: High spectral and temporal resolution infrared measurements from geostationary orbit. Journal of Atmospheric and Oceanic Technology. In press.

Schreiner, A.J., T.J. Schmit, and W.P. Menzel, 2001: Observations and trends of clouds based on GOES Sounder data, Journal of Geophysical Research.D.Atmospheres,. 106, D17, 20,349-20,363.

Seemann, S.W., E. E. Borbas, R. O. Knuteson, G. R. Stephenson, and H.-L. Huang, 2008: Development of a Global Infrared Land Surface Emissivity Database for Application to Clear Sky Sounding Retrievals from Multi-spectral Satellite Radiance Measurements. Journal of Applied Meteorology and Climatology, 47, 108-123

Smith, W. L., H. M. Woolf, and W. J. Jacob, 1970: A regression method for obtaining real-time temperature and geopotential height profiles from satellite spectrometer measurements and its application to Nimbus 3 "SIRS" observations. Monthly

Weather Review, 98, 582–603.

Smith, W. L. and H. M. Woolf, 1976: The use of eigenvectors of statistical covariance matrices for interpreting satellite sounding radiometer observations. Journal of the Atmospheric Sciences, 33, 1127–1140.

Smith, W. L., H. M. Woolf, C. M. Hayden, D. C. Wark, and L. M. McMillin, 1979: TIROS-N operational vertical sounder. Bulletin of the American Meteorological Society, 60, 1177–1187.

Smith, W. L., H.M. Woolf, C.M. Hayden, and A.J. Schreiner, 1985: The simultaneous retrieval export package. Tech. Proc. Second Int. TOVS Study Conf., Igls, Austria, CIMSS, 224–253.

Smith, W. L. and H. M. Woolf, 1988: A linear simultaneous solution for temperature and absorbing constituent profiles from radiance spectra. Tech. Proc. Fourth Int. TOVS Study Conf., Igls, Austria, CIMSS, 330–344.

Stephens, G.L., D.G. Vane, R.J. Boain, G.G. Mace, K. Sassen, Z. Wang, A.J. Illingworth, E.J. O'Connor, W.B. Rossow, S.L. Durden, S.D. Miller, R.T. Austin, A. Benedetti, and C. Mitrescu, 2002: The Cloudsat Mission And The A-Train, Bulletin of the American Meteorological Society, 83, 12, 1771-1790.

Susskind, J., C. D. Barnet, and J. M. Blaisdell, 2003: Retrieval of atmospheric and surface parameters from AIRS/AMSU/HSB data in the presence of clouds, IEEE Transactions on Geoscience Remote Sensing, 41, 2, 390–409.

Turner, D. D., B.M. Lesht, S.A. Clough, J.C. Liljegren, H.E. Revercomb, and D.C. Tobin, 2003: Dry bias and variability in Vaisala RS80-H radiosondes: The ARM experience. Journal of Atmospheric and Oceanic Technology, 20, 1, 117-132.

Wang, F., J. Li, T. J. Schmit, and S.A. Ackerman, 2007: Trade-off studies of a hyperspectral infrared sounder on a geostationary satellite. Applied Optics, 46, 200 - 209.

Warren, S.G., C.J. Hahn and J. London, 1985: Simultaneous occurrence of different cloud types. Journal of Applied Meteorology, 24, 4– 2267.

Wei, H., P. Yang, J. Li, B. B. Baum, H.-L. Huang, S. Platnick, Y. Hu, and L. Strow, 2004: Retrieval of semitransparent ice cloud optical thickness from Atmospheric Infrared Sounder (AIRS) measurements, IEEE Transactions on Geoscience Remote Sensing, 42, 2254– 2267.

Weisz, E., J. Li, J. Li, D.K. Zhou, H.-L. Huang, M.D. Goldberg, and P. Yang, 2007:

Cloudy sounding and cloud-top height retrieval from AIRS alone single field-of-view radiance measurements, Geophysical Research Letters, 34, 12.

Weisz, E., J. Li, W. P. Menzel, A. K. Heidinger, B. H. Kahn, and C. Y. Liu, 2007: Comparison of AIRS, MODIS, CloudSat and CALIPSO Cloud Top Height Retrievals. Geophysical Research Letters, Vol. 34, L17811.

Winker, D. M., B. H. Hunt, and M. J. McGill, 2007: Initial performance assessment of CALIOP, Geophysical Research Letters, 34, L19803, doi:10.1029/2007GL030135.

Wylie, D. P., D. L. Jackson, W. P. Menzel, and J. J. Bates, 2005: Global Cloud Cover Trends Inferred from Two decades of HIRS Observations. Journal of Climate, 18, 15, 3021–3031.

Zeng, Q.C. 1974, Principle of atmospheric Infrared remote sensing, Science Press, Beijing, 174pp. (in Chinese)

Zhou, D. K., W. L. Smith, X. Liu, A. M. Larar, S. A. Mango, and H.-L. Huang, 2007: Physically Retrieving Cloud and Thermodynamic Parameters from Ultraspectral IR Measurements, Journal of the Atmospheric Sciences, 64, 969-982.